UNIVERSITA' DEGLI STUDI DI PARMA

Dottorato di ricerca in Fisica

XXVII ciclo

Dynamics, Synchronization and Inverse problem in Mean Field Neural Networks with synaptic plasticity

Coordinatore:
Prof. Cristiano Viappiani

Tutor:
Prof. Raffaella Burioni

Dottorando: Matteo di Volo

Contents

Introduction

One of the most intriguing and mysterious issue that has been feeding the brain of scientists is the way brain itself works and how it produces questions, thoughts and reactions to external stimuli. The increasing refinement of experimental techniques has led to a detailed description of single units composing the brain, neurons. The network composed by neurons connecting together is thought to be the main system ruling brain's activities [1]. The language through which single neurons communicate with each others has been addressed to their electrical activity, able to stimulate other neurons, like in a electrical circuit. Physiological information about neural structure and activity was employed from the very beginning to construct effective mathematical models of brain functions. There is a large variety of models present in the literature, describing different physiological mechanisms with higher or lower degree of detail. For instance, the combination of complex single–neuron dynamics, noise and specific network topologies revealed quite crucial for reproducing experimental observations, like the spontaneous emergence of synchronized neural activity, both *in vitro* (see, e.g., [2]) and *in vivo*, and the appearance of peculiar fluctuations, the so–called "up–down" states, in cortical sensory areas [3, 4]. Nevertheless, every model is far from the real complexity and refinement that would be necessary to describe every physical mechanism present in neural dynamics. On the other hand, anatomical observations suggest that real neural networks are made up of a very large number of interacting neurons and, when dealing with large–scale or collective neural processes, one can expect that a high level of detail is not necessary in order to catch the fundamental aspects of collective dynamics. This can be argued observing that a single neuron does not play a crucial role for brain processes and cannot modify them significantly in case of inefficiency. Actually, it is well known that the brain activity is quite robust also with respect to relatively strong perturbations.

On the basis of these observations in this thesis the attention is mainly devoted to the collective dynamics of networks of neurons, that, in addition, is typically the easiest observable that is measured in experiments. In the perspective of considering a model describing the fundamental aspects of neural dynamics we consider a system of leaky integrate–and–fire (LIF) neurons, interacting via a synaptic current regulated by the short–term plasticity mechanism [5]. As a model for the underlying topology we consider randomly uncorrelated diluted networks (we take into account both dense and sparse networks) made of N nodes. We will show how such model is able to reproduce a very rich variety of dynamical phases. In particular, disorder on network structure yields a dynamical phase characterized by quasi–synchronous events (QSE). This means that a large fraction of neurons fire in a short time interval of a few milliseconds (ms), separated by uncorrelated firing activity lasting over some tens of ms. The resulting collective field generated by this model shows oscillations typically observed in *in vivo* setups. Furthermore, disorder on different model parameters (in particular on neurons excitability and connections), produces synchronization patterns observed in *in vitro* experiments, where bursts of neurons alternate with very long uncorrelated activity (lasting seconds) distributed according to a long tail statistics [2, 5].

Accordingly, disorder on model parameters, like network connections and neurons excitability, plays a crucial role for the emergent dynamics. Moreover, the large number of units and the redundancy of connections suggests that a mean–field approach can be the right mathematical tool for understanding the large–scale dynamics of neural network models. The thermodynamic limit, $N \to \infty$, is expected to provide the basic ingredients for an analytic treatment. On the other hand, the way such a thermodynamic limit is performed may wipe out any relation with the model features that are responsible, for finite N, of relevant dynamical properties. In this thesis we show how it is possible to derive a mean field model that keeps track of relevant inhomogeneities responsible for finite size dynamics, called heterogenous mean field (HMF), similar to the one recently introduced in the context of epidemiological spreading on networks [6, 7, 8]. Given a real finite size sample, the HMF model is able to reproduce its dynamics from the knowledge of the parameters probability distributions that can be picked up from the finite size system.

In the perspective of a *direct problem*, i.e. the investigation of the model dynamics for certain parameters distributions, such mean–field like equations can be studied analytically by introducing the return maps of the firing times. Furthermore, the HMF model sheds light on the role

of the network topology in the collective synchronization of the network. Another a big advantage in the introduction of such a mean field approach is the possibility to formulate and solve an *inverse problem*, that is addressed to the reconstruction of the network topological features from dynamic time series [9, 10, 11, 12]. The latter approach is particularly interesting when the direct investigation of the network is impossible or very hard to be performed.

In *local* approaches to inverse problems [9, 10, 11, 12], the network is reconstructed through the knowledge of long time series of single neuron dynamics, a methods that applies efficiently to small systems only. Actually, the signals emerging during neural time evolution are often records of the average synaptic activity from large regions of the cerebral cortex – a kind of observable much easier to be measured than signals coming from single neuron activities [13]. Furthermore, inspired by previous considerations, it is reasonable to expect that collective signals do not depend on the detail of the neuronal model considered, permitting a good position of the inverse problem with real data. Inferring the topological properties of the network from global signals is still an open and central problem in neurophysiology. In this thesis we show how it is possible to formulate and solve such a *global* version of the inverse problem, reconstructing the network topology that has generated a given global (i.e. average) synaptic-activity field.

Furthermore, we will show how it is possible to extend this approach to the reconstruction of different parameters distributions given the global signal. Finally, by considering the presence of inhibitory neurons, we will present the extension to this case, reconstructing network topology and fraction of inhibitory neurons from a finite size global signal.

The thesis is organized as follows. In the first Chapter the experimental observations of neural dynamics are described. Furthermore we describe how one can build up mathematical models of a neural network from the basis of physiological observations. In the second Chapter we report the main dynamical features of the dynamics relative to the model we take under consideration. In the third Chapter we describe how one can define a mean field model in the simplest case of a excitatory network with disorder only on network structure and how this approach leads to the formulation and solution of a global inverse problem where informations on the network topology are reconstructed from the knowledge of the collective electrical activity of the network. Finally, in the last chapter, we show how the overall procedure of mean field approach and inverse problem can be extended to a system in presence of inhibitory synapses

and to networks where disorder is applied on excitabilities of single neurons.

CHAPTER 1

Neural ensambles: synchronization and models

The brain is the organ acting as control system over the actions of the majority of animals. Its main role is to elaborate the sensory stimuli coming from the environment and drive the relative response of the body. A crucial issue that has attracted the attention of many scientists is the way this system works and how it elaborates and sends information. Thanks to more and more refined experimental techniques it has been possible to deduce that the answer lies in the cellular elements composing the brain. These cells, called neurons, are able to emit and propagate electrical potentials to other neurons, usually called spikes. The temporal sequence of these spikes is supposed to be the code through which neurons exchange information and regulate the response of muscles and the secretion of hormones. Accordingly, brain tissues generate electric fields that can be measured with electroencephalography (EEG) [14]. This technique, as other different measurements like MEG or FMRI, permits the definition and detection of a quantitative observable to describe brain's region activity [15, 13]. From a microscopic ground, accurate experimental techniques (like the so called patch clamp [16]) have permitted to measure single neuron electrical activity and how this activity is transmitted to other neurons. As a result, it has been possible to build up mathematical models that simulate the electrical activity of groups of neurons. These two ingredients permit to investigate the physical mechanism giving rise to specific collective activity of large regions of the brain through the comparison of model predictions and experimental observations. In this chapter some examples of these scientific developments are reported. In Sec. 1.1 we report some experimental observations of the electrical activity of neural ensembles. Given the microscopic organization of brain tissues composed by neurons connected to each other in Sec. 1.2 we recall the typical mathematical formalism that can be used to describe a group of dynamical

units that are connected through topological structures. In Sec. 1.3 we report the experimental observations about single neural electric activity that lead to the construction of the fundamental model for the single unit dynamics, called the leaky–integrate and fire (LIF), that will be considered in this thesis. Finally, in Sec. 1.4 we discuss how neurons transmit information to each other. In particular, we focus on the influence of the activity (the spikes) of a neuron on the neurons connected to it, and on the connections, and we discuss in details the model of coupling dynamics between neurons developed by Tsodyks, Uziel and Markram (TUM model). Combining these results we obtain a description of the activity of groups of neurons with a set of coupled differential equations, whose dynamics is the subject of this thesis.

1.1 Experimental observations of neural tissues

The brain is composed by neurons that are connected to each other. Anatomical evidence indicates that the density of neurons and connections is very high. In particular, it has been estimated that neurons in human brain have on average 7000 connections to other neurons. Furthermore, in cerebral cortex the density of neurons is about 10^4 neurons$/\mathrm{mm}^3$ [17]. The neuron is characterized by its membrane potential V which is the difference between the voltage outside and inside the main body of the cell, called soma. The membrane potential V sets, in absence of stimuli, at a resting potential. When V, because of external stimuli, exceeds a certain threshold value it rapidly rises and falls. This short change of V is called action potential and has a stereotyped shape. Each neuron has many branches, called dendrites, that receive the signal coming from other neurons. This signal is propagated along the axon which is the nerve fiber that carries the signal to dendritic projections of receiving neurons. They carry this information in the form of action potentials, starting at the soma and terminating at points where the axon makes contact with target cells, called synapse. Here the action potential of the neuron sending information affects the membrane potential of target neuron, increasing or decreasing it [18].

The anatomical structure is qualitatively the same for all neurons, even if different neurons can have different dendritic ramifications. As an example, in Fig. 1.1 we show three examples of neural structures where we can see that, apart from structural differences, neurons have a stereotyped organization composed by inputs (dendrites), elaboration center (soma or cell body) and output (axon). Apart from the chemical mechanisms ruling

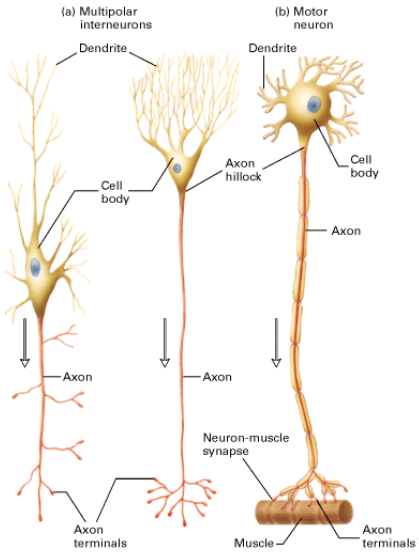

Figure 1.1: Examples of neural cells with different dendritic ramifications [19].

the dynamics of V and of the synaptic transmission (these will be treated in Sec. 1.3 and 1.4), from this phenomenological description it is clear that the electrical activity of neurons, i.e. their membrane potential dynamics, makes neural tissues able to generate electric fields.

The most famous and used technique to detect these fields is the electroencephalography, shortly called EEG [14]. The first record of human EEG dates back to 1924, by German physiologist and psychiatrist Hans Berger [20]. The main advantage of this technique is that is not invasive, as it reveals the electric field outside the scalp, while the main disadvantage is the limited spatial resolution [21]. Nevertheless, this method is still largely used in order to diagnose sleep disorders, coma, encephalopathies, and brain death. The electric fields generated by a single neuron cannot be detected by EEG, as their intensity is too small to be revealed outside the scalp. Accordingly, EEG signals are always the result of the constructive composition of single neurons electric fields and reflect the synchronization of the spiking time of neurons. Typically, neurons taking part to the global signal are thousands or millions and their synchronization gives rise to oscillations in their mean activity [22]. The observed EEG signals reveal oscillatory activity in certain frequency bands. The most famous and first to be discovered is the alpha band ($8-13$Hz), that can be well revealed during relaxed wakefulness. Nevertheless, other frequency bands have been observed like delta ($0.5-4$ Hz), theta ($4-8$ Hz), beta ($13-30$

Hz) and gamma ($30 - 70$ Hz) [14]. In Fig. 1.2 are reported some examples of collective oscillations detected by EEG. These observations reveal that

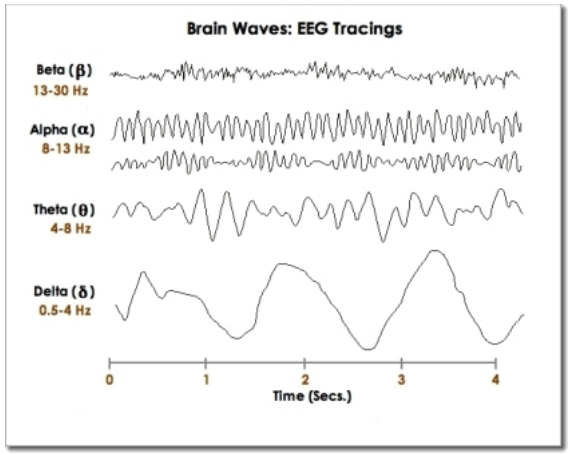

Figure 1.2: Some examples of EEG recordings [23].

synchronizations properties of neurons play a crucial role for the emergent dynamics and functionality of large brain areas. As an example, epilepsy is characterized by abnormal synchronous neuronal activity in the brain [14]. For completeness, let us indicate the existence of several other methods to study brain function exist, e.g. functional magnetic resonance imaging (fMRI) [13], positron emission tomography, magnetoencephalography (MEG) [15], from which the same deduction mentioned above can be done.

As fields coming from the mentioned method are the result of thousands or millions of single neural fields, much effort has been done in order to move the experimental analysis to a microscopic ground. A crucial step forward in this direction has been the possibility to build up neural cultures in laboratories, made up by real neural cells connected together. The main advantage of this approach is the possibility to have access to the dynamics of every single neuron, through a microelectrode array [24]. This is a patterned array of electrodes laid out in a transparent substrate used to detect neural activity and spiking patterns. Accordingly, it is possible to obtain the timing at which every neuron emits a spike and analyze the dynamics of the culture by collecting the activity of all neurons. As an example, in Fig.1.3 it is reported the observation from a culture of about fifty neurons. In particular, it is reported the raster plot of neural network. On the ordinates it is reported the neuron index and on abscissa the time. Every time a neuron emits a spike a dot is drawn at the

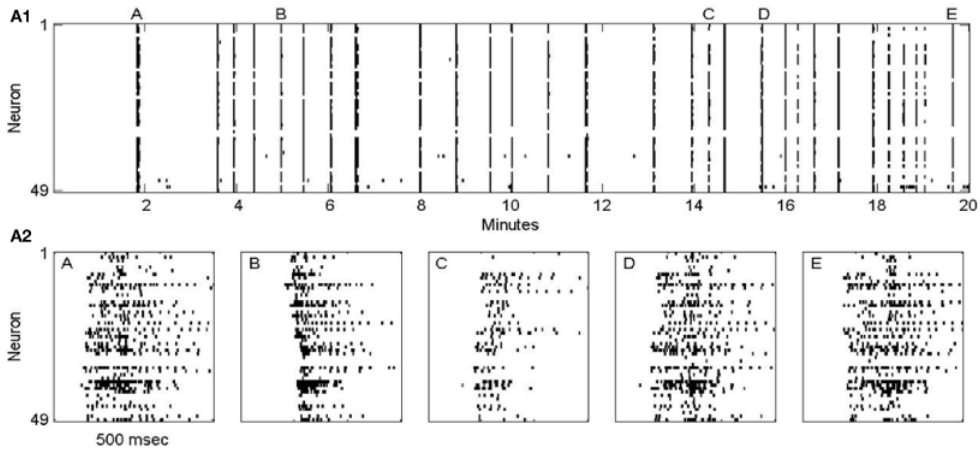

Figure 1.3: Typical raster plot of the recorded activity for coupled neural network. Each line corresponds to the recorded activity from a specific electrodes. Bars indicated neuronal firing [25].

relative time and neural index. The raster plot is a microscopic picture of the system dynamics, at variance with the EEG recordings presented previously. As typically happens in neural cultures observations, the dynamics is characterized by events of bursting, usually called population bursts (PB), where the majority of neurons fire in a short interval (typically of hundreds ms). At variance with oscillations of large populations observed in EEG recordings, in this case the collective activity shows peaks at irregular times (actually when the PB appears). In fact, the distribution of time lapse in between two consecutive PB (usually called IPBI) follows a long tail statistics with rare events [2]. Accordingly, also from this microscopic picture, it seems clear that synchronization between neurons is the fundamental aspect that determines the dynamics of the system.

Synchronization is a widely studied phenomenon that appears in many different frameworks and scientists have payed much attention in the theoretical mechanism yielding the observed synchronization patterns [26]. In particular, systems of dynamical units connected together can be studied through general mathematical models that apply in different fields. In the next section it will be shown how one can write down a model for dynamical units connected together that will be used in the rest of the thesis to investigate the dynamics proper of neural ensembles.

1.2 Model for dynamical units on extended networks

In previous section we have discussed the observed features of neural ensembles dynamics derived from experiments. At this point we can think about a mathematical model, with the aim to reproduce and interpret some observed synchronization characteristics observed in experiments.

1.2.1 Single unit and coupling dynamics

Let us start from the observation that a neuron can be schematized as a dynamical unit (the cell body) that can be described by a vector of time dependent variables, say $\mathbf{w}(t)$. In absence of external stimuli or connection with other units $\mathbf{w}(t)$ has its own dynamics, that can be written as

$$\dot{\mathbf{w}} = \mathbf{F}_\alpha(\mathbf{w}), \tag{1.1}$$

where the function $\mathbf{F}_\alpha$ represents the single unit dynamics and α is a set of parameters from which $\mathbf{F}$ depends. Notice that, for the sake of simplicity, we have not introduced an explicit dependence of $\mathbf{F}$ on time t as in all the cases usually studied for investigating oscillators and neural dynamics the dependence on t is implicit in $\mathbf{w}$.

Furthermore, each unit i receives a certain number of inputs that produces a change in the dynamical variable $\mathbf{w}_i$ of the cell body. In many models of oscillators, in particular in neural systems, the effect of node j on node i depends by the state of node j, in the case of neurons by its spike train. Thus, we consider this class of models by defining a general function $\mathbf{G}(\mathbf{w}_j)$ that rules the effect of unit j on unit i in the following sense

$$\dot{\mathbf{w}}_i = \mathbf{F}_\alpha(\mathbf{w}_i) + g\mathbf{G}(\mathbf{w}_j), \tag{1.2}$$

where g is the coupling strength. In general, also $\mathbf{G}$ depends on some parameters but they are not shown explicitly in Eq. (1.2) as in all the cases here considered they are fixed and do not change from neuron to neuron. Furthermore, in Eq. (1.2) $\mathbf{G}$ depends only from presynaptic terminal j. Nevertheless in many cases, like in the presence of inhibitory neurons (see Sec. 1.4), the dynamics depends also on the postsynaptic terminal i. We will treat this case as an extension of the main methods developed in this thesis in Sec4. Another example where $\mathbf{G}$ depends from postsynaptic neuron i are electrical coupling (see Sec. 1.4). Nevertheless we will not treat this case as the majority of neural coupling do not use this mechanism. The functions $\mathbf{F}$ and $\mathbf{G}$ depend on the specific system one wants to

analyze. In next sections we will show how we can define them to recover the fundamental properties of neural dynamics.

1.2.2 Structure of connections and network models

In order to study the dynamics of extended systems, like neural ensembles, one has to define the structure of connections between single units. Graph theory is the mathematical framework to characterize the network of connections [27, 28]. A graph can be defined as set V of nodes together with a set E of edges. Nodes represent the dynamical units of the system while edges the connections between single nodes. Graphs can be divided in two main families, undirected and directed graphs. The first class is characterized by edges with no preferential direction. This means that, if a connection exists between node i and j, the influence of one on each other is bidirectional. This case applies in epidemic spreading models where there is no directionality in the coupling between two nodes that infect each other when they come in contact [6]. On the contrary, in neural systems the coupling is directional as the axon of neuron i can come in contact to a dendrite of neuron j and not vice versa. Thus, neuron i can send spikes to neuron j but not necessarily neuron j affects neuron i dynamics. This class of graphs are called directed and the edges are usually called arcs or arrows. In order to make this difference clearer, in Fig. 1.4 we show two examples of directed and undirected graphs. A graph

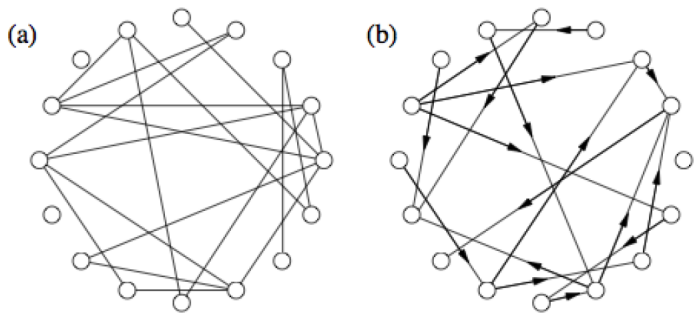

Figure 1.4: A undirected and directed graph is drawn on the left and right, respectively. Dots are nodes and lines or arrows undirected or directed links [29].

formed by N nodes can be represented by a NXN matrix ϵ, called adjacency matrix. Its entries ϵ_{ij} are 0 or 1. If node j is directly connected to

neuron i $\epsilon_{ij} = 1$, otherwise $\epsilon_{ij} = 0$. By definition, if the graph is undirected the adjacency matrix is symmetric. A first quantity that plays a fundamental role in the dynamics of the units is its connectivity. In the case of directed graph we can define two different connectivities. The in–degree connectivity $k^i_{in} = \sum_j \epsilon_{ij}$ and the out–degree connectivity $k^i_{out} = \sum_j \epsilon_{ji}$. For the sake of simplicity we define $k = k_{in}$ the in–degree or simply connectivity of node i. Given a certain graph of size N we can define $P(k)$ the in–degree or connectivity distribution of the network. In finite size samples this distribution is the envelop of the histograms obtained analyzing the connectivity of the nodes. Furthermore, as $k \in [0, N-1]$in order to avoid self loops, P needs to be suitably normalized. There are several ways to construct networks. In this thesis we will consider random and uncorrelated network [28]. A random network is a network constructed with some random process that can be defined by a probability distribution or by the random process which generates it. Uncorrelated graphs are graph for which the probability that a neuron with connectivity k is connected with a neuron with connectivity k' does not depend on k'. The most used model to generate random uncorrelated graphs is the Erdős–Rényi model [30]. It consists in choosing every couple of nodes (i, j) and connecting them with a certain probability p. The resulting connectivity distribution $P(k)$ turns out to be binomial

$$P(k) = \binom{N-1}{k} p^k (1-p)^{N-1-k}. \tag{1.3}$$

If the size N is sufficiently large and p is fixed the central limit theorem implies that $P(k)$ is a Gaussian distribution with average $\langle k \rangle = pN$ and variance $\sigma^2_k = Np(1-p)$.

Many networks, including World Wide Web links and social networks, show a power law distribution for $P(k)$, at variance with Erdős–Rényi model. The mostly used generative model for scale-free networks is Barabśi and Albert's generative model in which each new node creates links to existing nodes with a probability distribution proportional to the current nodes in-degree [31]. A cleaver way to construct random graphs with desired distribution $P(k)$ is the configuration model [32]. Chosen a normalized distribution $P(k)$, a sequence of N values of k $(k_1, k_2 \ldots, k_N)$ are extracted by $P(k)$. Then, randomly chosen k_i nodes indexes are assigned to each node i.

A crucial issue in graph theory and in particular for dynamical models arranged on graphs is the dependence of the structure on the size N. In order to show the size effects on network structure let us introduce the

specific connectivity $\tilde{k} = k/N$. As a result one has that $P'(\tilde{k}) = NP(\tilde{k}N)$. In particular, for the Erdős–Rényi network, in large ensembles and for fixed p, P' is a Gaussian with average $\langle\tilde{k}\rangle = p$ and standard deviation $\sigma_{\tilde{k}} = \sigma_k/N \sim 1/\sqrt{N}$. This result will be useful in next sections and shows that the relative fluctuations of connectivity go to zero in the thermodynamic limit (i.e. when $N \to \infty$). In this framework, an important classification in networks construction is based on the difference between sparse and dense/massive networks. Sparse networks are networks where the rescaled connectivity of neurons k/N goes to zero in thermodynamic limit. A massive network is a network where connectivities of neurons scale at least as the size N of neurons. In the case of Erdős–Rényi model this distinction is ruled by the dependence of p by N. If p/N does not go to zero in the thermodynamic limit the network is said massive and sparse otherwise.

1.2.3 Extended system model

We can now formulate a formal model for dynamical units on graphs. The dynamics of node i receiving input by node j is described by Eq.(1.2). To obtain the dynamics of node i on a graph we need to add the effect of all nodes sending outputs to i. If the structure of the network is described by the adjacency matrix ϵ_{ij} we can write, for each node $i \in [1, N]$

$$\dot{\mathbf{w}}_i = \mathbf{F}_\alpha(\mathbf{w}_i) + \frac{g}{N}\sum_j \epsilon_{ij}\mathbf{G}(\mathbf{w}_j). \tag{1.4}$$

Notice that the coupling term has been rescaled by the network size N. This choice depends on the choice of the network model we are considering. In the case of Eq. (1.4) we suppose that the network connectivities scale as the size N of the network, i.e. a massive network. In fact, we want the coupling term to remain finite in the thermodynamic limit and comparable at different sizes. If we are dealing with sparse networks it is more convenient to rescale by the average connectivity $\langle k\rangle$ in order to respect the mentioned requests. These model adjustments are not a prejudice of generality. In fact, in this thesis we want to refer to real neural systems that are always finite, i.e. N is a finite number. By considering the dynamics of a certain brain region, we will deal with a specific network of a certain size N with its own network structure. Thus, a real network is neither massive or sparse and, in the model describing that specific network, the choice of the term $1/N$ or $1/\langle k\rangle$ is just a rescaling of the coupling g. Nevertheless, if one wants to analyze the network at increasing size it

is necessary to choose the way to generate graphs at increasing values of N and to have a well defined model with the opportune rescaling of the coupling term.

In order to study the dynamics of neural ensembles we need a model for $\mathbf{F}$ and $\mathbf{G}$. In the next Sections we describe the experimental studies that have led to the model equations that will be used in this thesis.

1.3 Neuron dynamics

As introduced in Sec.1.1 the state of the neuron is described by its membrane potential V, defined as the voltage difference between the cell body of the cell and the extracellular liquid in which neurons are embedded. In absence of external stimuli V sets in a resting state V_r. Whenever V exceeds a certain threshold value, due to external stimuli, we observe a rapid increase of V (polarization) followed by a rapid decrease up to a value lower then the resting state. Then, a third phase called iperpolarization brings back V to the resting value V_r. This change of V in time is said action potential and has a stereotyped shape. In Fig. 1.5 we report its shape derived by an experiment in 1962, where we can see its time duration lasting around 2ms [33]. Much effort has been done in order to un-

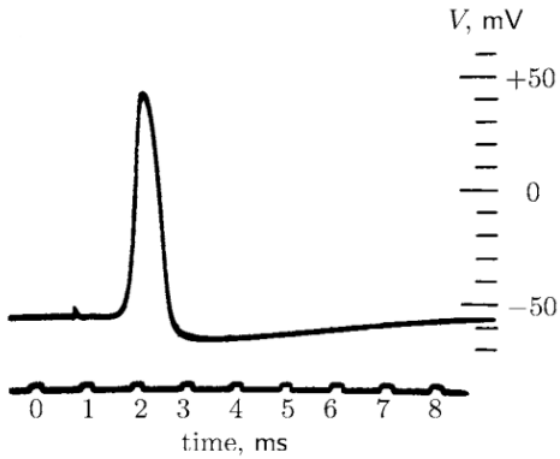

Figure 1.5: Oscilloscope traces from the voltage of a neuron recorded by Baker et.al. in 1962 [33].

derstand the mechanisms ruling the dynamics of V in absence of stimuli

and how it is able to generate the action potential. The pioneering experiment of Hodgkin and Huxley paved the way for possible understanding and modelization of neuron dynamics by performing experiments on the squid giant axon [34]. The large diameter of the axon provided a great experimental advantage for Hodgkin and Huxley as it allowed them to easily insert voltage electrodes. The electric activity of neurons is guided by ionic currents passing through the membrane. The dominant currents are generated by sodium (Na^+), potassium (K^+), calcium (Ca^{2+}) and chlor (Cl^-). The concentration of these ions are different inside and outside the cell and the electric gradients due to their mobility are responsible for the electrical activity of the cell body. In particular, the membrane permeability for these ions is the fundamental ingredient responsible for the generation of the action potential. Thanks to their experiment, Hodgkin and Huxley have been able to construct a suitable model for the permeability of the cell membrane to Calcium and Potassium allowing for an explanation of the action potential formation. The model proposed takes under consideration four dynamical variables for the dynamics of V. The complexity of the model, both for computational and purely analytical investigations, led to a reductionist approach for the neuron dynamics modelization [35]. Models later implemented, like Morris–Lecar model [36], use simpler dynamical equations with the aim to describe the fundamental characteristics of the neural dynamics. The simplest model in this direction is called leaky–integrate and fire (LIF) and it was proposed by Lapique [37]. This model does not care about the reproduction of the action potential dynamics. It takes under consideration two fundamental ingredients of neural dynamics: a spike is emitted whenever V reaches a certain threshold and then V returns rapidly to its reset value. The equation chosen to describe this dynamical features is

$$\tau_m \dot{V} = E_l + V_r - V \tag{1.5}$$

$$\text{if } \; V > V_{th} \rightarrow \text{spike emission and } \; V = V_r, \tag{1.6}$$

where V_r is the resting potential and τ_m is a time constant that takes into account the capacity of the cell membrane that, in this scheme, can be considered like a capacitor. The voltage E_l is present in all neural models and is due to the leakage current that, because of different concentrations of non–dominant ions inside and outside the cell, flows through the membrane. Finally, 1.6 is a hand–role taking into account that when V exceeds a certain threshold value V_{th} a spike is emitted to other neurons and V is reset to the resting state V_r. In this approximation the action potential is instantaneous and in the next session we will see how one can model the

effect of the spike train of the considered neuron. Let us introduce from the very beginning adimensional variables, i.e. we rescale appropriately time and voltages. In particular

$$t \to t/\tau_m \tag{1.7}$$

$$v = \frac{V - V_r}{V_{th} - Vr}. \tag{1.8}$$

As a result we obtain the following equation for the dynamics of v

$$\dot{v} = a - v, \tag{1.9}$$

where a is the rescaled leakage current, the resting value is $v = 0$ and the threshold value is $v_{th} = 1$. For the rest of the thesis we will consider only adimensional equations. Accordingly, in order to read the results in physical units, voltage and time have to be rescaled back. Typical values for parameters are $\tau_m = 30$ms, $V_r = -65$mV and $V_{th} = -55$mV [5, 35]. By looking at the comparison with Eq.(1.1) we have that $\mathbf{w} = v$ is a scalar and that $\mathbf{F}_\alpha(\mathbf{w}) = a - v$ plus the hand–role 1.6. In this case a is the only parameter of the single neuron dynamics.

Let us analyze the dynamical properties of LIF model for $v(t)$. If $a > 1$ v follows a periodic dynamics of period $T_v = \ln(a/(a-1))$ and spikes are emitted at regular piece (spiking regime). Accordingly, the time lapse between two consecutive spikes, inter–spike–interval (ISI), is constant and equal to T_v. On the contrary, if $a < 1$ the dynamics of v has a stable fixed point $v^* = a$ and the neuron does not emit spikes (silent regime). In Fig. 1.6 we show these two dynamical regimes. Accordingly, a plays the role of a bifurcation parameter with critical value $a_c = v_{th} = 1$. In order to obtain more complex spike trains one can use stocastic processes $\xi(t)$ in the form of additive noise in Eq.(1.9). For example, one may consider a random walk with boundaries. By changing the time correlation of the process one can obtain a wide range of spiking patterns [38]. This case will be taken in consideration in Sec. 2.2 when we will deal with some peculiar collective dynamics observed in neural cultures.

The LIF model has the advantage to be computationally efficient and analytically integrated in–between two consecutive spikes. It is not able to describe specific characteristics of neural dynamics as the action potential formation. Nevertheless, by using mathematical tools like the hand–rule 1.6, it is able to catch the fundamental properties of neural behaviors. Furthermore, it permits a clear interpretation of dynamical regimes observed in network structures. The main methods shown in this thesis can be applied also to more complex neural models. Nevertheless, we will deal

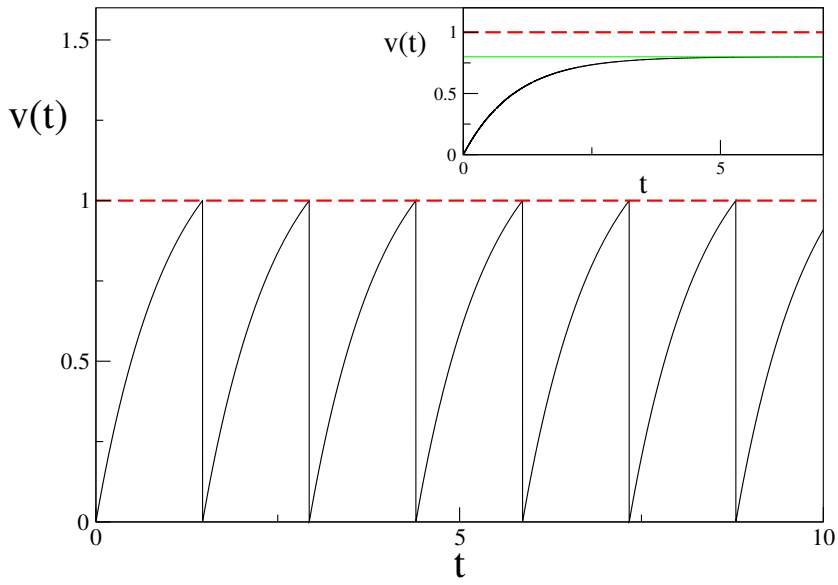

Figure 1.6: Dynamics of the membrane potential v. In the main picture we observe the spiking regime for $a = 1.3$. The dashed red line is the threshold value $v_{th} = 1$. In the inset we show the silent regime. In this case $a = 0.8$ (green continuous line).

with LIF neurons that will permit us a straightforward application of our approach and a clearer interpretation of the observed dynamics.

1.4 Neural coupling dynamics

Once investigated the dynamics of the single neuron and built up a model for the dynamics of the membrane potential in absence of stimuli from other neurons, it is necessary to take under consideration the coupling dynamics. From an experimental point of view this means to quantify the effect of the spike train of a neuron into the membrane potential of the receiving node. From a mathematical point of view this means to determine the function $\mathbf{G}(\mathbf{w})$ that, in the contest of LIF neural ensembles where $\mathbf{w} = v$, is a scalar function $G(v)$.

The electrical signal is transmitted from a neuron to the receiving neuron through a structure called synapse. Accordingly, neuron sending the spike is said presynaptic and the neuron receiving that information is said postsynaptic. There are two types of synapses: electrical and chemical [18]. In the firsts axon and dendrite come in contact and the elec-

trical signal passes directly from a neuron to the other [39]. Electrical synapses are pretty rare in nervous system which is mostly connected through chemical synapses. In chemical synapses, the axon does not come in contact with the dendrite and the region between these membranes is called synaptic cleft. When the cell body of the presynaptic neuron produces an action potential, it propagates pretty fast as a wave along the axon (around 25m/s, see [40] for details on the mechanisms of propagation). As soon as it arrives at the axon terminal it induces the opening of Calcium channels. The ratio between Ca^{2+} concentration inside and outside the cell is around 10^{-4} and this provokes a gradient of ions flowing inside the axon terminal. In the axon terminal are present vesicles that, whenever the calcium concentration increases around them, release molecules said neurotransmitter (or resources) [41]. These neurotransmitters bind to specific receptors in the membrane of the postsynaptic side of the synapse. This generates the opening of specific ionic channels that determine the postsynaptic current I_{syn} that rules the change in postsynaptic neural membrane potential, i.e. $\Delta v = I_{syn}\Delta t$ (notice that from now on all the variables and parameters are adimensional). In Fig. 1.7 we show a schematic description of this picture. There are different chemical type of

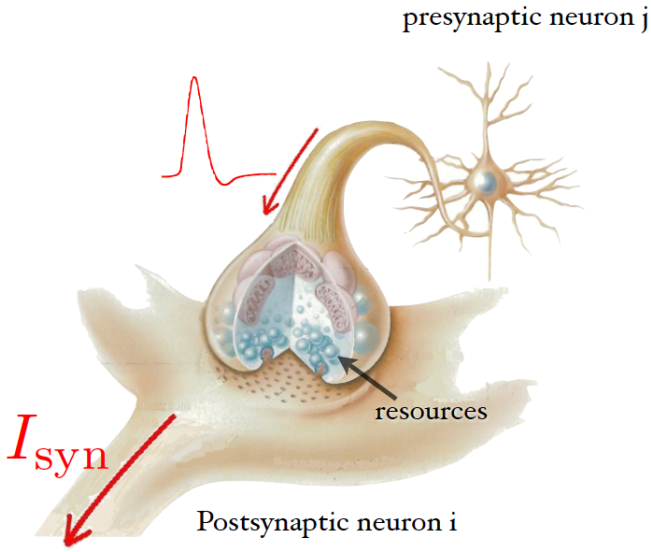

Figure 1.7: Chemical synapse's components [42].

neurotransmitter. One of the most famous is the amino acid **GABA**[43]. When this neurotransmitter is released, the current I_{syn} flowing in postsynaptic neuron is negative reducing postsynaptic neuron excitability. This

type of neurotransmitters are said inhibitory. On the contrary, glutamate is a neurotransmitter said excitatory as it generates a positive current I_{syn} in postsynaptic terminal. A neuron whose neurotransmitters are excitatory or inhibitory is said excitatory or inhibitory, respectively. In the rest of this thesis we use the term inhibitory or excitatory related to the neuron and not to the synapse, even if in some cases the same neuron produce either inhibitory or excitatory post–synaptic signal in the target cell. In general the percentage of inhibitory neurons is pretty low, around $10 - 30\%$ [44].

As the action potential has a stereotyped shape, the responsible of the intensity of postsynaptic current are the neurotransmitter properties. These properties are able to modify in time and change the efficiency of a synapse. Furthermore, it is possible that new synapses create thus changing the network structure. These mechanisms are called synaptic plasticity and they are generally thought to be responsible for memory and learning [45, 46]. There are two main forms of synaptic plasticity: long and short–term plasticity. They differ mainly for the time scales ruling the process. Furthermore, in short–term plasticity mechanism the synaptic efficiency depends only on the dynamics of pre–synaptic neuron, i.e. from its spike train, and does not affect the structure of connections, at variance with long–term forms of plasticity [47].

In this thesis we will take into account the short–term–plasticity mechanism. For this mechanism it has been built up a quite confident model that well reproduces the experimental observations. From the observation of the electrical activity of pairs of neocortical pyramidal neurons of the rat, in [48] it is reported a model for short–term–plasticity between excitatory neurons. It is based on the dynamics of synaptic resources (i.e. neurotransmitters) in function of presynaptic spike train. The resources can set in three different states. There is a fraction of available resources x, a fraction of active resources y and a fraction of inactive resources z. Their dynamics are described by the following dynamical equations for presynaptic neuron i

$$\dot{y}_i = -\frac{y_i}{\tau_{\text{in}}} + U x_i S_i \tag{1.10}$$

$$\dot{x}_i = \frac{z_i}{\tau_{\text{r}}} - U x_i S_i \tag{1.11}$$

$$\dot{z}_i = \frac{y_i}{\tau_{\text{in}}} - \frac{z_i}{\tau_{\text{r}}} \quad , \tag{1.12}$$

where $S_i(t) = \sum \delta(t - t_{n,i})$ is the spike train where each action potential is describer by a δ function that activates at the n–th action potential emitted

by neuron i, u is a parameter, τ_{in} and τ_{r} are said inactivation and recovery time, respectively. Notice that, by construction, the sum of all the fraction

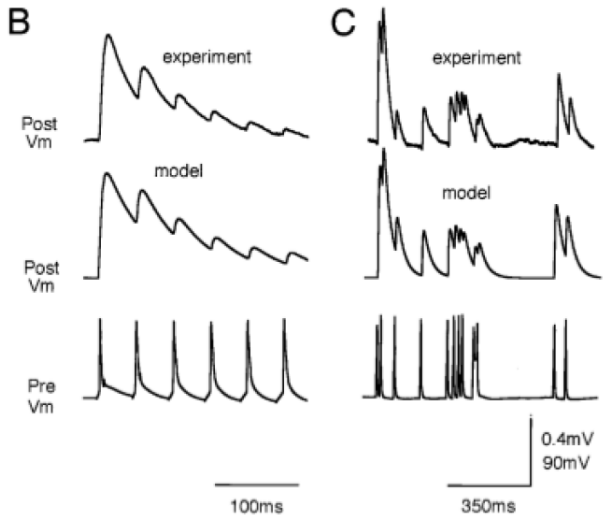

Figure 1.8: Comparison between experimental data and model for a couple of neurons. In B) it is reported the response to a regular activity of presynaptic neuron and in C) the case of non periodic activity [48].

of resources is equal to one, i.e. $x_i+y_i+z_i = 1$. Whenever a spike is emitted by neuron i a fraction U of the available resources x_i passes immediately from the available to the active state , i.e. $\Delta y_i = Ux_i$ and $\Delta x_i = -Ux_i$ (see the second term in Eq.s (1.10) and (1.11)). In between two consecutive spikes, the usage of the active resources y_i responsible for postsynaptic current $I_{syn,j}$ flowing in neuron j, causes their exponential inactivation with a time scale τ_{in}, in favor of an increase of inactive resources z_i of the same amount (see the first term in Eq.s (1.10) and (1.12)). In the meanwhile, the fraction of available resources recover exponentially, in a time scale τ_{r}, the fraction of inactive resources (see the first term of Eq. (1.11) and the second one of Eq. (1.12)). Accordingly, the postsynaptic current is proportional to the fraction of active resources y_i, i.e. $I_{syn,j} = Ay_i$. In Fig.1.8 it is reported the comparison between the model and experimental recordings where the accordance is quite good. The mechanism described by Eq.s (1.10)–(1.12) is called depressive. In fact, if the presynaptic neuron fires with high frequency, the synapse efficiency becomes negligible as there are no more available resources.

From the model above described, the dynamics of every node i in a

system of N purely excitatory neurons can be written as follows

$$\dot{v}_i = a - v_i + \frac{g}{N}\sum_j \epsilon_{ij} y_j \tag{1.13}$$

$$\dot{y}_i = -\frac{y_i}{\tau_{\rm in}} + U(1 - y_i - z_i)S_i \tag{1.14}$$

$$\dot{z}_i = \frac{y_i}{\tau_{\rm in}} - \frac{z_i}{\tau_{\rm r}}, \tag{1.15}$$

where we suppose that the proportional factor A between y and the post-synaptic current between neurons is the same for every couple.

In general, real systems are composed by a relatively small fraction if inhibitory neurons. Experimental observations show that between pyramidal excitatory neurons and inhibitory inter–neurons another mechanism in addition to the depressive one is present in synapses. This mechanism is called facilitation and can be introduced by increasing the synapses efficiency at every spike. In the language of Eq.s (1.10)–(1.12) this can be introduced by turning the parameter U in a dynamical variable $u(t)$. In particular, in its evolution equation for the presynaptic neuron i becomes the following [49]

$$\dot{u}_i = -\frac{u_i}{\tau_f} + U_f(1 - u_i)S_i, \tag{1.16}$$

where U_f is a parameter that determines the increase of u at the arrival of the spike and τ_f is the facilitation time constant that comes into play in between two consecutive spikes. These results have been merged in a model for the dynamics of a population of both excitatory and inhibitory neurons developed by Tsodyks, Uziel and Markram, named TUM model [5]. In this model the facilitation mechanism comes into play when the postsynaptic neuron is inhibitory. Furthermore, the recovery time scale $\tau_{\rm r}$ is different when postsynaptic neuron is inhibitory or excitatory. In particular, from phenomenological data, if postsynaptic neuron is inhibitory $\tau_{\rm r} = \tau_{\rm r}^I = 3.4$ and if postsynaptic neuron is excitatory $\tau_{\rm r} = \tau_{\rm r}^E = 26.6$ in rescaled units. Other parameter values are $\tau_{\rm in} = 0.2$, $U = 0.5$ for excitatory postsynaptic neuron, $U_f = 0.08$ and $g = 30$ [5]. Accordingly, when inhibitory neurons are taken under consideration, each synaptic variable

depends both from postsynaptic j and presynaptic neuron i

$$\dot{v}_i = a - v_i + \frac{g}{N}\sum_{j\neq i}\epsilon_{ij}y_{ij} \tag{1.17}$$

$$\dot{y}_{ij} = -\frac{y_{ij}}{\tau_{\text{in}}} + u_{ij}(1 - z_{ij} - y_{ij})S_j \tag{1.18}$$

$$\dot{z}_{ij} = \frac{y_{ij}}{\tau_{\text{in}}} - \frac{z_{ij}}{\tau_{\text{r}}^{ij}}. \tag{1.19}$$

If neuron i is excitatory $u_{ij} = U$ for every j, otherwise it is a function of time

$$\dot{u}_{ij} = -\frac{u_{ij}}{\tau_{\text{f}}} + U_f(1 - u_{ij})S_j. \tag{1.20}$$

Furthermore, $\tau_{\text{r}}^{ij} = \tau_{\text{r}}^{I}$ if i is inhibitory and $\tau_{\text{r}}^{ij} = \tau_{\text{r}}^{E}$ if i is excitatory, for every presynaptic neuron j.

In the rest of this thesis we will call TUM model the model for short–term plasticity in both purely excitatory or excitatory and inhibitory systems.

CHAPTER 2

Purely excitatory network: dynamics on random structures

In the previous chapter we have shown the possibility to build up models of neural ensembles. The experimental advances on the chemical processes responsible for neural activity lead to the formulation of many models of neural dynamics that differ for the microscopic mechanism taken under consideration. Accordingly, the diversity of microscopic models can produce different dynamical regimes characterized by different synchronization pattern [26, 50, 3, 4, 57]. The choice of the model has to be done as a function of what we are interested in investigating. In this thesis we are mainly interested in the relation between inhomogeneity among neurons, like the structure of connections, and the collective dynamics, i.e. global fields. For this purpose it is reasonable to suppose that the collective dynamics does not depend crucially on the detail of the model one takes under consideration. Furthermore, the heterogeneous mean field approach we are going to develop in this thesis is quite general and can be applied to different models. Accordingly, in order to show its implementation and analyze the collective dynamics emerging in these systems, we consider a quite simple model able to reproduce several dynamical regimes typically observed in experimental setups. In particular we consider random uncorrelated networks of LIF neurons equipped with the mechanism of short term plasticity (TUM model).

This chapter is divided in two man sections, depending on the emerging dynamical regime we are interested in analyzing. In Sec. 2.1 we show that the model considered shows collective oscillations ruled by inhomogeneity in network connections. Furthermore, the finite size dynamics is chaotic and the maximum Lyapunov exponent goes to zero in the thermodynamic limit. In Sec. 2.2 we introduce disorder and noise in neurons

excitability, a crucial ingredient to observe the dynamics characterized by bursts typically observed in in vitro neural cultures.

2.1 Collective oscillations of neurons in spiking regime

In this Section we investigate the dynamics of the deterministic model of Eq.s (1.13)–(1.15), where neurons have the same leakage current $a = 1.3$ (i.e. they are in periodic firing regime). Furthermore, following phenomenological data [5], we fix the ratio $\tau_{\rm r}/\tau_{\rm in} = 133$ and $g = 30$. We consider Erdös-Renyi dense random networks where the average connectivity scales as the system size N. In the first subsection we analyze the dynamics of finite size samples and in the second subsection we investigate the dependence on the size N and the stability properties of the dynamics.

2.1.1 Finite size dynamics

Given the complexity of the differential equations describing finite size systems the prevalent tool to investigate the dynamics of the network is a numerical simulation. A major advantage in this direction comes from the possibility of transforming the set of differential equations into an event–driven map [50, 51]. In fact, these differential equations can be formally integrated from time $t_{\rm n}$ to time $t_{\rm n+1}$, where $t_{\rm n}$ is the instant of time immediately after the n-th spike in the network. The resulting map for neuron i reads

$$\begin{aligned} z_i(n+1) &= z_i(n)e^{-\frac{\tau(n)}{\tau_{\rm r}}} \\ &\quad + \frac{\tau_{\rm r}}{\tau_{\rm r}-\tau_{\rm in}} y_i(n)\left(e^{-\frac{\tau(n)}{\tau_{\rm r}}} - e^{-\frac{\tau(n)}{\tau_{\rm in}}}\right) \end{aligned} \tag{2.1}$$

$$v_i(n+1) = v_i(n)e^{-\tau(n)} + a\left(1-e^{-\tau(n)}\right) + gF_i(n) \tag{2.2}$$

$$\begin{aligned} y_i(n+1) &= y_i(n)e^{-\frac{\tau(n)}{\tau_{\rm in}}} \\ &\quad + u\left[1 - \frac{\tau_{\rm r}}{\tau_{\rm r}-\tau_{\rm in}} y_i(n)\left(e^{-\frac{\tau(n)}{\tau_{\rm r}}} - \frac{\tau_{\rm in}e^{-\frac{\tau(n)}{\tau_{\rm in}}}}{\tau_{\rm r}}\right)\right. \\ &\quad \left. - z_i(n)e^{-\frac{\tau(n)}{\tau_{\rm r}}}\right]\delta_{i,s}, \end{aligned} \tag{2.3}$$

where $\tau(n) = t_{n+1} - t_n$ is the n-th inter–spike–interval (ISI) in the network and $F_i(n)$ has the following expression,

$$F_i(n) = \frac{\tau_{\text{in}}}{\tau_{\text{in}} - 1}\left(e^{-\frac{\tau(n)}{\tau_{\text{in}}}} - e^{-\tau(n)}\right)\frac{1}{N}\sum_{j\neq i}\epsilon_{ij}y_j(n), \tag{2.4}$$

with the sum running over the index j of all presynaptic neurons of neuron i. Notice that $\tau(n)$ can be determined by computing the time

$$\tau_i(n) = \ln\left[\frac{a - v_i(n)}{a + gF_i(n) - 1}\right],\ i = 1, \cdots N \tag{2.5}$$

needed by the ith neuron to reach the threshold value and thereby selecting the shortest one,

$$\tau(n) = \inf_i\{\tau_i(n)|i = 1, 2, \cdots, N\}.$$

Numerical simulations show that in the fully coupled case ($\epsilon_{ij} = 1, \forall i, j$), generic initial conditions always converge towards a synchronized regime with all neurons firing simultaneously [52]. This is a standard scenario that can be observed in many networks of identical fully coupled phase-oscillators. In particular, the same behavior is found in networks without plasticity, when the transmitted pulse has an infinitely fast rise time, like e.g. exponential or δ-pulses [53, 54]. Notice that the event–driven algorithm in Eqs. (2.1-2.3) has to be suitably modified in order to remove the ambiguities that emerge when the synchronous state is approached: because of the finite computer precision, the identification of the firing neuron may not yield a unique index. This problem can be straightforwardly overcome by reducing the dynamics of the synchronized neurons to that of a single one.

The stability of this regime, can be assessed by determining the evaporation exponent Λ [55], i.e. the convergence rate of a hypothetical single neuron that is subject to the mean field generated by the network.

By integrating the dynamical equations over one period τ, one obtains implicit equations that allow determining τ and the synaptic variables, $\tilde{y}$ and $\tilde{z}$, immediately after the firing event,

$$ae^{-\tau} = a + g\frac{\tau_{\text{in}}}{\tau_{\text{in}} - 1}\left(e^{-\frac{\tau}{\tau_{\text{in}}}} - e^{-\tau}\right)\tilde{y} - 1 \tag{2.6}$$

$$\tilde{y} = \tilde{y}e^{-\frac{\tau}{\tau_{\text{in}}}} + u(1 - \tilde{z} - \tilde{y}e^{-\frac{\tau}{\tau_{\text{in}}}}) \tag{2.7}$$

$$\tilde{z} = \tilde{z}e^{-\frac{\tau}{\tau_{\text{r}}}} + \frac{\tau_{\text{r}}}{\tau_{\text{r}} - \tau_{\text{in}}}\tilde{y}\left(e^{-\frac{\tau}{\tau_{\text{r}}}} - e^{-\frac{\tau}{\tau_{\text{in}}}}\right). \tag{2.8}$$

We now determine the evaporation exponent by estimating how the potential of a probe neuron, forced by the mean field generated by the network, converges towards the synchronized state. The membrane potential of each neuron follows the evolution equation

$$\dot{v}(t) = a - v(t) + gY(t). \tag{2.9}$$

For the probe neuron, the synaptic activity $Y(t)$ is to be considered as a periodic non-autonomous forcing. The stability analysis will be performed by following the evolution of the distance between the probe neuron and the synchronized cluster. Let us consider an initial condition, where the potential of the network neurons has just been reset ($v_j = 0$), while the probe neuron is lagging behind ($v(0) = 1 - \delta(0)$). The time s needed by the probe neuron to reach the threshold (i.e the temporal distance from the synchronized cluster) is implicitly given by the condition

$$(1-\delta(0))e^{-s} + a(1-e^{-s}) + \frac{g\tau_{\text{in}}}{\tau_{\text{in}}-1}\left(e^{-\frac{s}{\tau_{\text{in}}}} - e^{-s}\right)\tilde{y} = 1\,. \tag{2.10}$$

Over the time s, the potential of the network neurons increases from 0 to

$$\begin{aligned}\delta(s) &= a(1-e^{-s}) + g\frac{\tau_{\text{in}}}{\tau_{\text{in}}-1}\left(e^{-\frac{s}{\tau_{\text{in}}}} - e^{-s}\right)\tilde{y} \\ &= 1 - (1-\delta(0))e^{-s},\end{aligned} \tag{2.11}$$

which represents the distance when the probe-neuron potential has been reset, as well. From Eq. (2.9) it then follows that the later evolution follows the equation

$$\dot{\delta} = -\delta \tag{2.12}$$

so that

$$\delta(\tau) = \delta(s)e^{s-\tau}. \tag{2.13}$$

and the evaporation exponent is

$$\Lambda = \lim_{\delta(0)\to 0}\frac{\delta(\tau)}{\delta(0)} = \ln\left[\frac{a+g\tilde{y}}{a+g\tilde{y}-1}\right] - \tau\,. \tag{2.14}$$

By obtaining τ and $\tilde{y}$ from Eqs. (2.6)–(2.8) one can estimate Λ. The dependence of the evaporation exponent on τ_{in} is plotted in Fig. 2.1 (see the lower curve). The exponent Λ is always negative, meaning that the probe neuron will attach back to the cluster firing simultaneously with the rest of the neurons (i.e. the synchronous state is locally stable). If one started

assuming that the single neuron is ahead of the cluster, a different exponent would be obtained (see the upper curve in Fig. 2.1). The behaviour for small τ_{in} is somehow surprising since, by looking at Eq.s (2.2) and (2.4) the effect of the coupling tends to vanish for $\tau_{\text{in}} \to 0$. In order to clarify this point, we perform a perturbative analysis. From Eqs. (2.6,2.11,2.13), under the assumption of τ_{in} and $\delta(0)$ small, one finds

$$\delta(\tau) = \frac{a-1}{a}(\delta(0) + s) \tag{2.15}$$

At the same time, Eq. (2.10) reduces to

$$s(a-1) + a\tilde{y}\tau_{\text{in}}\left(1 - e^{-s/\tau_{\text{in}}}\right) = \delta(0) \tag{2.16}$$

If $s \ll \tau_{\text{in}}$, we are in the regime of infinitesimal perturbations; the exponential in the above equation can be expanded, giving rise to

$$s = \frac{\delta(0)}{a - 1 + g\tilde{y}} \tag{2.17}$$

By then replacing in Eq. (2.15) one finally obtains

$$\frac{\delta(\tau)}{\delta(0)} = \frac{(a-1)(a+g\tilde{y})}{a(a-1+g\tilde{y})} \tag{2.18}$$

The logarithm of the r.h.s. is just the evaporation exponent for $\tau_{in} = 0$. If, instead, $\tau_{\text{in}} \ll s$, the exponential in Eq. (2.16) can be neglected, giving rise to

$$s = \frac{\delta(0) - g\tilde{y}\tau_{\text{in}}}{a-1} \tag{2.19}$$

Again with the help of Eq. (2.15) one obtains

$$\delta(\tau) = \delta(0) - \frac{g}{a}\tilde{y}\tau_{\text{in}} \tag{2.20}$$

Equations (2.18,2.20) tell us that whenever the time separation s between the probe neuron and the cluster is larger than the decay time τ_{in} the physical distance decreases linearly in time with a coefficient that becomes increasingly small with τ_{in}. However, as soon as the distance becomes on the order of τ_{in}, an exponential convergence sets in that is ruled by an exponent that remains finite even for arbitrarily small τ_{in} values.

This analysis reveals a rather awkward property, namely that the solution is stable against negative perturbations and unstable otherwise (see

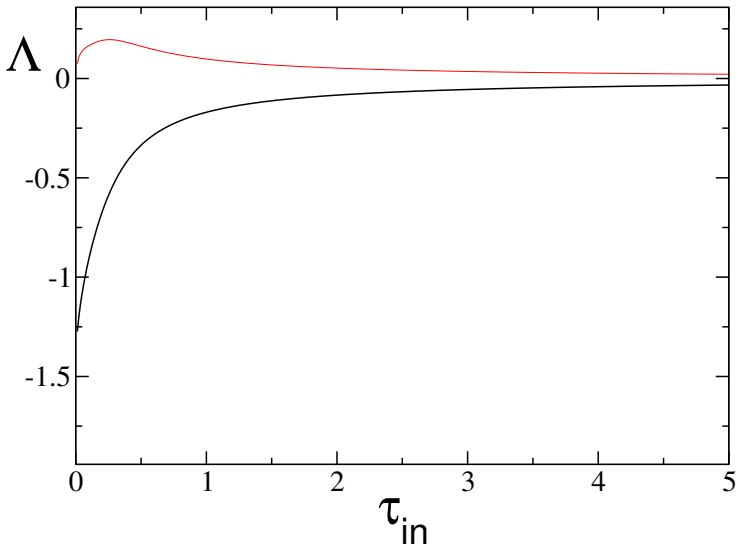

Figure 2.1: Evaporation exponents Λ as a function of $\tau_{\rm in}$: the lower (black) curve and the upper (red) curve refer resp. to the left (see Eq. (2.14)) and right exponent. We have used the following rescaled parameters: $g = 21$, $u = 0.5$ $a = 1.3$ and $\tau_{\rm r} = 133\tau_{\rm in}$. [52]

the left and right exponent in Fig. 2.1). This is because the periodic solution selected by the network belongs to a homoclinic cycle that is obtained from the collapse of a stable with an unstable solution. This property was already proved in Ref. [56] with reference to the TUS model in the absence of synaptic plasticity. In this case, one can apply the same mathematical formalism, since the synchronized regime is characterized by a sequence of exponential pulses. In the case of a fully coupled network, the asymmetric stability of the synchronous regime has no relevant consequences, since the neurons that possibly escape while being ahead of the cluster, are eventually attracted when they approach the cluster from the opposite side. We will see that this property has instead relevant consequences as soon as disorder is added to the network.

A second remarkable property is that the synchronized state is stable for all parameter values and Λ remains finite even in the limit $\tau_{\rm in} \to 0$, when the coupling vanishes. In fact, when the synaptic time scales $\tau_{\rm in}$ and $\tau_{\rm r}$ are significantly smaller than the typical ISI, the active transmitter variable, $y_i(t)$, exhibits a short pulse (of finite height and duration $\tau_{\rm in}$) so that the membrane potential of all connected neurons increases by an

amount

$$\Delta v_i(n) = g\tau_{\text{in}} e^{-\tau(n)} \frac{u}{N}.$$

which evidently vanishes for $\tau_{\text{in}} \to 0$. Nevertheless, the synchronized state is characterized by a finite stability, because it is surrounded by a tiny basin of attraction (of size τ_{in}). As a result, this model does not reduce, for $\tau_{\text{in}} \to 0$ to a standard LIF network with δ pulses [57] and the stability of the synchronized state differs by a finite amount.

The stability of the synchronous state in homogeneous globally coupled network seems to depend strongly on the smoothness of the receiving field $F_i(t)$ (i.e. on the dynamics of $y_j(t)$). In different models, like the α model [58] in absence of plasticity, the field $F_i(t)$ is not discontinuous at the spiking time. Accordingly, also in globally coupled network the synchronous state loses its stability and a partial synchronous state arises [59]. Every neuron is quasi–periodic characterized by the same two frequencies but their electrical activity interfere constructively giving rise to non trivial collective oscillations [60].

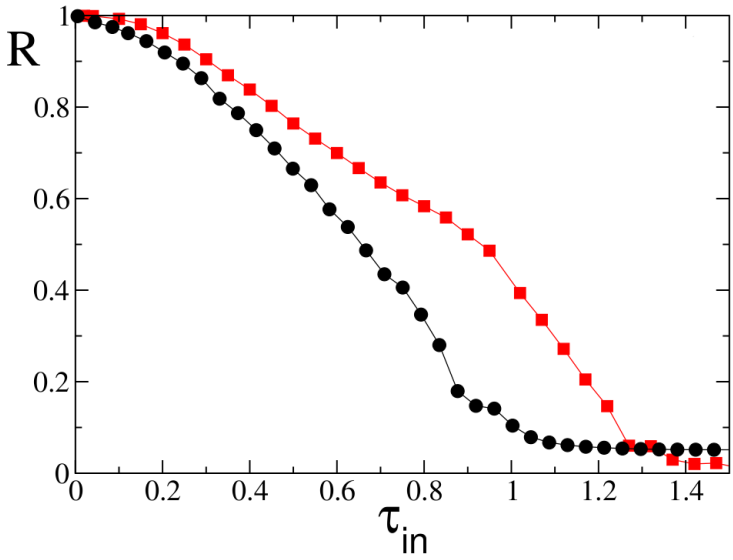

Figure 2.2: The Kuramoto order parameter R as a function of τ_{in} for a diluted network of $N = 500$, (black) circles, and $N = 5,000$, (red) squares. The values of R have been obtained by averaging over a time span of $4{\cdot}10^4$ time units, after discarding a transient of $N \cdot 10^3$ iterations of the map [52].

The introduction of inhomogeneity in network structure gives rise to a partial synchronous regime. We consider an Erdös-Renyi (ER) network

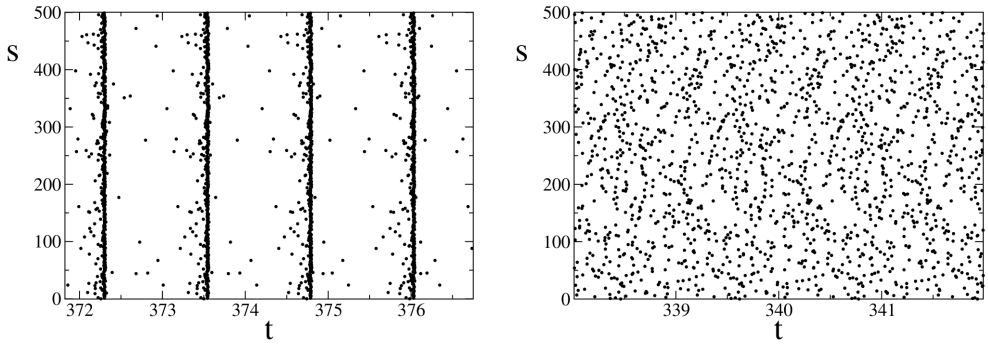

Figure 2.3: In left and right panel we report the firing patterns for resp. $\tau_{\rm in} = 0.2, 1.2$: s is the index of the neuron firing at time t and the ordering is fixed according to the randomly–seeded initial condition [52].

where the average connectivity, $\langle k \rangle = p \times N$, is an extensive quantity. It is instructive to characterize the network dynamics by monitoring the Kuramoto parameter [61],

$$R = \left\langle \left| \frac{1}{N} \sum_i e^{i\theta_i} \right| \right\rangle \tag{2.21}$$

$$\theta_i(t) = 2\pi \frac{t - t_i(m)}{t_i(m+1) - t_i(m)}, \tag{2.22}$$

where $\langle \cdot \rangle$ denotes a time average, $t_i(m)$ the m–th spike emitted by neuron i and $\theta_i(t)$ is the phase of neuron i at time $t \in [t_i(m), t_i(m+1)]$. The phase $\theta_i(t)$ is useful in order to characterize synchronization between the spiking times of neurons. In fact, if all neurons fire simultaneously, $\theta_i(t)$ rotate in phase and $R = 1$. On the contrary, if the spiking of neurons is uncorrelated, $\theta_i(t)$ are uniformly distributed in $[0, 2\pi]$ and $R = 0$. In Fig. 2.2 we plot the Kuramoto parameter R versus the decay time $\tau_{\rm in}$ for a network with 500 neurons (see the lower curve). For $\tau_{\rm in} \to 0$, the evolution is perfectly synchronous ($R = 1$), but upon increasing $\tau_{\rm in}$, the degree of synchrony is progressively lost until an almost asynchronous regime sets in (for $\tau_{\rm in} >\approx 1$). The raster plots obtained for different parameter values reported in Fig. 2.3 help to visualize the underlying dynamics. In particular, synchrony manifests itself as sharp quasi–synchronous–event (QSE) for $\tau_{\rm in} = 0.2$, which spread in time when $\tau_{\rm in}$ is increased, and eventually disappear for $\tau_{\rm in} \sim 1.2$. Let us fix our attention on the partially synchronized phase (i.e. $\tau_{\rm in} = 0.2$) where collective oscillations of global fields arise. In Fig. 2.4 we plot the global attractor of the system, by plot-

ting each pair ($Y(t)$,$Z(t)$). We observe that, apart from fluctuations due

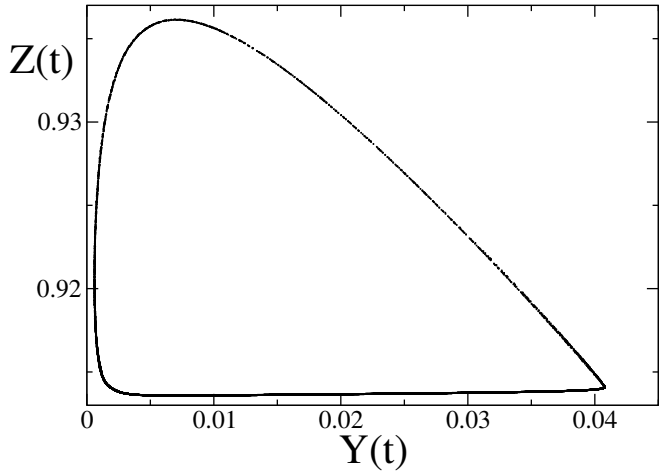

Figure 2.4: Global attractor of the QSE dynamical phase represented by the average synaptic fields $Y(t)$ and $Z(t)$ for $N = 10^4$ and $\tau_{\text{in}} = 0.2$. Data are reported after discarding a transient of $N \cdot 10^3$ iterations of the map [52].

to finite size effects, the collective dynamics is periodic. An interesting point to be addressed is the microscopic organization giving rise to such a collective activity. At variance with the globally coupled model the heterogeneity of the network produces a profund difference in the dynamics of different neurons. In fact, we observe that neurons can be divided in two families, depending on their dynamics. The first family shows, apart from finite size fluctuations, a periodic dynamics and its components are called *locked* neurons. The second one shows a quasi periodic dynamics characterized by two frequencies and its components are called *unlocked* neurons. In order to characterize the dynamics of neuron i we use the time interval between two consecutive spikes m and $m+1$, namely the inter–spike interval of neuron i $ISI_i(m) = t_i(m+1) - t_i(m)$. In Fig. 2.5 we report the microscopic attractor for two neurons belonging to two different families by plotting $ISI(m+1)$ vs $ISI(m)$ for the considered neurons. We observe that the locked neuron fires periodically with always the same ISI while the unlocked one spend sometimes firing with the same frequency of the locked neurons and then anticipates its firing until it turns back firing with the same frequency of locked neurons. This microscopic scenario is present in all locked and unlocked neurons, in the sense that the microscopic attractor for locked neurons is the same, as well as for unlocked neurons. What one observes by following the dynamics of neurons in time is that locked neurons not only fire with the same fre-

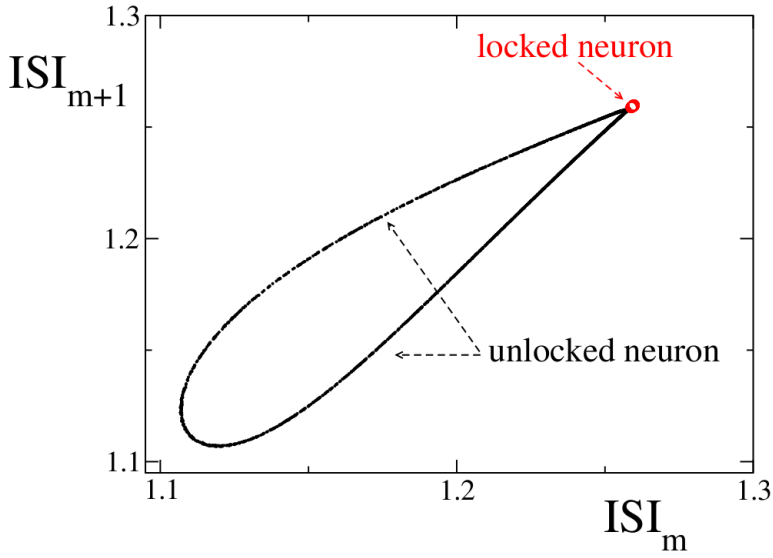

Figure 2.5: ISI return map for a locked neuron, (red) open circles, and an unlocked neuron, (black) dots (data have been collected in the same simulation of Fig.2.4) [52].

quency but also their phases θ_i are locked in phase, i.e. they fire almost simultaneously with a small delay fixed in time. This is the reason why they are called locked. Furthermore, they always take part to the quasi synchronous event (see the raster plot in the left panel of Fig. 2.3) and make the greatest contribution to the Kuramoto parameter R. Unlocked neurons do not fire periodically and typically fire in between two quasi synchronous events. After firing in the QSE they anticipate their firing with respect to locked neurons and then turn back to take part in the cluster. While locked neurons share the same periodicity of the global field $Y(t)$, unlocked neurons tend to have different average firing frequency. Nevertheless, unlocked neurons play a crucial role as they produce a collective field that contributes to $Y(t)$ in such a way to sustain the overall dynamics.

As a result, this model shows how collective oscillations are non trivial and arise as a complex organization of microscopic dynamics. For the sake of completeness let us remark that non trivial collective oscillations are typically observed in coupled oscillators or neurons models on extended systems [26, 62] evidencing the robustness of this qualitative scenario with respect to the detail of the model considered. As in the model here reported this characteristic emerges with the introduction of topological disorder, in the next chapter it will be shown how a heteroge-

neous mean field approach permits to perform a stability analysis clarifying what is the topological ingredient acting as a bifurcation parameter to generate this difference in single neurons dynamics.

2.1.2 Size scaling behavior and chaoticity

The dynamics presented in previous section is strongly dependent on structural disorder. This is pretty clear from the observation that in globally coupled network all neurons are synchronized, independently from the parameter's values of the model, while the introduction of disorder gives rise to a complex organization of single units yielding partial synchronous or asynchronous regimes. The Erdös-Renyi model for network construction gives the possibility to investigate the size effect in the model, i.e. the dynamics at increasing values of N. In Fig. 2.6 we plot the number of unlocked neurons in the network N_u in function of N, for fixed dilution $p = 0.7$. We observe that the fraction of unlocked neurons, namely N_u/N,

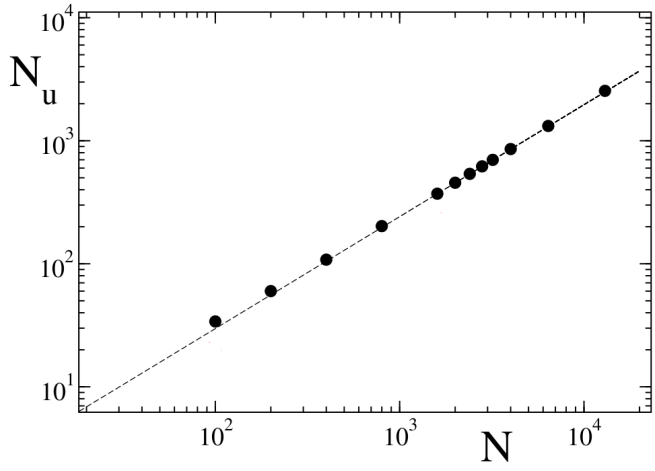

Figure 2.6: Number of *unlocked* neurons N_{u} as a function of the size N. The (black) dashed line is a power law fit with exponent $\eta = 0.90 \pm 0.01$. The measures have been averaged over 5 different realizations of the disorder (the corresponding error bars are smaller than the symbols) [52].

goes to zero increasing N. This means that the dynamics at increasing N is different, e.g. the collective field $Y(t)$, as the Kuramoto parameter R, takes different quantitative values. This is a direct consequence of how one constructs the succession of graphs at increasing N. In the next chapter we will show how it is possible to construct networks at different sizes N sharing the same dynamics, also from a quantitative point of view.

Another issue to be addressed in this framework is the stability of the network dynamics. This can be done by computing the Lyapunov exponents of the network in partially synchronous regime by using the standard algorithm by Benettin et al. [63]. In Fig. 2.7a we show the spectrum of the Lyapunov exponents in a network of $N = 50$ neurons and for the phenomenological value $\tau_{\rm in} = 0.2$. There exists a small positive component as it can be appreciated from the inset, which reveals the chaotic nature of the dynamics. More precisely, the Kaplan–Yorke dimension [64] is approximately equal to 12, i.e. we are facing a very thin attractor embedded into a configuration space of much higher dimension. The chaotic

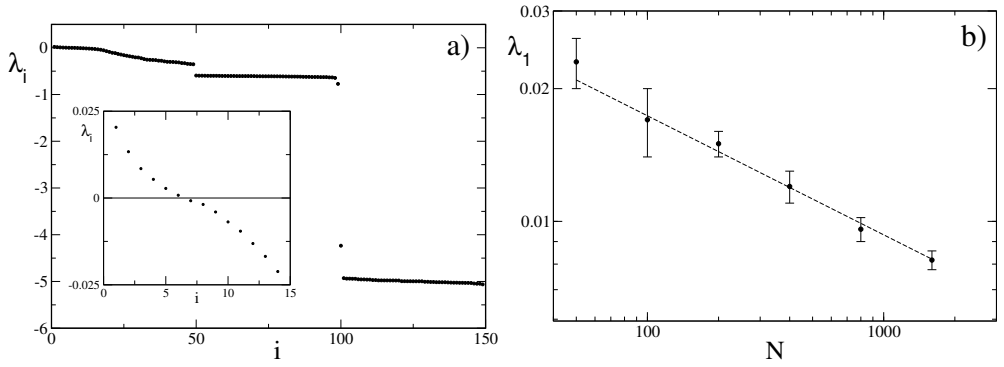

Figure 2.7: a) The spectrum of Lyapunov exponents for a diluted network of size $N = 50$. In the inset we report a zoom of the spectrum to show the presence of six positive exponents. In b) it is shown the maximum Lyapunov exponent λ_1 as a function of the number of neurons N: the measures of λ_1 have been averaged over 10 different realizations of the network (the error bars refer to the maximum deviation from the average). A power-law fit is reported (dashed line) with decay exponent $\delta = 0.27 \pm 0.01$. In both cases we have considered $\tau_{\rm in} = 0.2$ [52].

nature of the evolution is not at all surprising, given the nonlinear character of the model. On the other hand, in the thermodynamic limit, one expect chaos to disappear. In fact, as shown in Fig. 2.7b, the maximum Lyapunov exponent λ_1 vanishes in the limit $N \to \infty$. This is consistent with previous studies in the absence of synaptic plasticity (see, e.g. [50]), although the convergence is here significantly slower, $\lambda_1 \propto N^{-\delta}$ with $\delta = 0.27 \pm 0.01$, instead of $\delta = 1/2$, as expected on the basis of simple statistical arguments. This effect, again, is due to the way one constructs the network. In fact, increasing N, not only statistical fluctuations vanish as $1/\sqrt{N}$ but also the dynamics itself changes qualitatively (e.g. the number of unlocked neurons increase) yielding different Lyapunov exponents. In [52] it is reported an argument to explain the unusual exponent δ com-

bining the scaling of unlocked neurons and of statistical fluctuations. In the next Chapter we will explain better this point. In particular, it will be shown how the usual statistical scaling is recovered when one constructs networks in such a way to conserve the dynamics from a qualitative and a quantitative point of view (apart from statistical fluctuations).

2.2 Bursting behavior in networks with neurons in silent regime

Collective oscillations arise in many in vivo experiments and a quite simple model as that taken here under consideration is able to reproduce such a collective phenomena. Nevertheless, as discussed in Sec 1.1, different regimes can arise, usually in in vitro conditions. These regimes are characterized by quite long periods (1 to 100 seconds) where a small fraction of all neurons emits uncorrelated spikes. These periods are separated by bursting events lasting around 100–200 ms where almost all neurons emit more then one spike, called population bursts (PB). The time interval between two consecutive PB, called inter PB interval (IPBI), is not regular and follows a long tail statistics [2, 65, 66]. In order to have a quantitative comparison one can observe that, given the phenomenological value $\tau_m = 30$ms, the time interval between two consecutive QSE is around 30/50 ms. Furthermore, there are also qualitative differences. First, PB are separated by non regular time intervals (i.e. the global field $Y(t)$ is not periodic) and secondly in the PB all neurons fire more then once, at variance with QSE that are guided by locked neurons firing just once for every event. This scenario remains the same also changing the time scales of synaptic plasticity or the coupling g. In fact, as neurons are in a firing regime ($a = 1.3$) and being the network fully excitatory (i.e. synaptic coupling get the potential v closer to the spiking threshold), the maximum time interval between two consecutive spikes of a neuron is $\tau_m \ln(a/(a-1)) \sim 44$ms. As a result, topological disorder is not enough to reproduce this scenario that seems to be due to different model characteristics. Accordingly, fixing the topology to be a Erdös-Renyi network with dilution $p = 0.7$, in order to obtain a scenario similar from a qualitative and a quantitative point of view to in vitro observations one has to change the excitability of neurons. Nevertheless, by getting a near to 1 the dynamics is qualitatively the same of the QSE one with collective oscillations, even if the time lapse in between two QSE can increase [69]. In order to observe a qualitative change in the dynamics we need to work with neurons in silent regime, i.e. $a < 1$. Nevertheless, if all neurons are

in silent regime the network does not show spontaneous activity [69]. Accordingly, one can suppose that every neuron i receives external current $a_i(t)$ not constant in time. In particular, let us consider i.i.d. stochastic variables, that evolve in time according to a random walk between fixed boundaries, $a_{\min}$ and $a_{\max}$, so that the average external current is defined as $\bar{a} = (a_{\max} + a_{\min})/2$. At each step of the random walk the values of $a_i(t)$ are independently updated by adding or subtracting with equal probability a fixed increment Δa. Whenever the value of $a_i(t)$ crosses one of the two boundaries, it is reset to the same boundary value. The introduction of this stochastic component prevents the possibility to use the event driven algorithm to simulate the dynamics. As a result, we integrate the dynamics at steps. The value of the integration time step has been set $\Delta t = 9 \cdot 10^{-4}$ expressed in the adimensional time unit (in physical units $\Delta t = 2.7 \cdot 10^{-5}$s). The choice of this value of Δt guarantees a sufficient time sampling of dynamics over the range of parameter values explored in this paper. Moreover, in numerical simulations we have assumed that each step of the random walk occurs at each integration time step of the dynamics. The results hereafter reported have been obtained by fixing $a_{\max} - a_{\min} = 0.1001$, so that the parameter space can be explored by varying the parameters Δa and $\bar{a}$ only. These parameters play a crucial role for the emerging dynamics. In fact, Δa determines the time correlation of noise and $\bar{a}$ the average excitability of neurons. In Fig. 2.8 we plot the autocorrelation function defined by

$$f(\tau) = \frac{\langle a(t+\tau)a(t)\rangle - \langle a(t)\rangle^2}{\sigma^2} \quad , \tag{2.23}$$

where $\langle \dots \rangle$ represents an average over time and realizations and $\sigma^2 = \langle (a(t) - \langle a(t)\rangle)^2\rangle$ is the variance. Accordingly, we can change Δa to obtain the desired correlation time τ_c. As reported in [69], the role of $\bar{a}$ is essentially that of moving the dynamics from a QSE regime where the global field shows collective oscillations to a PB regime where QSE turn into PB and the time lapse in between two consecutive PB is not regular anymore. When $\bar{a}$ is bigger then the critical value $a_c = 1$ one observes QSE separated by almost regular time intervals. For $\bar{a}$ sufficiently below a_c we observe two main qualitative changes in the dynamics. First, incoherent neural activity extends over much longer time lapses and follows a long tail statistics. Secondly, the QSE turn into PB lasting around 200 ms. The correlation time τ_c determines the shape of the tail in the probability distribution of the inter–PB–interval (IPBI). As shown in [69], if τ_c is smaller then the typical values of $IPBI$ the tail has an exponential shape.

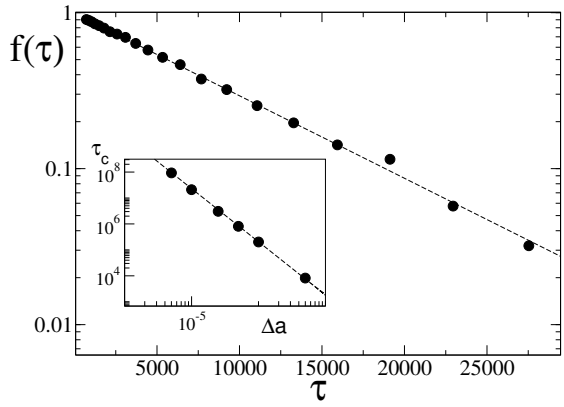

Figure 2.8: Log-lin plot of the time autocorrelation function $f(\tau)$ for $a_{\max} = 1.0001$, $a_{\min} = 0.9000$. The time variable τ is expressed in units of the random walk step. The dashed line is the fit with the function $\exp(-\tau/\tau_c)$, with $\tau_c = (0.081 \pm 0.004)10^5$ (in physical units $\tau_c = (0.22 \pm 0.01)$s). The dependence in log-log sale of τ_c on Δa (for the same values of $a_{\max}$ and $a_{\min}$) is shown in the inset: the dashed line is obtained by a fit with the power–law $\tau_c = A_0 \Delta a^{-\gamma}$, where $\gamma = 2.05 \pm 0.01$ and $A_0 = (1.296 \pm 0.004)10^{-3}$ (in physical units $A_0 = (3.50 \pm 0.01)10^{-8}$s). Data here reported have been obtained averaging over 10^3 realizations and 10^3 time lapses (see Eq. 2.23) [69].

Increasing τ_c over the typical values of IPBI the tail turns to have a power law behavior, that is generally detected in experiments [2]. In Fig. 2.10 we report the raster plot and the IPBI probability distribution that shows a power law behavior.

As previously remarked, PB last around 200 ms. At variance with dynamical scenario characterized by up–down states, their duration is stereotyped and can be controlled by a suitable choice of the synaptic time scale τ_{in}, that in these simulations case amounts to 18 ms. Moreover, the average available synaptic resources (see the green curve in Fig. 2.10) are recovered over the much longer time scale, in our case $\tau_r = 2.4$ s, so that in the meanwhile new firing neurons are no more able to produce an avalanche. Before a new avalanche may occur one has to wait a time lapse of the order of τ_r and this is the reason why one can observe the cutoff close to 1s in the IPBI statistics in Fig. 2.10.

Let us remark that, as conjectured by many authors (e.g. see [67, 68]), typical features of neural activity can be reproduced with a model near to critical conditions or to some bifurcation point for parameters. This situation is in accordance with the present scenario. In particular, power law distributions of the sporadic unsynchronized neural activity observed

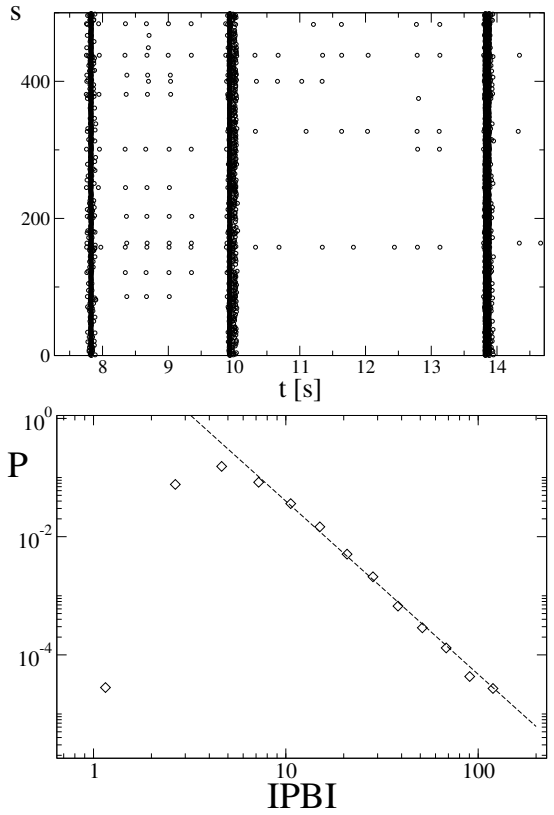

Figure 2.9: Dynamics of a network of $N = 500$ excitatory LIF neurons with $\bar{a} = 0.95005$ and $\Delta a = 6 \cdot 10^{-6}$ (correlated noise, $\tau_c \sim 1700$s) The synaptic parameter values are $u = 0.5$, $g = 7$, $\tau_{\rm in} = 0.6$ and $\tau_{\rm r} = 80$. In the upper panel it is reported the raster plot. In the lower panel it is shown the probability density functions P of IPBI of a network. Data is plotted by a suitable exponential binning of the support of the variables. The solid lines are power–law fits, with exponent $\alpha = -2.93 \pm 0.05$ for IPBI. Data have been obtained with a statistics of $5 \cdot 10^4$ events [69].

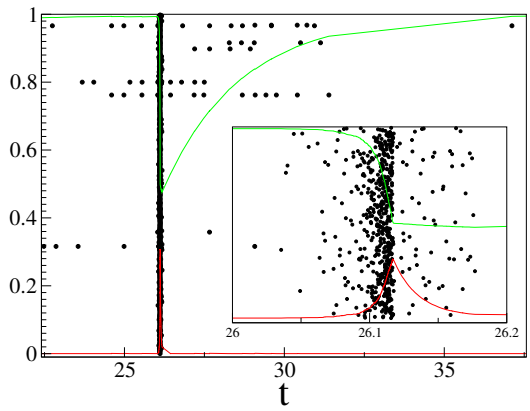

Figure 2.10: Dynamics of a network of $N = 500$ excitatory LIF neurons in the presence of plasticity with $\bar{a} = 0.95005$ and $\Delta a = 6 \cdot 10^{-6}$ (correlated noise): the rescaled neuron index k/N is reported as a function of time t (in seconds). The evolution of the average synaptic fields $Y_i(t)$ and $X_i(t)$ are also reported (red and green curves, respectively). In the inset we show a zoom of a PB event. The synaptic parameter values are $u = 0.5$, $g = 7$, $\tau_{\rm in} = 0.6$ and $\tau_{\rm r} = 80$. [69]

in experiments (e.g. see [2]) can be recovered by choosing sufficiently correlated noise for values of a just below, but sufficiently close to the critical value $a_c = 1$.

The PB dynamical phase here reported can be reproduced also in absence of topological disorder and noise. In particular, by considering a globally coupled network and a disorder in leakage currents of neurons a_i (notice that these variables do not depend on time anymore), one can obtain the PB dynamical regime. Consistently for the results reported in presence of noise, one has to extract the a_i's from a distribution $P(a)$ extending to values a lower then the critical value $a_c = 1$. In Fig. 2.11 we repoprt the the statistics of $IPBI$ and in the inset the dynamics of the global field $Y(t)$ for a uniform distribution $P(a)$ in the interval $[0.9005, 1.006]$. The difference with respect to the correlated noise case is that the IPBI distribution turns back to be an exponential instead of a power law.

In conclusion, the model here used is able to reproduce a wide variety of observed behaviors by equipping the model of the disorder component suitable for certain dynamical phases. Nevertheless, given the complexity of dynamical equations, the dynamics at finite size N is difficult to be addressed if not with numerical simulations. In the next chapter we show how one can analyze finite size dynamics by a mean field approach in the case of spiking excitatory neurons in random network.

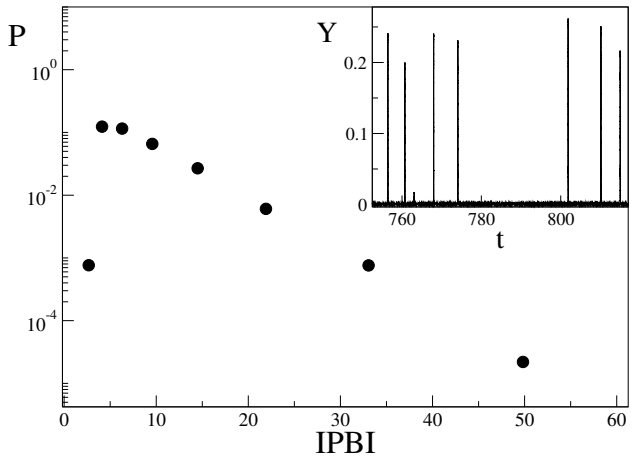

Figure 2.11: Dynamics of a globally coupled network of $N = 500$ excitatory LIF neurons, where the currents a have been extracted from a uniform distribution $P(a)$ in the interval $[0.9005, 1.006]$. The synaptic parameter values are $u = 0.5$, $g = 1.2$, $\tau_{\text{in}} = 0.6$ and $\tau_{\text{r}} = 80$. We report the probability density functions P of IPBI of the network in log–lin scale. Data is plotted by a suitable exponential binning of the support of the variables and have been obtained with a statistics of $5 \cdot 10^4$ events. In the inset we plot the time evolution of the global field $Y(t)$.

CHAPTER 3

Heterogeneous mean field and global inverse problem for random networks of excitatory neurons

In previous chapters we have seen how a minimal biologically inspired model of neural ensembles is able to reproduce some observed features of neural dynamics detected in experiments. The model analysis has been performed through numerical simulations of finite size samples as the complexity of equations does not allow for a straightforward analytical treatment (apart from the case of homogeneous system, i.e. all–to–all structure). Accordingly, in this chapter we describe how one can take a step forward for the comprehension of the dynamics of the model, by manipulating the differential equations of the system.

The starting point is the observation that real neural networks (e.g. those producing the fields one usually measures in laboratories) are made up by a finite number of elements. Thus, the main point addressed in this chapter is the way one can analyze the dynamics of a finite sample of neurons. The method hereafter reported is based on a mean field approximation and is quite general, making it applicable to a wide range of dynamical models on extended structures. Accordingly, we show its implementation in a simple case of excitatory network in spiking regime, where disorder is present only on network structure. Nevertheless, this simple setup has the advantage to reproduce non trivial synchronization patterns with the emergence of oscillations in global fields.

The mean field model we will obtain permits a deeper understanding of the role of the network structure and how it drives the system to the partially synchronous self organized dynamics presented in previous chapter. Furthermore it gives the possibility to formulate and solve a global inverse problem. Starting from the dynamical signal of the average synaptic-activity

field, the method provides with good accuracy the in–degree distribution $P(\tilde{k})$ (see Sec. 1.2) of the finite size network that produced it. This chapter is structured as follows. In Sec. 3.1 it will be shown how it is possible to perform a mean field approach in this system and under which assumption. In Sec. 3.2 we will analyze the resulting mean field model in order to investigate the direct problem, that is the influence of the network structure for the dynamics of neurons. Finally, in Sec.3.4 we will show how one can formulate and solve the global inverse problem in different network structures.

3.1 Thermodynamic limit and mean field approximation

In this section we discuss how to describe the finite finite size dynamics of the model discussed in Sec.2.1 through a mean field approximation. First of all, let us point out the reference system we want to address with this analysis. Let us consider a finite size sample made of N neurons connected through a random uncorrelated network (see Sec. 1.2). Given a single sample, i.e. let us imagine a real group of neurons, one can define the distribution of specific in degrees $P(\tilde{k})$ as the envelope of the histogram ideally obtained from the finite size sample with adjacency matrix of elements ϵ_{ij}. The dynamics of the model can then be obtained by integrating the equations (1.13)–(1.15).

A possible way to investigate the dynamics is to perform the thermodynamic limit that is expected to provide the basic ingredients for an analytic treatment. This approach involves the construction of ideal networks at increasing size with respect to the reference system one we want to investigate. Nevertheless, the way such a construction is performed may wipe out any relation with the topological features that are responsible of the observed relevant dynamical properties. Accordingly, the construction needs to be done in such way that the dynamics of the network at every sufficiently large size N maintains the same features. As shown in Sec.2.2 the Erdős–Rényi way to construct network at different size N with fixed dilution p does not have this propriety. In fact, the fraction of unlocked neurons changes increasing N and the dynamics in the thermodynamic limit is completely synchronous. Accordingly, this procedure does not keep track of the ingredient responsible for the emergent dynamics. The dynamics observed in finite size samples is the resultant of a mixture of locked and unlocked neurons. As a consequence, this separation (i.e. the relative fraction of locked and unlocked neurons) needs to remain unchanged in order to observe the same dynamical behavior.

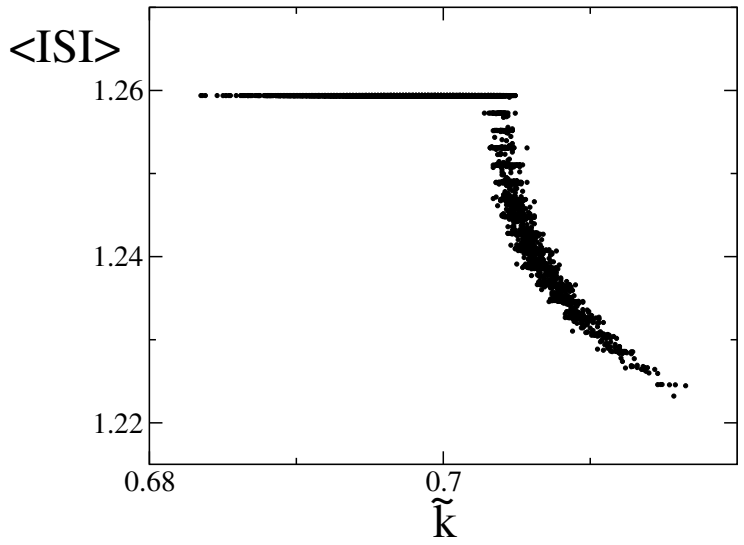

Figure 3.1: Average inter spike interval (ISI) of neurons in function of specific connectivity $\tilde{k} = k/N$ for a Erdős–Rényi network of $N = 10^4$ neurons with dilution $p = 0.7$. Averages have been obtained by sampling 10^4 firing events for each neuron, after discarding a transient of $N \cdot 10^4$ iterations of the map [52].

In Fig. 3.1 it is reported the average ISI of neurons in function of their rescaled connectivity $\tilde{k} = k/N$ for a Erdős–Rényi network of $N = 10^4$ neurons with dilution $p = 0.7$. We observe a plateau at low connectivity of neurons sharing the same spiking frequency. These neurons are the locked neurons taking part at the QSE. The other neurons, with higher connectivity values, have higher spiking frequency and are the non–periodic unlocked neurons (see Fig.2.5).

From this picture it is quite clear that a crucial role for the microscopic organization of neurons (and as a consequence for the dynamics of the system) is the disorder in the connectivity. One can expect that what really matters is not the absolute connectivity k but the fluctuations of the relative connectivity $k/\langle k \rangle$. Nevertheless, for the construction of network at increasing size we will consider massive networks for which the average connectivity scales as the size N. Accordingly, the parameter whose distribution needs to be maintained in order to observe similar dynamical features is the specific connectivity $\tilde{k}$. A possible way to construct network with the same distribution $P(\tilde{k})$ is the following [32, 70]. For every neuron i it is extracted its specific connectivity $\tilde{k}_i$ from the distribution $P(\tilde{k})$ and then $\tilde{k}N$ presynaptic neurons are assigned randomly. No-

tice that the distribution $P(\tilde{k})$ is takes values for $\tilde{k} \in (0, 1]$ and has to be suitably normalized. In particular, if $P(\tilde{k})$ is a truncated Gaussian distribution, the dynamics reproduces the scenario discussed in Sec. 2.1 and shown in Fig. 3.1 for an Erdös–Renyi random graph. The overall scenario can be further analyzed by plotting the raster plot of a finite size network where the indexes of neurons are ordered according to their connectivity (see Fig. 3.2). We observe unlocked neurons at high connectivity (i.e. high index values) and at low connectivity (i.e. very low index values). Furthermore the maroon crosses represent the mean field $Y(t) = 1/N \sum_j y_j(t)$ that shows peaks at the QSE event.

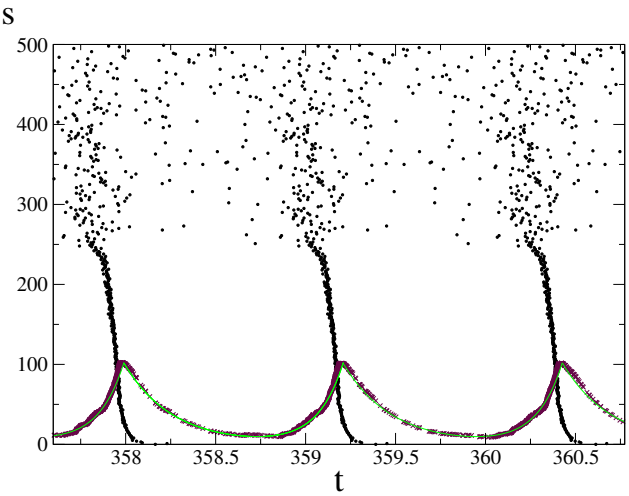

Figure 3.2: Raster plot of a randomly diluted network containing 500 neurons, ordered along the vertical axis according to their in–degree. The distribution $P(\tilde{k})$ is a Gaussian with $\langle \tilde{k} \rangle = 0.7$, standard deviation $\sigma_{\tilde{k}} = 0.077$. A black dot in the raster plot indicates that neuron s has fired at time t. The maroon crosses are the global field $Y(t)$ and the green (light grey) continuous curve is its analytic fit by the function $Y_f(t) = Ae^{-\frac{t}{\tau_1}} + B(e^{\frac{t}{\tau_2}} - 1)$, that repeats over each period of $Y(t)$; the parameter values are $A = 2 \cdot 10^{-2}$, $B = 3.56 \cdot 10^{-6}$, $\tau_1 = 0.268$ and $\tau_2 = 0.141$. Notice that the amplitude of both $Y(t)$ and $Y_f(t)$ has been suitably rescaled to be appreciated on the same scale of the Raster plot [71].

In order to check that this construction is the appropriate one in Fig.3.3 we show the time-average of ISI vs $\tilde{k}$, here defined as $\overline{ISI}(\tilde{k})$. One can clearly observe the plateau of locked neurons and the crossover to unlocked neurons. Notice that in this case, at variance with what observed in Erdős–Rényi network, there is a family of unlocked neurons at low values of $\tilde{k}$. This family is not observed in Erdős–Rényi case (see Fig.3.1)

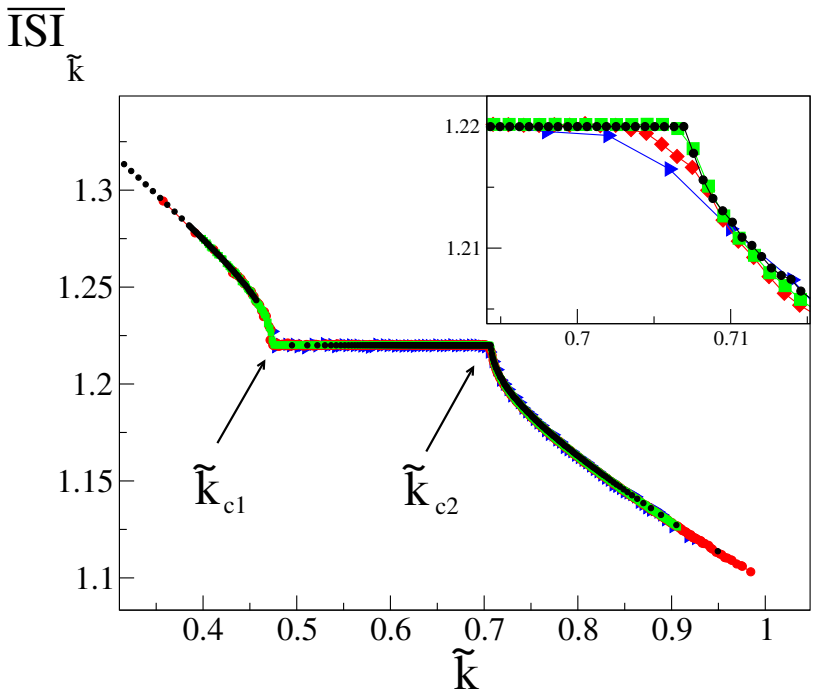

Figure 3.3: Time average of inter-spike intervals $\overline{ISI}(\tilde{k})$ vs $\tilde{k}$ from a Gaussian distribution with $\langle\tilde{k}\rangle = 0.7$ and $\sigma_{\tilde{k}} = 0.077$ and for three networks with $N = 500$ (blue triangles), $N = 5000$ (red diamonds), $N = 20000$ (green squares). For each size, the average is taken over 8 different realizations of the random network. We have also performed a suitable binning over the values of $\tilde{k}$, thus yielding the numerical estimates of the critical values $\tilde{k}_{c1} \approx 0.49$ and $\tilde{k}_{c2} \approx 0.70$. In the inset we show a zoom of the crossover region close to $\langle\tilde{k}\rangle = 0.7$. Black dots are the result of simulations of the mean field dynamics (see Eq.s (3.3)–(3.6)) with $M = 307$ [70].

because the standard deviation of $\tilde{k}$, namely $\sigma_{\tilde{k}}$, is too small and cannot be decided a priori (apart from changing p). Remarkably, networks of different sizes ($N = 500,\ 5000$ and 20000) feature the same dependence of $\overline{ISI}(\tilde{k})$ on $\tilde{k}$. There is not a sharp transition from locked to unlocked neurons, because for finite N the behavior of each neuron depends not only on its $\tilde{k}$, but also on neighbor neurons sending their inputs. Nevertheless, in the inset, the crossover appears to be sharper and sharper for increasing N, as expected for true critical points. Furthermore, the fluctuations of $\overline{ISI}(\tilde{k})$ over different realizations, by $P(\tilde{k})$, of three networks of different size exhibit a peak around $\tilde{k}_{c1}$ and $\tilde{k}_{c2}$, while they decrease with N as $\sim N^{-1/2}$ (data not shown). Thus, the qualitative and quantitative features

of the QSE at finite sizes are expected to persist in the thermodynamic limit, where fluctuations vanish and it will be shown that the dynamics of each neuron depends only on its in–degree.

In summary, given a reference sample with its own distribution $P(\tilde{k})$, one needs to construct ideal network at increasing sizes keeping fixed $P(\tilde{k})$. In this way, it is possible preserve the dynamics from a quantitative and a qualitative point of view, apart from statistical fluctuations.

3.2 Heterogeneous mean field model

The network construction described in previous section preserves the dynamics of the system at each size N. This is true in particular in the thermodynamic limit, i.e. $N \to \infty$. The dynamics of the model in this limit can be a addressed through an approximation based on the finite size fluctuations vanishing in this limit. In particular, let us consider a neuron i in the ideal infinite structure, characterized by the distribution $P(\tilde{k})$ of the finite sample of reference. The field Y_i received by this neuron is

$$Y_i(t) = \frac{1}{N} \sum_j \epsilon_{ij} y_j(t) = \frac{1}{N} \sum_{j \in I(i)} y_j, \tag{3.1}$$

where $I(i)$ is the set of k_i neurons transmitting to neuron i. In the thermodynamic limit, as the network is massive, the connectivity k_i goes to infinity and, given the randomness of the network (i.e. the choice of presynaptic neurons $j \in I(i)$ is random) one can assume that

$$\frac{1}{k_i} \sum_{j \in I(i)} y_j \to \frac{1}{N} \sum_j y_j = Y(t) \tag{3.2}$$

in the limit $N \to \infty$. Accordingly, by combining Eq.s (3.1) and (3.2) one finds that, in the thermodynamic limit, the field received (apart from the coupling factor g) by every neuron i is $Y_i = \tilde{k}_i Y$. Let us point out that for finite but large values of the connectivity of neurons Eq. (3.2) is an approximation equivalent to say that the average of a large but finite number of fields chosen randomly in the network is approximately equivalent to the average over all neurons in the network. We will show that this approximation is valid also when one considers sparse networks and typically is well satisfied by a quite small value of $\langle k \rangle$ is sufficient (e.g. $\langle k \rangle \sim 50$). The mean field hypothesis permits to forget about the detail of the network structure, i.e. which neurons fire to the reference neuron i. In order

to determine the dynamics of neuron i it is sufficient to know its specific connectivity $\tilde{k}_i$. Accordingly, we can write a dynamical equation for the class of neurons sharing the same specific connectivity $\tilde{k}$. The evolution equations for each class $\tilde{k}$ read

$$\dot{v}_{\tilde{k}}(t) = a - v_{\tilde{k}}(t) + g\tilde{k}Y(t) \tag{3.3}$$

$$\dot{y}_{\tilde{k}}(t) = -\frac{y_{\tilde{k}}(t)}{\tau_{\text{in}}} + u(1 - y_{\tilde{k}}(t) - z_{\tilde{k}}(t))S_{\tilde{k}}(t) \tag{3.4}$$

$$\dot{z}_{\tilde{k}}(t) = \frac{y_{\tilde{k}}(t)}{\tau_{\text{in}}} - \frac{z_{\tilde{k}}(t)}{\tau_{\text{r}}} \quad , \tag{3.5}$$

where $v_{\tilde{k}}$, $y_{\tilde{k}}$ and $z_{\tilde{k}}$ are the membrane potential, fraction of active and inactive resources of the class of neurons with in–degree $\tilde{k}$, respectively and the mean field $Y(t)$ needs to be consistently written in order sum over all the microscopic fields $y_{\tilde{k}}$ weighted for the fraction $P(\tilde{k})d\tilde{k}$ of neurons present in that specific class

$$Y(t) = \int_0^1 P(\tilde{k}) y_{\tilde{k}}(t) d\tilde{k}. \tag{3.6}$$

Notice that $\tilde{k}$ is a continuous variable in the interval $(0, 1]$ and the infinite set of equations (3.3)–(3.6) is the mean field model relative to a finite size sample characterized by the distribution $P(\tilde{k})$. This model is said heterogeneous mean field (HMF) because it keeps track of the inhomogeneity present in finite size realization. The overall procedure applies to a wide class of network dynamics of the type described in Eq.(1.4). Actually, the method can be extended to a more general class of the type

$$\dot{\boldsymbol{w}}_i = \mathcal{F}\Big(\boldsymbol{w}_i, \frac{g}{N}\sum_{j\neq i}\epsilon_{ij}\mathbf{G}(\boldsymbol{w}_j)\Big) \quad , \tag{3.7}$$

where the vector $\boldsymbol{w}_i$ represents the state of the site i, $\mathcal{F}(\boldsymbol{w}_i, 0) = \mathbf{F}$ is the single site dynamics (see Eq. (1.4)), g is the coupling strength, $\mathbf{G}(\boldsymbol{w}_j)$ is the coupling function and $\epsilon_{i,j}$ is the adjacency matrix of the directed uncorrelated network. In this case, calling $E(t)$ the mean field, the evolution equations corresponding to Eq.s (3.3)–(3.6) read

$$\dot{\boldsymbol{w}}_{\tilde{k}} = \mathcal{F}\Big(\boldsymbol{w}_{\tilde{k}}, g\tilde{k}E(t)\Big) \tag{3.8}$$

$$E(t) = \int_0^1 P(\tilde{k}) G(\boldsymbol{w}_{\tilde{k}}(t)) d\tilde{k}. \tag{3.9}$$

Despite this set of equations (3.3)–(3.6) cannot be solved explicitly, they provide a great numerical advantage with respect to direct simulations of large systems. Actually, the basic features of the dynamics of such systems can be effectively reproduced (modulo finite–size corrections) by exploiting a suitable sampling of $P(\tilde{k})$. One can subdivide the support $(0,1]$ of $\tilde{k}$ by M values $\tilde{k}_i$ $(i = 1, \cdots, M)$, in such a way that $\int_{\tilde{k}_i}^{\tilde{k}_{i+1}} P(\tilde{k})d\tilde{k}$ is constant (importance sampling). Notice that the integration of the discretized HMF equations is much less time consuming than the simulations performed on a random network. For instance, numerical tests indicate that the dynamics of a network with $N = 10^4$ neurons can be confidently reproduced by an importance sampling with $M = 300$.

The effect of the discretization of $\tilde{k}$ on the HMF dynamics can be analyzed by considering the distance $d(Y_{M_1}(t), Y_{M_2}(t))$ between the global activity fields $Y_{M_1}(t)$ and $Y_{M_2}(t)$ (see Eq.(3.6)) obtained for two different values M_1 and M_2 of the sampling, i.e.:

$$d(Y_{M_1}(t), Y_{M_2}(t)) = \left(\frac{1}{T} \sum_{i=1}^{T} \frac{(Y_{M_1}(t_i) - Y_{M_2}(t_i))^2}{Y_{M_1}(t_i)^2} \right)^{\frac{1}{2}}. \tag{3.10}$$

In general $Y(t)$ exhibits a quasi periodic behavior and $d(Y_{M_1}(t), Y_{M_2}(t))$ is evaluated over a time interval equal to its period T. In order to avoid an overestimation of $d(Y_{M_1}(t), Y_{M_2}(t))$ due to different initial conditions, the field $Y_2(t)$ is suitably translated in time in order to make its first maximum coincide with the first maximum of $Y_1(t)$ in the time interval $[1, T]$. In Fig. 3.4 we plot $d_M = d(Y_M, Y_{M/2})$ as a function of M. We find that $d_M \sim 1/\sqrt{M}$, thus confirming that the finite size simulation of the HMF dynamics is consistent with the HMF model ($M \to \infty$).

This result shows that the HMF model is well defined and that its dynamics can be exploited by a quite reduced computational cost. To check its validity in Fig.3.3 we compare $\overline{ISI}(\tilde{k})$, obtained from the HMF equations for $M = 307$, with the same quantity computed by direct simulations of networks up to size $N = 2 \times 10^4$. The agreement is remarkable evidencing the numerical effectiveness of the method and the capacity of the HMF model to reproduce finite size dynamics.

3.3 HMF: the direct problem

In this Section we report the main results one can obtain through the HMF model in the framework of the direct problem, i.e. given a distribution

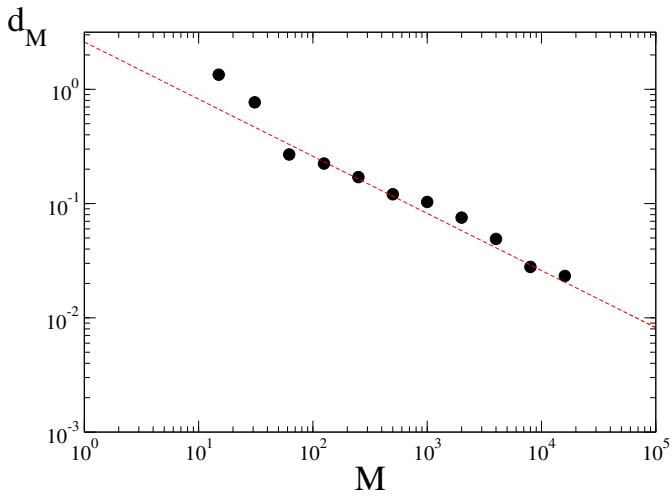

Figure 3.4: The effect of sampling the probability distribution $P(\tilde{k})$ with M classes of neurons in the HMF dynamics. Finite size effects are controlled by plotting the distance between the activity fields obtained for two sampling values M and $M/2$, $d_M = d(Y_M(t), Y_{M/2}(t))$ (defined in the text), vs. M. The red dashed line is the power law $1/\sqrt{M}$. Data is obtained for a Gaussian distribution $P(\tilde{k})$, with $\langle\tilde{k}\rangle = 0.7$ and $\sigma_{\tilde{k}} = 0.077$ [71].

$P(\tilde{k})$ how it drives the microscopic and collective dynamics. The, we report on the chaoticity of the HMF model through the calculation of the Lyapunov exponents, i.e. orbit separation. Furthermore we show that the overall method can be applied in the case of sparse networks and that the mean field approximation remains valid also for quite low when connectivity values.

3.3.1 Stability analysis and chaoticity

In the HMF equations, once the global field $Y(t)$ is known, the dynamics of each class of neurons with in-degree $\tilde{k}$ can be determined by a straightforward integration, and we can perform the stability analysis that Tsodyks et al. applied to a similar model [56]. As an example, we have considered the system studied in Fig.3.2 and 3.3. The global field $Y(t)$ of the HMF dynamics has been obtained using the importance sampling for the distribution $P(\tilde{k})$. For sufficiently large M the discretized HMF dynamics allows one to obtain a precise fit of the periodic function $Y(t)$ and to estimate its period T. As an instance of its periodic behavior, in Fig.3.2 we report also $Y(t)$ (maroon crosses) and its fit (green continuous line and the formula in the caption). The fitted field is exactly periodic

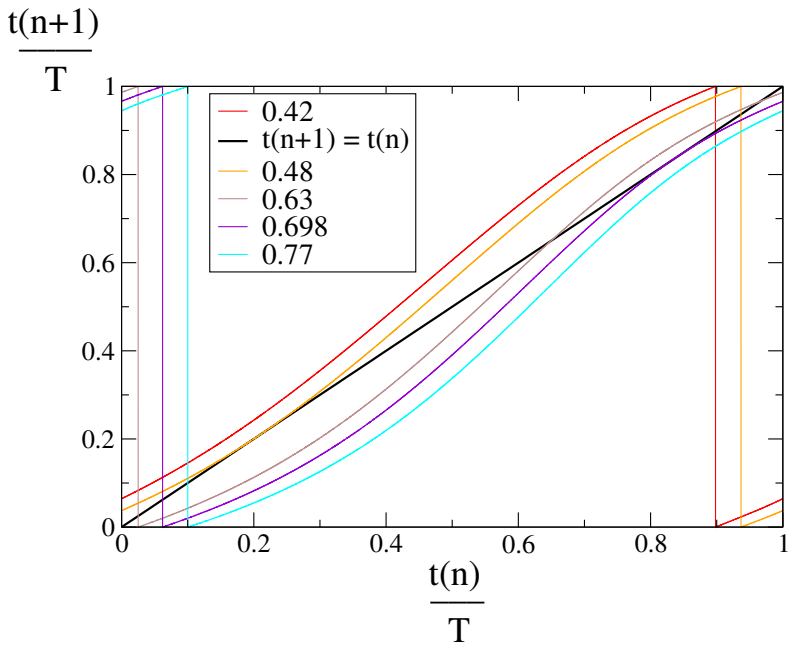

Figure 3.5: The return map $R_{\tilde{k}}$ in Eq. (3.12) of the rescaled variables $t_{\tilde{k}}(n)/T$ for different values of $\tilde{k}$, corresponding to lines of different colors, according to the legend in the inset: the black line is the bisector of the square [70].

and is a good approximation of the global field that one expects to observe in the mean field model corresponding to an infinite discretization M. As a result, the analysis performed using this periodic field are relative to the dynamics of the HMF model, i.e. in the limit $M \to \infty$. Let us call $Y_f(t)$ the fitted field, continuous and periodic in time, with period T. Accordingly, Eq. (3.3) can be approximated by

$$\dot{v}_{\tilde{k}}(t) = a - v_{\tilde{k}}(t) + g\tilde{k}Y_f(t). \tag{3.11}$$

Notice that, by construction, the field $Y_f(t)$ features peaks at times $t = nT$, where n is an integer. In this way we can represent Eq. (3.11) as a discrete single neuron map. In practice, we integrate Eq.(3.11) and determine the sequence of the (absolute value of the) firing time–delay, $t_{\tilde{k}}(n)$, of neurons with in–degree $\tilde{k}$ with respect to the reference time nT. The return map $R_{\tilde{k}}$ of this quantity reads

$$t_{\tilde{k}}(n+1) = R_{\tilde{k}} t_{\tilde{k}}(n). \tag{3.12}$$

In Fig. 3.5 we plot the return map of the rescaled firing time–delay $t_{\tilde{k}}(n)/T$ for different values of $\tilde{k}$. We observe that in-degrees $\tilde{k}$ corresponding to locked neurons (e.g., the brown curve) have two fixed points $t^s_{\tilde{k}}$ and $t^u_{\tilde{k}}$, the first one is stable (the derivative of the map $R_{\tilde{k}}$ is < 1) and the second unstable (the derivative of the map $R_{\tilde{k}}$ is > 1). Clearly, the dynamics converges to the stable fixed point displaying a periodic behavior. In particular, the firing times of neurons $\tilde{k}$ are phase shifted of a quantity $t^s_{\tilde{k}}$ with respect the peaks of the fitted global field. The orange and violet curves correspond to the dynamics at the critical in-degrees $\tilde{k}_{c1}$ and $\tilde{k}_{c2}$ where the fixed points disappear (see Fig.(3.3)). The presence of such fixed points influences also the behavior of the unlocked component (e.g., the red and light blue curves). In particular, the nearer $\tilde{k}$ is to $\tilde{k}_{c1}$ or to $\tilde{k}_{c2}$, the closer is the return map to the bisector of the square, giving rise to a dynamics spending longer and longer times in an almost periodic firing. Afterwards, unlocked neurons depart from this almost periodic regime, thus following an aperiodic behavior. As a byproduct, this dynamical analysis allows to estimate the values of the critical in–degrees. For the system of Fig.3.2, $\tilde{k}_{c1} = 0.48$ and $\tilde{k}_{c2} = 0.698$, in very good agreement with the numerical simulations (see Fig. 3.3).

A further investigation of the HMF model concerns its stability properties. From the picture described in Sec.2.2 it is clear that the dynamics of every finite size sample shows deterministic chaos. Nevertheless, in the thermodynamic limit and in the mean field model one expects fluctuations to vanish, yielding a non chaotic dynamics. Using the deterministic map (3.12), one can tackle in full rigor the stability problem of the HMF model. The existence of stable fixed points for the locked neurons implies that they yield a negative Lyapunov exponent associated with their periodic evolution.

As for the unlocked neurons, their Lyapunov exponent, $\lambda_{\tilde{k}}$, can be calculated numerically by the time-averaged expansion rate of nearby orbits of map (3.12):

$$\lambda_{\tilde{k}}(n) = \frac{1}{n}\sum_{j=1}^{n} \log\left[\frac{|\delta(j)|}{|\delta(0)|}\right], \tag{3.13}$$

where $\delta(0)$ is the initial distance between nearby orbits and $\delta(j)$ is their distance at the j–th iterate, so that

$$\lambda_{\tilde{k}} = \lim_{n\to\infty} \lambda_{\tilde{k}}(n) \tag{3.14}$$

if this limit exists. The Lyapunov exponents for the unlocked component vanish as $\lambda_{\tilde{k}}(n) \sim 1/n$. According to these results, one expects that the

maximum Lyapunov exponent $\lambda_{\max}(M)$ goes to zero in the limit $M \to \infty$. In fact, at each finite M, $\lambda_{\max}$ can be evaluated by using the standard algorithm by Benettin et al. [63]. In Fig.3.6 we plot $\lambda_{\max}$ as a function of the discretization parameter M. Thus, $\lambda_{\max}(M)$ is positive, behaving approximately as $M^{-\gamma}$, with $\gamma \sim 1/2$ (actually, we find $\gamma = 0.55$).

The scenario in any discretized version of the HMF dynamics is the following: *(i)* all *unlocked neurons* exhibit positive Lyapunov exponents, i.e. they represent the chaotic component of the dynamics; *(ii)* $\lambda_{\max}$ is typically quite small, and its value depends on the discretization parameter M and on $P(\tilde{k})$; *(iii)* in the limit $M \to \infty$ $\lambda_{\max}$ and all $\lambda_{\tilde{k}}$'s of unlocked neurons vanish, thus converging to a quasi periodic dynamics, while the *locked neurons* persist in their periodic behavior.

The same scenario is observed in the dynamics of random networks built with the HMF strategy, where the variance of the distribution $P(\tilde{k})$ is kept independent of the system size N, so that the fraction of locked neurons is constant.

For the LIF dynamics in an Eördos–Renyi random network with N neurons, it was found that $\lambda_{\max}(N) \approx N^{-0.27}$ in the limit $N \to \infty$ (see Fig. 2.7). According to the argument proposed in [52], the value of the power-law exponent is associated to the scaling of the number of unlocked neurons, N_u with the system size N, namely $N_u \sim N^{0.9}$. The same argument applied to HMF dynamics indicates that the exponent $\gamma \sim 1/2$, ruling the vanishing of $\lambda_{\max}(M)$ in the limit $M \to \infty$, stems from the fact that the HMF dynamics keeps the fraction of unlocked neurons constant.

This picture shows that the HMF model describes the backbone of the microscopic and macroscopic dynamical attractors (see Fig.s 2.4 and 2.5), delaying finite size fluctuations. This permits some easier treatments of the equations (e.g. the map 3.12), being confident with the fundamental aspects of finite size samples dynamics.

3.3.2 The role of $P(\tilde{k})$

Still in the perspective of the *direct problem*, the HMF equations provide further insight on how the network topology influences the dynamical behavior. In particular, in this Section we will analyze the different collective dynamics that may emerge for choices of $P(\tilde{k})$ other than the Gaussian case, discussed in the previous section. We will focus mainly in two different distributions. The first one is a power–law distribution

$$P(\tilde{k}) = A\tilde{k}^{-\alpha}, \tag{3.15}$$

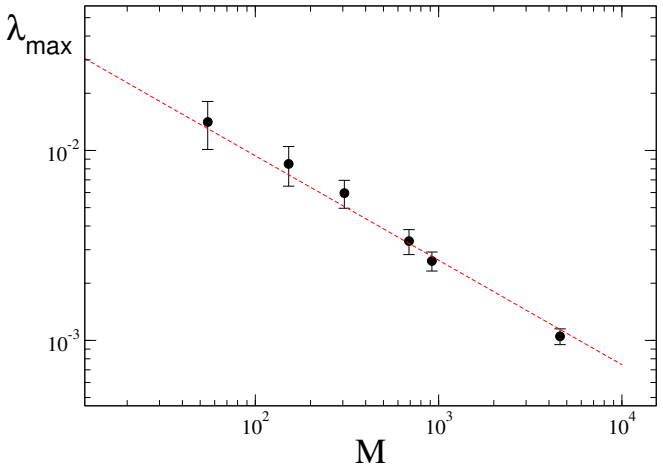

Figure 3.6: The maximum Lyapunov exponent $\lambda_{\max}$ as a function of the sampling parameter M: $\lambda_{\max}$ has been averaged also over ten different realizations of the network (the error bars refer to the maximum deviation from the average). The dashed red line is the powerlaw $M^{-\gamma}$, with $\gamma = 0.55$ [71].

where the constant A is given by the normalization condition $\int_{\tilde{k}_m}^{1} P(\tilde{k})d\tilde{k} = 1$. The lower bound $\tilde{k}_m$ is introduced in order to maintain A finite. For simplicity, we fix the parameter $\tilde{k}_m$ and analyze the dynamics by varying α. Notice that the standard deviation $\sigma_{\tilde{k}}$ of distribution (3.15) decreases for increasing values of α. Another distribution, generating an interesting dynamical phase, is

$$P(\tilde{k}) = B\exp\left(-\frac{(\tilde{k}-p_1)^2}{2\sigma_s^2}\right) + B\exp\left(-\frac{(\tilde{k}-p_2)^2}{2\sigma_s^2}\right), \tag{3.16}$$

i.e. the sum of two Gaussians peaked around different values, p_1 and p_2, of $\tilde{k}$, with the same variance σ_s^2. B is the normalization constant such that $\int_0^1 P(\tilde{k}) = 1$. In the rest of this Section we fix $p_1 = 0.5$.

We have found that, in general, the fraction of locked neurons increases as $P(\tilde{k})$ becomes sharper and sharper, while synchronization is eventually lost for broader distributions. In Fig. 3.7 we report the fraction of locked neurons, $f_l = \int_{\tilde{k}_{c1}}^{\tilde{k}_{c2}} P(\tilde{k})d\tilde{k}$ (actually in Figure it s reported the percentage), as a function of the standard deviation $\sigma_{\tilde{k}}$, for different kinds of $P(\tilde{k})$ (single or double–peaked Gaussian, power law) in the HMF equations. In all cases, there is a critical value σ^* of $\sigma_{\tilde{k}}$ above which f_l vanishes, i.e. QSE disappear. This asynchronous dynamical phase is characterized by a mean field $Y(t)$ exhibiting fluctuations due to finite size effects and

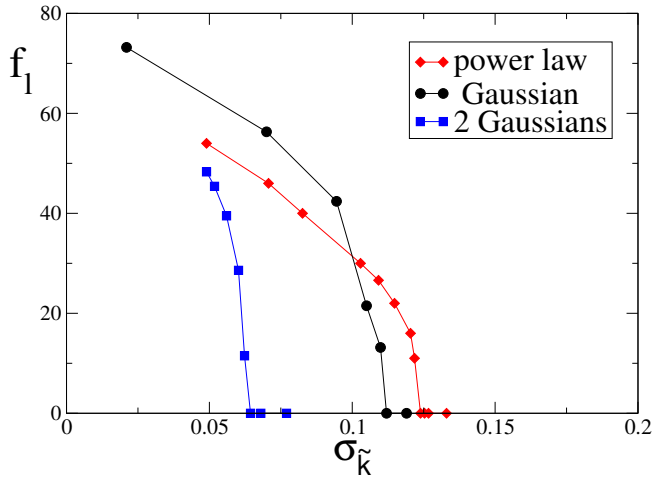

Figure 3.7: The fraction of locked neurons (actually we report the percentage), f_l, as a function of the standard deviation $\sigma_{\tilde{k}}$ of the distributions: truncated Gaussian with $\langle \tilde{k} \rangle = 0.7$ (black dots); truncated superposition of two Gaussians (both with standard deviation $\sigma_s = 0.03$), one centered at $p_1 = 0.5$ and the other one at a varying value p_2, that determines the overall standard deviation $\sigma_{\tilde{k}}$ (blue squares); truncated power law distribution with $\tilde{k}_m = 0.1$ (red diamonds). In the last case the value of the standard deviation is changed by varying the exponent α, while the average $\langle \tilde{k} \rangle$ changes accordingly. Lines have been drawn to guide the eyes [70].

in the thermodynamic limit it tends to a constant value Y^*. From Eq.s (3.3)–(3.5), one obtains that in this regime each neuron with in–degree $\tilde{k}$ fires periodically with a period

$$T_{\tilde{k}} = \ln \left[\frac{b + g\tilde{k}Y^*}{b + g\tilde{k}Y^* - 1} \right],$$

while its phase depends on the initial conditions. The phases of neurons are correlated in such a way to distribute properly yielding an asynchronous state, i.e. the Kuramoto parameter $R = 0$ (see Eq. (2.21)). As a further remark, in this case all the Lyapunov exponents $\lambda_{\tilde{k}}$ are negative.

The generality of this scenario points out the importance of the relation between $P(\tilde{k})$ and the average synaptic field $Y(t)$.

This picture signals a very interesting dynamical transition between the quasi-synchronous phase ($\sigma_{\tilde{k}} < \sigma^*$) to a multi-periodic phase ($\sigma_{\tilde{k}} > \sigma^*$), where all neurons are periodic with different periods.

Let us take under consideration now the single cases of power law and double Gaussian distributions. In the case of the power law the dynam-

ics for relatively high α is very similar to the quasi–synchronous regime observed for $\sigma_{\tilde{k}} < \sigma^*$ in the Gaussian case (see Fig. 3.2). By decreasing α one can observe again a transition to the asynchronous phase observed for $\sigma_{\tilde{k}} > \sigma^*$ in the Gaussian case. Accordingly, also for the power–law distribution (3.15) a phase with locked neurons may set in only when there is a sufficiently large group of neurons sharing close values of $\tilde{k}$. In fact, the group of locked neurons is concentrated at values of $\tilde{k}$ quite close to the lower bound $\tilde{k}_m$, while in the Gaussian case they concentrate at values smaller than $\langle \tilde{k} \rangle$.

A more complex scenario appears for the double Gaussian of Eq. (3.16). If σ_s is very large ($\sigma \gtrsim 0.1$), the situation is the same observed for a single Gaussian with large variance, yielding a multi–periodic asynchronous dynamical phase.

For intermediate values of σ_s i.e. $0.05 \lesssim \sigma \lesssim 0.1$, the dynamics of the network can exhibit a quasi–synchronous phase or a multi–periodic asynchronous phase, depending on the value of Δ. In fact, one can easily realize that this parameter tunes the standard deviation of the overall distribution: small separations amount to broad distributions.

Finally, when $\sigma_s \lesssim 0.05$, a new dynamical phase appears. For small

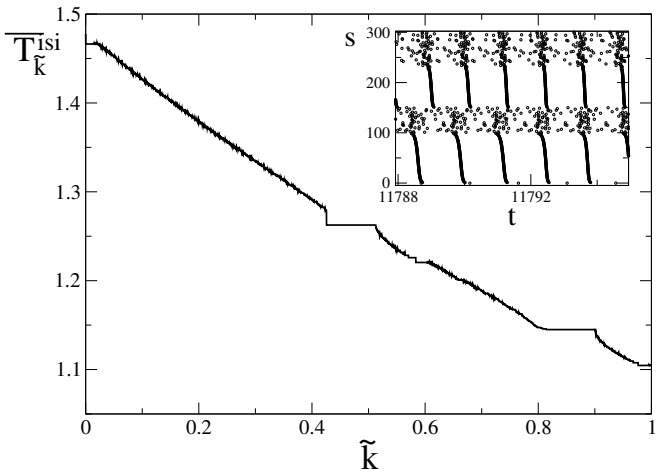

Figure 3.8: The time average of the inter–spike interval $\overline{T^{isi}_{\tilde{k}}}$ vs. $\tilde{k}$ for the probability distribution $P(\tilde{k})$ defined in Eq.(3.16), with $\Delta = |p_2 - p_1| = 0.4$, and $\sigma_s = 0.03$. We have obtained the global field $Y(t)$ simulating the HMF dynamics with a discretization with $M = 300$ classes of neurons. We have then used $Y(t)$ to calculate T^{isi} of neurons evolving Eq. (3.3). In the inset we show the raster plot of the dynamics: as in Fig.1, neurons are ordered along the vertical axis according to their in–degree [71].

values of Δ (e.g. $\Delta \approx 0.1$) , we observe the usual QSE scenario with one family of locked neurons (data not shown). However, when Δ is sufficiently large (e.g. $\Delta \approx 0.4$), each peak of the distribution generates its own group of locked neurons. More precisely, neurons separate into three different sets: two locked groups, that evolve with different periods, T_1 and T_2, and the unlocked group. In Fig.3.8 we show the dependence of the average inter spike interval, here called $\overline{T^{isi}_{\tilde{k}}}$, on $\tilde{k}$ and the raster plot of the dynamics (see the inset) for $\sigma_s = 0.03$.

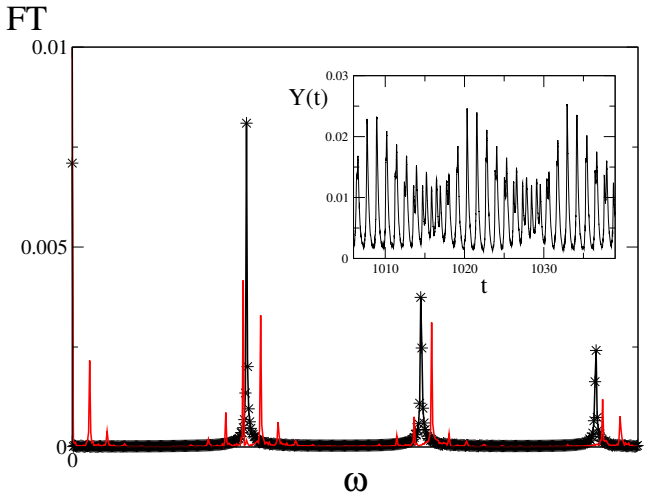

Figure 3.9: The frequency spectra of the global activity field $Y(t)$ for different in–degree probability distributions. The black spectrum with stars has been obtained for the HMF dynamics with $M = 350$, generated by the power law probability distribution $P(\tilde{k}) \sim \tilde{k}^{-4.9}$ (see Eq.(3.15)), with $\tilde{k}_m = 0.1$: in this case there is a unique family of locked neurons generating a periodic global activity field $Y(t)$. The red continuous line spectrum has been obtained for a random network of $N = 300$ neurons generated by the double Gaussian distribution (see Eq.(3.16)) described in Fig.s 6 and 7: in this case two families of locked neurons are present while, as reported in the inset, $Y(t)$ exhibits a quasi–periodic evolution [71].

Notice that the plateaus of locked neurons extend over values of $\tilde{k}$ on the left of p_1 and p_2. In the inset of Fig. 3.9 we plot the global activity field $Y(t)$: the peaks of the signal represent the quasi-synchronous firing events of the two groups of locked neurons. One can also observe that very long oscillations are present over a time scale much larger than T_1 and T_2. They are the effect of the *firing synchrony* of the of two locked families. In fact, the two frequencies $\omega_1 = 2\pi/T_1$ and $\omega_2 = 2\pi/T_2$ are in general not commensurate, and the resulting global field is a quasi–periodic function. This can be better appreciated by looking at Fig.3.9, where we report the

frequency spectrum of the signal $Y(t)$ (red continuous curve). We observe peaks at frequencies $\omega = n\omega_1 + m\omega_2$, for integer values of n and m. For comparison, we report also the spectrum of a periodic $Y(t)$, generated by the HMF with power law probability distribution (3.15), with $\alpha = 4.9$ (black curve with stars): in this case the peaks are located at frequencies multiples of the frequency of the locked group of neurons.

On the basis of this analysis, we can conclude that slow oscillations of the global activity field $Y(t)$ may signal the presence of more than one group of topologically homogeneous (i.e. locked) neurons. Moreover, we have also learnt that one can generate a large variety of global synaptic activity fields by selecting suitable in-degree distributions $P(\tilde{k})$, thus unveiling unexpected perspectives for exploiting a sort of *topological engineering* of the neural signals. For instance, one could investigate which kind of $P(\tilde{k})$ could give rise to an almost resonant dynamics, where ω_2 is close to a multiple of ω_1.

3.3.3 HMF in sparse networks

In this section we analyze the effectiveness of the HMF approach for sparse networks, i.e. networks where the neurons degree does not scale linearly with N and, in particular, the average degree $\langle k \rangle$ is independent of the system size. In this context, the coupling term describing the membrane potential of a generic neuron i, in a network of N neurons, evolves according to the following equation:

$$\dot{v}_i = a - v_i + \frac{g}{\langle k \rangle} \sum_{j \neq i} \epsilon_{ij} y_j, \tag{3.17}$$

while the dynamics of y_i is the same of Eq.s (1.10)–(1.12). The coupling therm is now independent of N, and the normalization factor, $\langle k \rangle$, has been introduced in order to compare models with different average connectivity. The structure of the adjacency matrix ϵ_{ij} is determined by choosing for each neuron i its in-degree k_i from a probability distribution $P(k_i)$ (with support over positive integers) independent of the system size.

On sparse networks the HMF model is not recovered in the thermodynamic limit, as the fluctuations of the field received by each neuron of in–degree k_i do not vanish for $N \to \infty$. Nevertheless, for large enough values of k_i, one can expect that the fluctuations become negligible in such a limit, i.e. the synaptic activity field received by different neurons with the same in-degree is approximately the same. Eq. (3.17) can be turned

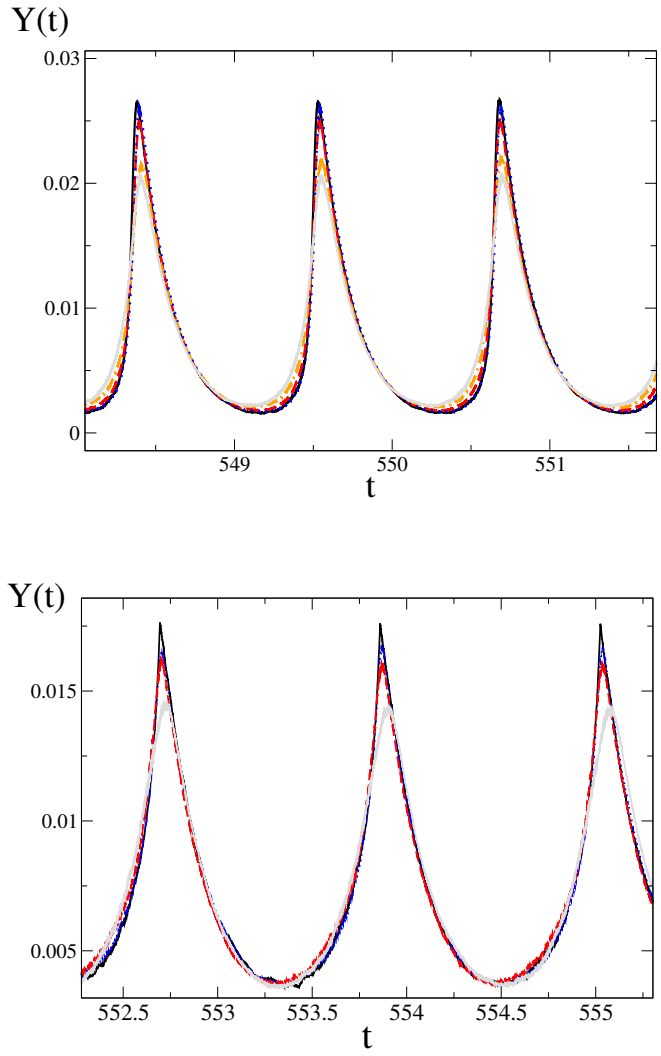

Figure 3.10: Comparison of the global synaptic activity field $Y(t)$ from sparse random networks with the same quantity generated by the corresponding HMF dynamics. We have considered sparse random networks with $N = 10^4$ neurons. In the upper panel we consider a Gaussian probability distributions $P(k)$ with different averages $\langle k \rangle$ and variances σ_k, such that $\sigma_k / \langle k \rangle = 0.06$: $\langle k \rangle = 10, 20, 60, 100$ correspond to the grey continuous curve, orange dots and segments, red segments and blue dots, respectively. The black continuous line represents $Y(t)$ from the HMF dynamics ($M = 10^3$), where $\hat{P}(\hat{k})$ is a Gaussian probability distribution with $\langle \hat{k} \rangle = 1$ and $\sigma_{\hat{k}} = \sigma_k / \langle k \rangle = 0.06$. In the lower panel we consider the scale free case with fixed power exponent α and different k_m: $k_m = 10, 30, 70$ correspond to the grey continuous line, red segments and blue dots, respectively. The black continuous line represents $Y(t)$ from the HMF dynamics ($M = 10^3$), where $\hat{P}(\hat{k}) = (\alpha - 1)\hat{k}^{-\alpha}$ with cutoff $\hat{k}_m = 1$. Notice that in both cases decreasing $\langle k \rangle$ decreases the peak of the curve with respect to the HMF curve peak [71].

into a mean–field like form as follows

$$\dot{v}_i = a - v_i + \frac{g}{\langle k \rangle} k_i Y \ , \tag{3.18}$$

where $Y(t)$ represents the global field, averaged over all neurons in the network. This implies that the equation is the same for all neurons with in–degree k_j, depending only on the ratio $\hat{k}_i = k_i/\langle k \rangle$. Consequently, also in this case one can read Eq. (3.18) as a HMF formulation of Eq. (3.17), where each class of neurons $\hat{k}$ evolves according to to Eq.s (3.3)–(3.5), with $\hat{k}$ replacing $\tilde{k}$, while the global activity field is given by the relation $Y(t) = \int_0^\infty \hat{P}(\hat{k}) y_{\hat{k}}(t) d\hat{k}$.

In order to analyze the validity of the HMF as an approximation of models defined on sparse networks, we consider two main cases: (*i*) $\hat{P}(\hat{k})$ is a truncated Gaussian with average $\langle \hat{k} \rangle = 1$ and standard deviation $\sigma_{\hat{k}}$; (*ii*) $\hat{P}(\hat{k}) = (\alpha - 1)\hat{k}^{-\alpha}$ is a power–law (i.e., scale free) distribution with a lower cutoff $\hat{k}_m = 1$. The Gaussian case (*i*) is an approximation of any sparse model, where $P(k_j)$ is a discretized Gaussian distribution with parameters $\langle k \rangle$ and σ_k, chosen in such a way that $\sigma_{\hat{k}} = \sigma_k/\langle k \rangle$. The scale free case (*ii*) approximates any sparse model, where $P(k_j)$ is a power law with exponent α and a generic cutoff. Such an approximation is expected to provide better results the larger is $\langle k \rangle$, i.e. the larger is the cutoff k_m of the scale free distribution. In Fig. 3.10 we plot the global field emerging from the HMF model, superposing those coming from a large finite size realization of the sparse network, with different values of $\langle k \rangle$ for the Gaussian case (upper panel) and of k_m for the scale free case (lower panel). The HMF equations exhibit a remarkable agreement with models on sparse network, even for relatively small values of $\langle k \rangle$ and k_m. This analysis indicates that the HMF approach works also for non–massive topologies, provided the typical connectivities in the network are large enough, e.g. $\langle k \rangle \sim \mathcal{O}(10^2)$ in a Gaussian random network with $N = 10^4$ neurons (see Fig. (3.10)).

Finally, let us point out again that a real network, i.e. the reference finite size sample one wants to address, is neither sparse or massive as its size N is fixed. Accordingly, the use of massive or sparse graphs to construct networks at increasing size represents just two different possibilities. The rescaling factor $\langle k \rangle$ or N in the real network is a fixed number and can be seen as a rescaling of the coupling g. The only difference is that for the massive construction the HMF is exact in the limit $N \to \infty$ while in the sparse case the HMF equations are always an approximation. On the other hand, the analysis of the sparse construction shows that the

mean field hypothesis is satisfied also for quite small values of neurons connectivities.

3.4 HMF: global inverse problem, from synaptic activity to network topology

A central problem in the contest of neural network dynamics is the reconstruction of neural connectivities from experimental observations. This is a typical inverse problem and has been mainly addressed through in *local* approaches [9, 10, 11, 12]. In this way the network is reconstructed through the knowledge of long time series of single neuron dynamics, a methods that applies efficiently to small systems only. Actually, the signals emerging during neural time evolution are often records of the average synaptic activity from large regions of the cerebral cortex – a kind of observable likely much easier to be measured than signals coming from single neuron activities [14, 15, 13]. Inferring the topological properties of the network from global signals is still an open and central problem in neurophysiology. In this section we investigate the possibility of formulating and solving such a *global* version of the inverse problem, reconstructing the network topology that has generated a given global (i.e. average) synaptic-activity field. The solution of such an inverse problem could also imply the possibility of engineering a network able to produce a specific average signal.

3.4.1 Formulation and solution to the global inverse problem

The HMF approach allows to implement the inverse problem and leads to the reconstruction of the distribution $P(\tilde{k})$ from the knowledge of $Y(t)$. If the global synaptic activity field $Y(t)$ is known, each class of neurons of in-degree $\tilde{k}$ evolves according to the equations:

$$\dot{\mathsf{v}}_{\tilde{k}}(t) = a - \mathsf{v}_{\tilde{k}}(t) + g\tilde{k}Y(t) \tag{3.19}$$

$$\dot{\mathsf{y}}_{\tilde{k}}(t) = -\frac{\mathsf{y}_{\tilde{k}}(t)}{\tau_{\mathsf{in}}} + u(1 - \mathsf{y}_{\tilde{k}}(t) - \mathsf{z}_{\tilde{k}}(t))\tilde{S}_{\tilde{k}}(t) \tag{3.20}$$

$$\dot{\mathsf{z}}_{\tilde{k}}(t) = \frac{\mathsf{y}_{\tilde{k}}(t)}{\tau_{\mathsf{in}}} - \frac{\mathsf{z}_{\tilde{k}}(t)}{\tau_{\mathsf{r}}} \quad . \tag{3.21}$$

Notice that the variable $\mathsf{v}(t)$, $\mathsf{y}(t)$, $\mathsf{z}(t)$ can take values that differ from the variables generating the field $Y(t)$, i.e. $v(t)$, $y(t)$, $z(t)$, as they start from

different initial conditions. However, the self consistent relation for the global field $Y(t)$ implies:

$$Y(t) = \int_0^1 P(\tilde{k}) \mathsf{y}_{\tilde{k}}(t) d\tilde{k} \ . \tag{3.22}$$

If $Y(t)$ and $\mathsf{y}_{\tilde{k}}(t)$ are known, this is a Fredholm equation of the first kind in $P(\tilde{k})$ [72]. In the general case of Eq. (3.7), calling $E(t)$ the global measured external field, the evolution equations corresponding to Eq.s (3.19)–(3.21) read

$$\dot{\mathbf{w}}_{\tilde{k}} = \mathcal{F}\Big(\mathbf{w}_{\tilde{k}}, g\tilde{k}E(t)\Big) \tag{3.23}$$

and the Fredholm equation for the inverse problem is

$$E(t) = \int_0^1 P(\tilde{k}) G(\mathbf{w}_{\tilde{k}}(t)) d\tilde{k} \ . \tag{3.24}$$

In the case of our LIF model, as soon as a locked component exists, Eq. (3.22) can be solved by a functional Montecarlo minimization procedure applied to a sampled $P(\tilde{k})$. At variance with the *direct problem*, $P(\tilde{k})$ is the unknown function and, accordingly, we have to adopt a uniform sampling of the support of $\tilde{k}$. A sufficiently fine sampling has to be used for a confident reconstruction of $P(\tilde{k})$ (See Appendix A).

To check our inverse method, we choose a distribution $P(\tilde{k})$, evolve the system and extract the global synaptic field $Y(t)$. We then verify if the procedure reconstructs correctly the original distribution $P(\tilde{k})$. In panels (a), (b) and (c) of Fig. 3.11 we show examples in which $Y(t)$ has been obtained from the simulation of the HMF with different $P(\tilde{k})$ (Gaussian, double peak Gaussian and power law). We can see that the method determines confidently the original distribution $P(\tilde{k})$. Notice that the method fails as soon as the locked component disappears, as explained in the methods section. Remarkably, the method can recognize the discontinuity of the distribution in $\tilde{k} = \tilde{k}_{\min}$ and the value of the exponent of the power law $\alpha = 4.9$.

This test means that for the HMF model the global inverse problem can be formulated and solved for global fields showing collective oscillations. Nevertheless, the HMF is a good representation of the dynamics of a finite size sample characterized by a distribution $P(\tilde{k})$. Accordingly, in panel (d) of Fig.3.11, we show the result of the inverse problem for the distribution $P(\tilde{k})$ obtained from a global signal generated by a finite size realization with $N = 500$ and $\langle k \rangle = 350$. The significant agreement indicates that the

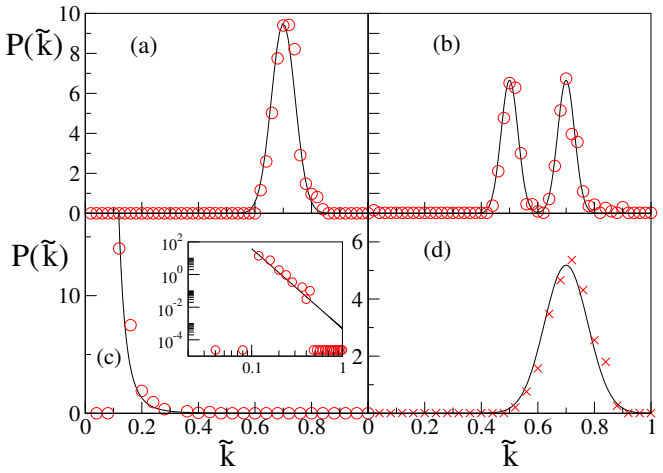

Figure 3.11: Inverse problem for $P(\tilde{k})$ from the global field $Y(t)$. Panels (a), (b) and (c) show three distributions of the kind considered in Fig. (4) (black continuous curves) for the HMF equations and their reconstructions (circles) by the inverse method. The parameters of the three distributions are $\sigma_{\tilde{k}} = 0.043$, $\tilde{k}_2 = 0.7$ and $\alpha = 4.9$. In panel (d) we show the reconstruction (crosses) of $P(\tilde{k})$ (black continuous line) by the average field $Y(t)$ generated by the dynamics of a *finite size* network with $N = 500$ [70].

HMF and its inverse problem are able to infer the in–degree probability distribution $P(\tilde{k})$ even for a realistic finite size network. This last result is particularly important, as it opens new perspectives for experimental data analysis, where the average neural activity is typically measured from finite size samples with finite but large connectivity.

Finally, let us point out that in many experiments one has access to the global field $V(t)$. Nevertheless, integrating over k Eq. (3.3) one has

$$Y(t) = \frac{a - \dot{V}(t) - V(t)}{g\langle k \rangle}. \tag{3.25}$$

Thus, again, one can write a self consistency equation with the unknown distribution $P(k)$.

3.4.2 Robustness with respect to noise

In this section we want to study the robustness of the HMF equations and of the corresponding inverse problem procedure in the presence of noise. This is quite an important test for the reliability of the overall HMF approach. In fact, a real neural structure is always affected by some level

of noise, that, for instance, may emerge in the form of fluctuations of ionic or synaptic currents.

For the sake of simplicity, here we introduce noise by turning the external current a, in Eq. (3.3), from a constant to a time and neuron dependent stochastic processes $a_{\tilde{k}}(t)$. Precisely, the $a_{\tilde{k}}(t)$ are assumed to be i.i.d. stochastic variables, that evolve in time as a random walk with boundaries, $a_{\min}$ and $a_{\max}$ (the same rule adopted in Sec. 2.2). Accordingly, the average value, $\bar{a}$ of $a_{\tilde{k}}(t)$ is given by the expression $\bar{a} = (a_{\min} + a_{\max})/2$, while the amplitude of fluctuations is $\delta = a_{\max} - a_{\min}$. At each step of the walk, the values of $a_{\tilde{k}}(t)$ are independently updated by adding or subtracting, with equal probability, a fixed increment Δa. Whenever the value of $a_{\tilde{k}}(t)$ crosses one of the boundaries, it is reset to the boundary value.

Since the dynamics has lost its deterministic character, its numerical integration cannot exploit an event driven algorithm, and one has to integrate Eq.s (3.3) –(3.5) by a scheme based on explicit time discretization. The results reported hereafter refer to an integration time step $\Delta t = 9 \cdot 10^{-4}$, that guarantees an effective sampling of the dynamics over the whole range of parameter values that we have explored. We have assumed that Δt is also the time step of the stochastic evolution of $a_{\tilde{k}}(t)$.

Here we consider the case of uncorrelated noise, that can be obtained by a suitable choice of Δa (see Fig. 2.8). In our simulations $\Delta a = 10^{-2}$, that yields a value $\mathcal{O}(10^{-2})$ of the correlation time of the random walk with boundaries. This value, much smaller than the value $\mathcal{O}(1)$ typical of T^{isi}, makes the stochastic evolution of the external currents, $a_{\tilde{k}}(t)$, an effectively uncorrelated process with respect to the typical time scales of the neural dynamics. In Fig. 3.12 we show $Y(t)$, produced by the discretized HMF dynamics with $M = 4525$ and for a Gaussian distribution $P(\tilde{k})$, with $\langle \tilde{k} \rangle = 0.7$ and $\sigma_{\tilde{k}} = 0.0455$. Curves of different colors correspond to different values of δ. We have found that up to $\delta \simeq 0.1$, i.e. also for non negligible noise amplitudes ($\bar{a} = 1$), the HMF dynamics is practically unaffected by noise. By further increasing δ, the amplitude of $Y(t)$ decreases, as a result of the desynchronization of the network induced by large amplitude noise.

Also the inversion procedure exhibits the same robustness with respect to noise. As a crucial test, we have solved the inverse problem to recover $P(\tilde{k})$ by injecting the noisy signal $Y(t)$ in the noiseless equations (3.19)–(3.21), where $a = \bar{a}$ (see Fig.3.12). The reconstructed distributions $P(\tilde{k})$, for different δ, are shown in Fig. 3.13. For relatively small noise amplitudes ($\delta < 0.1$) the recovered form of $P(\tilde{k})$ is quite close to the original

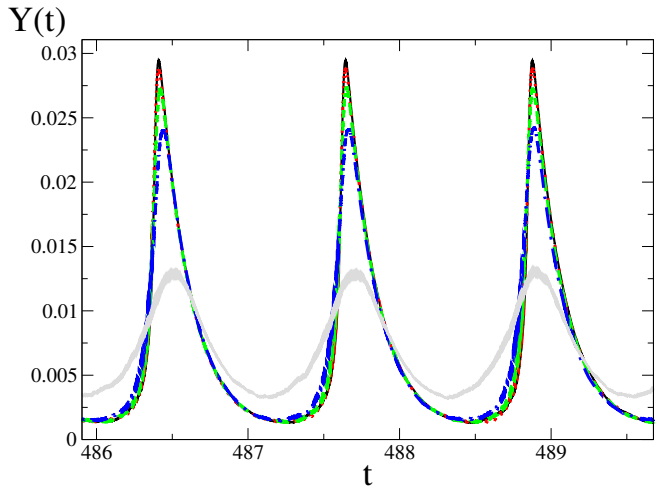

Figure 3.12: The global activity field $Y(t)$ of the HMF dynamics, sampled by $M = 4525$ classes of neurons, for a gaussian probability distribution $P(\tilde{k})$, with $\langle\tilde{k}\rangle = 0.7$ and $\sigma_{\tilde{k}} = 0.0455$. Lines of different colors and style correspond to different values of the noise amplitude, δ, added to the external currents $a_{\tilde{k}}(t)$. Notice that increasing δ decreases the peak of the curve. In particular, $\delta = 0$ (black continuous line), $\delta = 0.1$ (red dots), $\delta = 0.15$ (green segments), $\delta = 0.2$ (blue dots and segments) and $\delta = 0.3$ (grey continuous line) [71].

one, as expected because the noisy $Y(t)$ does not differ significantly from the noiseless one. On the contrary, for relatively large noise amplitudes ($\delta > 0.1$), the recovered distribution $P(\tilde{k})$ is broader than the original one and centered around a shifted average value $\langle\tilde{k}\rangle$. The dynamics exhibits much weaker synchrony effects, the same indeed one could observe for the noiseless dynamics on the lattice built up with this broader $P(\tilde{k})$ given by the inversion method.

As a matter of fact, the global neural activity fields obtained by experimental measurements are unavoidably affected by some level of noise. Accordingly, it is worth investigating the robustness of the inversion method also in the case of noise acting directly on $Y(t)$. In order to tackle this problem, we have considered a simple noisy version of the global synaptic activity field, defined as $Y_\delta(t) = (1 + \eta(t))Y(t)$, where the random number $\eta(t)$ is uniformly extracted, at each integration time step, in the interval $[-\frac{\delta}{2}, \frac{\delta}{2}]$.

In Fig. 3.14 we show the distributions $P(\tilde{k})$ obtained for different values of δ. We can conclude that the inversion method is quite stable with respect to this additive noise. In fact, even for very large signal–to–noise ratio (e.g. low–right panel of Fig. 3.14, where $\delta = 0.8$) the main features of

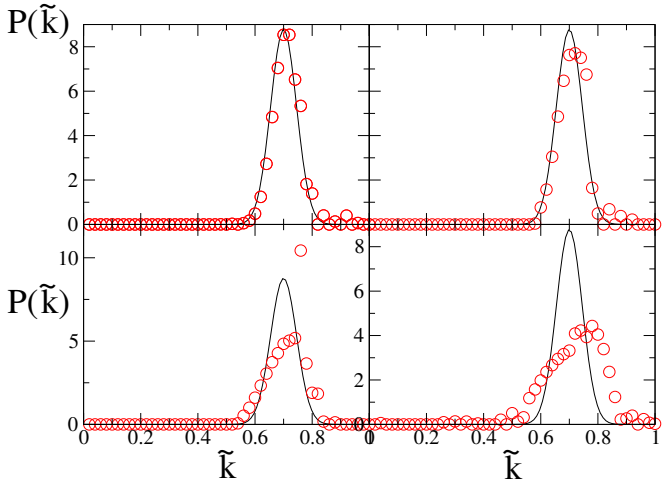

Figure 3.13: Solution of the inverse problem by the HMF equations in the presence of noise added to the external currents. We consider the same setup of Fig. 9 and we compare, for different values of the noise amplitude δ, the reconstructed probability distribution $P(\tilde{k})$ (red circles) with the original gaussian distribution (black line): the upper–left panel corresponds to the noiseless case ($\delta = 0$), while the upper–right, the lower–left and and the lower–right correspond to $\delta = 0.1, 0.2, 0.3$, respectively [71].

the original distribution are still recovered, within a reasonable approximation.

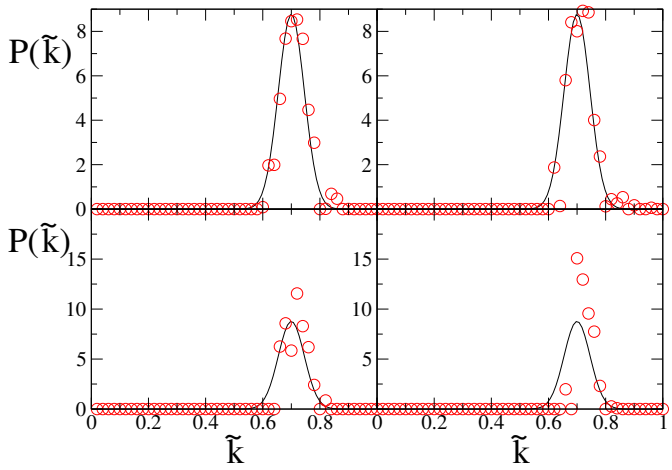

Figure 3.14: Solution of the inverse problem by the HMF equations in the presence of noise added to the activity field. We consider the same setup of Fig. 9, where now $a = 1$ and $Y_\delta(t) = (1-\eta(t))Y(t)$ (the random variable $\eta(t)$ is extracted from a uniform probability distribution in the interval $[-\delta/2, \delta/2]$). We compare, for different values of the noise amplitude δ, the reconstructed probability distribution $P(\tilde{k})$ (red circles) with the original gaussian distribution (black line): the upper–left, the upper–right, the lower–left and and the lower–right panels correspond to $\delta = 0.1, 0.4, 0.8, 1.2$, respectively [71].

CHAPTER 4

Extension of HMF and inverse problem: bursting behavior and inhibitory neurons

The heterogeneous mean field presented in previous section has turned to bee quite useful, specially for the possibility to solve a global inverse problem. The main idea is to keep track of the inhomogeneity responsible for the overall dynamics. Accordingly, this technique can be applied to different kinds of models of dynamical units on extended graphs. For example, Eq.(3.9) shows how one can follow the same method for different models in a similar setup where neurons are identical apart from diversity induced by disorder in network structure. Nevertheless, the idea can be used in different setups, where neurons are different because of non–topological inhomogeneities. In this Section we report two main examples, whose derivation comes from experimental observations of neural ensembles. The first one is the introduction of inhibitory neurons, that have been observed to play a crucial role in the dynamics of groups of neurons [73]. In this case the main difficulty to overcome is the dynamical role of synaptic plasticity that turns to be much more complicated (see Eq.s (1.17)–(1.20)). Nevertheless, even in this case a heterogeneous mean field approach can be applied and the resulting HMF model permits the formulation and solution of a global inverse problem. In this case the fraction of inhibitory neurons, the probability distribution of excitatory and inhibitory in degrees are reconstructed form the average signal of the overall network. Another example hereafter reported is the application of this method to the model described in Sec. 2.2. In this case the finite size dynamics is strongly influenced by statistical fluctuations and the overlap between HMF and finite size dynamics is not straightforward. Nevertheless, its application and the formulation of the inverse problem permits the reconstruction of the probability distribution of the disorder present in the network.

Accordingly, this chapter is divided in two man sections: Sec. 4.1 referring to the model with inhibitory neurons and Sec. 4.4 relative to the case of disorder on the excitability of neurons.

4.1 HMF for networks of inhibitory and excitatory neurons

Many of the brain activities emerge as the combined effect of excitatory and inhibitory components associated to synaptic plasticity [74]. In fact, neural networks in cortical area exhibit quite complex scale-free structures, where, typically, inhibitory neurons play the role of hubs [73], that control and moderate the action of excitatory neurons. It is well known that in mammalian brains the fraction of inhibitory neurons is close to 10-30%: it seems plausible to conjecture that such number should have been determined by evolutionary constraints, aiming at the effectiveness of brain functions. On the other hand, only recently it has been proposed a possible explanation of how such a rate between inhibitory and excitatory neurons is able to optimize the performances of a neural network [75]. All of these considerations indicate that models of neural networks aiming at reproducing a great deal of brain functions should take into account the presence of a proper fraction of excitatory and inhibitory neurons, organized on a suitable topological structure of the network. In this Section it is shown how one can generalize the HMF technique developed in previous chapter in test examples of network structures with inhibitory neurons. The finite size model needs to take under consideration the presence of a facilitation mechanism when inhibitory neurons are present in the network as described in Eq.s (1.17)–(1.20).

Let us define, also in this case, $\tilde{k} = k/N$ the rescaled in–degree, where $k \in [0, N-1]$. In general, inhibitory and excitatory neurons may have different in–degree connection distributions, namely $P_I(\tilde{k})$, $P_E(\tilde{k})$. In particular, $P_I(\tilde{k})$ or $P_E(\tilde{k})$ is the probability that an inhibitory or an excitatory neuron receives $\tilde{k}$ inputs from the other neurons of the network. In this setup we are making the assumption that inhibitory and excitatory neurons have typically the same number of outputs.

A possible way to construct realizations at size N with the determined probability distributions is the following. The network is composed by $f_I N$ inhibitory and $f_E N$ excitatory neurons, where f_I and f_E are the fractions of inhibitory and excitatory neurons in the network. For each neuron i, if it is excitatory we extract its rescaled in–degree from the distribution

$P_E(\tilde{k})$ and we assign randomly these $\tilde{k}_E N$ inputs. If it is inhibitory we use the same procedure using the distribution $P_I(\tilde{k})$.

For massive uncorrelated networks, we can generalize the result of the previous Chapter, so that the system in the thermodynamic limit is described by an heterogeneous mean field (HMF) model. In this case, anologously to the pure excitatory network, where the dynamics of each neuron only depend on its in-degree, we can expect the dynamics of a single neuron to be determined by two parameters only, namely its two in–degrees, received by inhibitory and excitatory neurons respectively (in Fig. 4.1 we will show that this is the case and the finite size dynamics can be well reproduced by the HMF model). These in-degrees encode all the relevant information on the adjacency matrix ϵ_{ij}. Even if obtained in the thermodynamic limit and for massive networks, the results of the HMF approach have been shown to hold in a much wider regime, and they are able to reproduce effectively the dynamics of a sparse uncorrelated network of large but finite size, as soon as the average degree is large enough, i.e. $k_i \gtrsim 50$.

Due to the randomness of the topology, the field received by a inhibitory neuron for $N \to \infty$ converges to $g\tilde{k}(-f_I Y_{II}(t) + f_E Y_{IE})$, where Y_{II} and Y_{IE} are the average fields produced respectively by inhibitory neurons on a generic inhibitory neuron, and by excitatory neurons on a generic inhibitory neuron. Consistently, the field received by a generic excitatory neuron converges to $g\tilde{k}(-f_I Y_{EI} + f_E Y_{EE})$. Thus, the dynamics of a neuron is characterized by its rescaled degree $\tilde{k}$ and its type, inhibitory I or excitatory E. Accordingly, its membrane potential dynamical equations read

$$\dot{v}^E_{\tilde{k}} = a - v^E_{\tilde{k}} + g\tilde{k}(-f_I Y_{EI}(t) + f_E Y_{EE}) \tag{4.1}$$

$$\dot{v}^I_{\tilde{k}} = a - v^I_{\tilde{k}} + g\tilde{k}(-f_I Y_{II}(t) + f_E Y_{IE}). \tag{4.2}$$

These equations determine the spike train of the considered class of neurons $S^{I/E}_{\tilde{k}}$. From this spike train, by denoting $(\cdot, *)$ one of the four ordered $I vs. E$ pairs, we can write the synaptic activity for each $(\cdot, *)$, where the presynaptic class $*$ has degree $\tilde{k}$. In this case we need to write dynamical

equations for each pair $(\cdot, *)$

$$\dot{y}_{\tilde{k}}^{(\cdot,*)} = -\frac{y_{\tilde{k}}^{(\cdot,*)}}{\tau_{\text{in}}} + u_{\tilde{k}}^{(\cdot,*)} x_{\tilde{k}}^{(\cdot,*)} S_{\tilde{k}}^{*} \tag{4.3}$$

$$\dot{x}_{\tilde{k}}^{(\cdot,*)} = \frac{z_{\tilde{k}}^{(\cdot,*)}}{\tau_{\text{r}}^{\cdot}} - u_{\tilde{k}}^{(\cdot,*)} x_{\tilde{k}}^{(\cdot,*)} S_{\tilde{k}}^{*} \tag{4.4}$$

$$x_{\tilde{k}}^{(\cdot,*)} + y_{\tilde{k}}^{(\cdot,*)} + z_{\tilde{k}}^{(\cdot,*)} = 1, \tag{4.5}$$

$$\tag{4.6}$$

where $u_{\tilde{k}}^{(\cdot,*)} = U$ if $\cdot$ is excitatory, otherwise

$$\dot{u}_{\tilde{k}}^{(\cdot,*)} = -\frac{u_{\tilde{k}}^{(\cdot,*)}}{\tau_{\text{f}}} + U_f\Big(1 - u_{\tilde{k}}^{(\cdot,*)}\Big) S_{\tilde{k}}^{*}. \tag{4.7}$$

Notice that the value of $\tau_{\text{r}}^{\cdot}$ depends from the $\cdot$ type of the postsynaptic terminal as well. The equations are closed by the global fields consistency:

$$Y_{\cdot,*} = \int_0^1 P_*(\tilde{k}) y_{\tilde{k}}^{(\cdot,*)} d\tilde{k}. \tag{4.8}$$

We introduce two global fields useful in the rest of the paper, i.e. the global field received by inhibitory neurons $Y_I = -f_I Y_{II}(t) + f_E Y_{IE}$, and that received by excitatory neurons $Y_E = -f_I Y_{EI}(t) + f_E Y_{EE}$.

4.2 The dynamical effects of inhibition

The different dynamics of synaptic activity, when postsynaptic neurons are inhibitory or excitatory, play a crucial role for the emergent collective behavior of the network. An interesting first insight on the global dynamics can be grasped directly from a simplified version of HMF equations. In particular, if the dynamics of the two types of synapses were the same, the presence of a certain fraction of f_I inhibitory neurons would have the same effect of $2f_I$ random cuts in the network links.

In fact, as the same presynaptic neuron would produces identical fields, both towards inhibitory or excitatory postsynaptic neurons, we would have $y_{\tilde{k}}^{E} = y_{\tilde{k}}^{I} = y_{\tilde{k}}$, where $y_{\tilde{k}}^{E/I}$ is the field produced by the class of neurons with degree $\tilde{k}$ towards a postsynaptic neuron of type E/I. Thus, the field received from inhibitory and excitatory neurons would be the same. Then, the field received by a neuron with degree $\tilde{k}$ is $g\tilde{k}\int_0^1 \Big[f_E P_E(\tilde{k}) -$

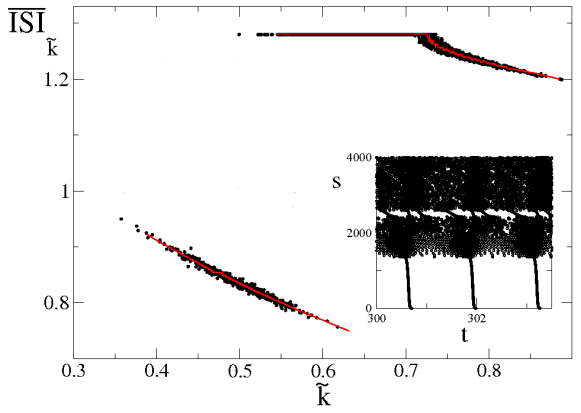

Figure 4.1: Average inter spike interval for a network of $N = 5000$ neurons (black dots) with $f_I = 0.1$ and related HMF dynamics (continuous line). The distributions P_I and P_E are Gaussians with $\langle \tilde{k}_I \rangle = 0.5$, $\langle \tilde{k}_E \rangle = 0.7$, $\tilde{\sigma}_I = 0.04$ and $\tilde{\sigma}_E = 0.056$. In the inset it is reported the raster plot for the HMF dynamics, notice that indexes such that $s \geq 2000$ represent inhibitory neurons. Furthermore, for each subgroup of inhibitory or excitatory neurons, neural indexe s has been ordered according to their connectivity $\tilde{k}$.

$f_I P_I(\tilde{k})\Big] y_{\tilde{k}}(t) d\tilde{k}$. If the term in square brackets has a definite sign, one can see that the network is equivalent to a completely inhibitory or excitatory (depending on the sign) network with an effective probability distribution $F(\tilde{k}) = \Big| f_E P_E(\tilde{k}) - f_I P_I(\tilde{k}) \Big|$. In particular, if $P_E = P_I$ the introduction of a fraction of inhibitory neurons f_I is equivalent to an effective dilution in the network, i.e. to perform $2f_I$ cuts of the links. If the term in square brackets has no definite sign, $F(\tilde{k})$ is not a probability distribution so that the real dynamics does not correspond to an equivalent model on a network of only excitatory or inhibitory neurons.

The global dynamics is much richer when the difference between excitatory and inhibitory neurons is fully taken into account, and this dynamics is well reproduced by the HMF approach. In Fig. 4.1 we report the comparison between finite size and mean field dynamics in a network with 10% of inhibitory neurons. In particular, we plot the average inter-spike interval ISI of each neuron as a function of the neuron in-degree $\tilde{k}_i$. Henceforth we fix the parameters of the model at phenomenological values [5]: $\tau_{\rm in} = 0.2$, $\tau_{\rm f} = 33.25$, $g = 30$ and $a = 1.3$. Excitatory neurons split in two families, namely periodic (locked) neurons, observed for $\tilde{k} < \langle \tilde{k} \rangle$, and aperiodic ones (unlocked) for $\tilde{k} > \langle \tilde{k} \rangle$. Inhibitory neurons fire with a higher frequency and are not periodic. Nevertheless, the global activity

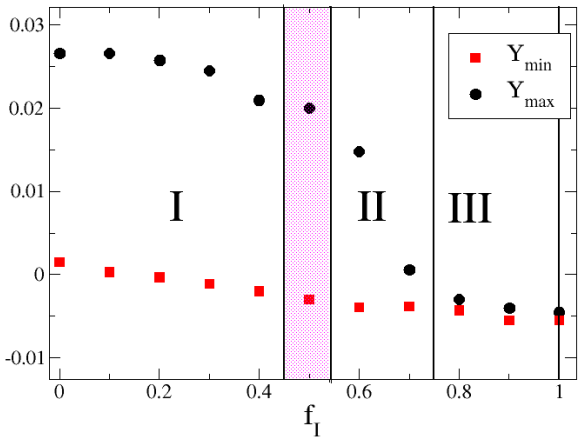

Figure 4.2: Maximum (black dots) and minimum (red squares) values of the global field $Y_E(t)$ as a function of the fraction on inhibitory neurons f_I. The distributions $P_{E/I}$ are the same of Fig. 4.1.

fields Y_E and Y_I show periodic oscillations, giving evidence of a level of synchrony supported by the presence of locked neurons [73]. In the inset we report the raster plot of the dynamics, putting into evidence the microscopic organization of neurons. On the ordinates it is reported the index of the firing neuron at time t and in abscissa the time t. Notice that the first half of indexes are excitatory and the second half are inhibitory. In both groups the indexes of neurons have been ordered according to their in–degree.

Let us now study the behavior of the model as a function of the fraction f_I of inhibitory neurons. At increasing f_I, the level of synchrony of the network decreases. In Fig. 4.2 we show that the global field Y_E tends to have a smaller excursion from its average. In fact, the more inhibitory neurons are present in the network, the more neurons are unsynchronized. In particular in Fig. 4.2 we plot the maximum (black dots) and minimum (red squares) values of the global field Y_E as a function of f_I. From this picture the dynamical phases of the model can be divided in three main regimes. In the first regime (regime I) the network is dominated by excitatory neurons. In first panel of Fig. 4.3 we plot the average inter spike interval as a function of $\tilde{k}$ for $f_I = 0.2$. We see that a great part of excitatory neurons are locked in phase yielding the QSE that one can see also in the inset of Fig. 4.1. The inhibitory neurons are

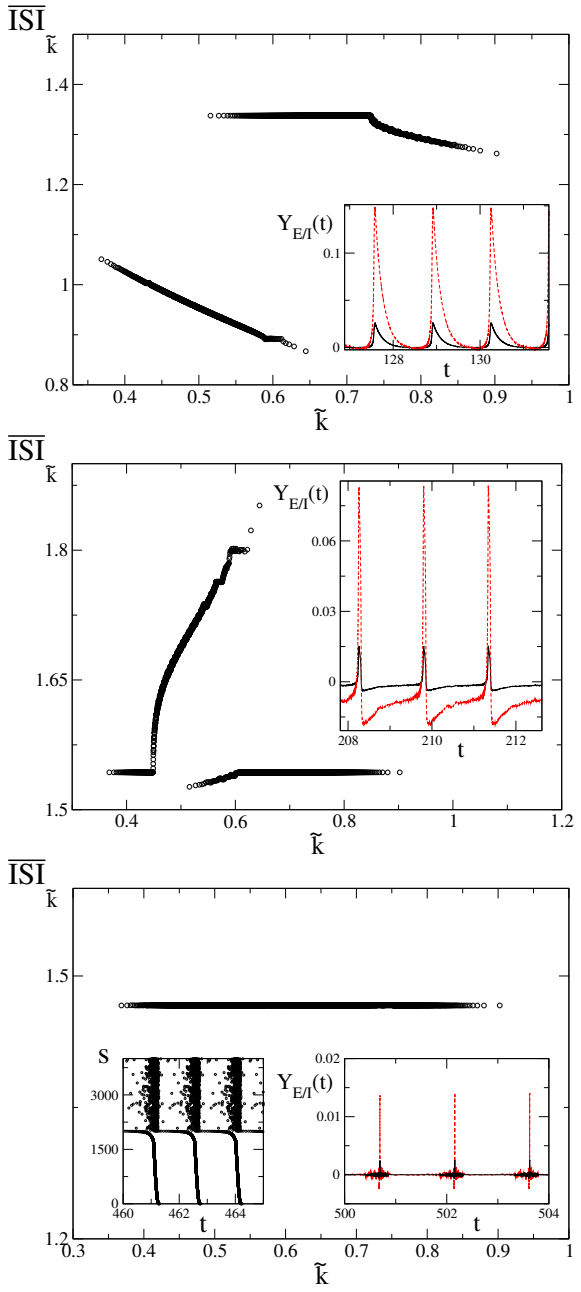

Figure 4.3: Network organization with different inhibitory fractions. In the upper panel it is reported the average inter spike interval for the HMF dynamics in presence of a fraction of 20% (black circles) of inhibitory neurons. In the inset we show the field received by an inhibitory neuron (red dashed curve) and by an excitatory neuron (black continuous curve). In the lower panels we observe the same plot for a network with a fraction $f_I = 0.6$ and $f_I = 0.5$ of inhibitory neurons. The raster plot of the dynamics is reported for the case $f_I = 0.5$ on the left inset of the last panel. The distributions P_I and P_E are Gaussians with $\langle \tilde{k}_I \rangle = 0.5$, $\langle \tilde{k}_E \rangle = 0.7$, $\tilde{\sigma}_I = 0.04$ and $\tilde{\sigma}_E = 0.056$.

mainly unlocked in phase and fire at a lower frequency. In the inset we plot the global field received by an excitatory and a inhibitory neuron, where we can see that the two fields are both positive and that the field received by inhibitory neurons is higher as a direct consequence of the facilitation mechanism that increases the synaptic efficiency during fast firing activity. When the network is dominated by inhibitory neurons one observes two dynamical phases. For very high values of f_I (regime III) one observes an asynchronous phase where the global fields do not show oscillations. For sufficiently low fraction of inhibitory neurons (regime II) one still observes partial synchronization with QSE. Nevertheless, see second panel of Fig. 4.3, the microscopic organization is different from region I. By looking at the inset it can be seen that inhibitory neurons receive a more intense field at each time t but now this field has great excursion to negative values. Accordingly inhibitory neurons are not faster then excitatory neurons anymore. In particular, some inhibitory neurons lock at the same frequency of excitatory neurons but the unlocked group of inhibitory neurons fires now at a lower frequency (just compare the two first panels of Fig. 4.3). At the edge between these different phases there is a optimal balance between excitatory and inhibitory neurons where the dynamics is different. The dynamical phase of this region (dashed in Fig. 4.2) is summerized in the third panel of Fig. 4.3. We can see in the inset the Y_E and Y_I are mostly fluctuating around zero apart from very narrow peaks of activity. In this regime all neurons, either excitatory and inhibitory, are pririodic with the same firing frequency. Nevertheless the organization of the spiking time of neurons is non trivial (see the raster plot inside the third panel of Fig. 4.3). There are some neurons firing in a short time interval, i.e. their phases differ for a short time lapse. These neurons give rise to a QSE that appears when we observe the peaks of the field Y_E and Y_I. Other neurons fire in between two consecutive QSE but, at variance to the cases before examined, are still periodic of the same period of the neurons taking part to the QSE. Accordingly in this balanced case, collective oscillations arise thanks to a complex organization of the phases of periodic neurons.

4.3 A relation between global excitatory and inhibitory fields

As we have seen, due to the different dynamics of inhibitory and excitatory synapses, the spike train emitted by inhibitory and excitatory neurons is different, as they receive different fields. As a consequence, the field generated by excitatory and inhibitory neurons is different, even if

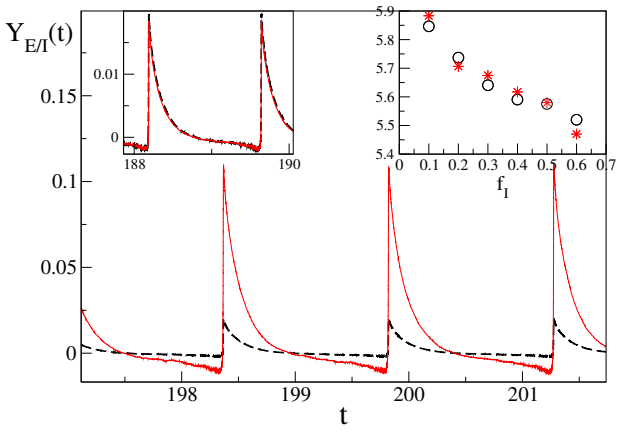

Figure 4.4: Time evolution of $Y_I(t)$ (red continuos line) and $Y_E(t)$ (black dashed line). In the inset on the left the field $Y_I(t)$ has been rescaled using the common period of the global fields and the factor obtained analytically (see text). In the inset on the right we show the comparison between the scale factor deduced from simulations (black circles) and that obtained analytically (red stars).

the postsynaptic terminal is of the same type. Thus, one has to consider the four different fields $Y_{EI}(t)$, $Y_{IE}(t)$, $Y_{II}(t)$ and $Y_{EE}(t)$.

Nevertheless, we can consider two main global fields received by neurons with a certain degree, namely Y_E and Y_I, that are the global fields received by excitatory and inhibitory neurons respectively.

Fig. 4.4 displays such fields, as obtained from a simulation of the HMF model. We observe that, apart from fluctuations, these fields have the same shape once rescaled by a factor (see the inset in Figure). Neurons taking part in the generation of these two fields are the same, namely all neurons with certain degree $\tilde{k}$, properly weighted with the distributions P_E and P_I. The difference lies in the different synaptic dynamics of u, that comes into play at the firing event when the postsynaptic neuron is inhibitory or excitatory. Thus, in between two spikes of the network, the fields Y_I and Y_E follow the same dynamics, i.e. an exponential decay with the same time constant τ_{in}. With these observations, it is possible to obtain a scaling of the two fields with an heuristic argument, based on the different dynamical equations of the synaptic coupling when postsynaptic terminal is inhibitory or excitatory.

Let us consider a specific neuron (excitatory or inhibitory) that, ruled by its spike train, generates postsynaptic fields $y^E(t)$ or $y^I(t)$ depending on postsynaptic terminal. Suppose this neuron emits spikes at a constant piece as locked neurons do (actually with the same period of the global

fields), i.e. its synaptic activity fields are periodic of period T. By looking at Eq.s (4.3)–(4.7) one can impose the periodic solution and find out the relative field $y^{E/I,*}(t)$. The dynamics of $y^{E,*}(t)$ and $y^{I,*}(t)$ is the same apart from a rescaling as, by construction $y^{E/I,*}(t) = y^{E/I,*}(t+T)$ and in between two consecutive spikes the dynamics is just an exponential decay with the same exponent τ_{in}. The solution can be obtained by integrating the equations over time T and imposing the existence of fixed point $(\tilde{y}^{E/I,*}, \tilde{z}^{E/I,*}, \tilde{u}^{E/I})$. The resulting equations are:

$$\tilde{y}^{E,*} = \frac{U}{1 - e^{-\frac{T}{\tau_{\text{in}}}}\left(1 + U + \frac{U\tau_{\text{r}}^E}{\tau_{\text{r}}^E - \tau_{\text{in}}}\right)\left(e^{-\frac{T}{\tau_{\text{r}}^E}} e^{\frac{T}{\tau_{\text{in}}}} - 1\right)} \tag{4.9}$$

$$\tilde{y}^{I,*} = \frac{\tilde{u}^I}{1 - e^{-\frac{T}{\tau_{\text{in}}}}\left(1 + \tilde{u}^I + \frac{\tilde{u}^I\tau_{\text{r}}^I}{\tau_{\text{r}}^I - \tau_{\text{in}}}\right)\left(e^{-\frac{T}{\tau_{\text{r}}^I}} e^{\frac{T}{\tau_{\text{in}}}} - 1\right)} \tag{4.10}$$

$$\tilde{u}^I = U_f \frac{e^{-\frac{T}{\tau_f}}}{1 - e^{-\frac{T}{\tau_f}} + U_f e^{-\frac{T}{\tau_f}}}. \tag{4.11}$$

For locked neurons displaying the same periodicity T of the global fields, Equations (4.9-4.11) provide the proportionality constant relating the local fields $y_{\tilde{k}}^{E/I,*}(t)$; since the main contribution to the global signals is given by locked neurons, we expect that the global fields $Y^E(t)$ and $Y^I(t)$ display the same proportionality relation. The panels of Fig. 4.4 show indeed that numerical simulations confirm the estimated prediction for the ratio between $Y^E(t)$ and $Y^I(t)$. We point out that this argument applies in the regimes of collective oscillations studied in this paper, where neurons are typically periodic or quasi–periodic.

4.3.1 Inverse problem

The HMF model permits the formulation and the solution of a global inverse problem. In general, in experiments one has more easily access to global fields. Accordingly we suppose to measure the global field received by neurons, i.e. $Y(t) = f_E Y_E(t) + f_I Y_I(t)$. The unknown parameters are the distributions $P_E(\tilde{k})$, $P_I(\tilde{k})$ and f_I.

Using the proportionality constant evaluated in the previous section one can, by evaluating the periodicity of $Y(t)$, write the fields $Y_E(t)$ and $Y_I(t)$ as a function of $Y(t)$ and of the unknown fraction f_I. Therefore, for each value of f_I one obtains a local field $y_{\tilde{k}}^{(*,\cdot)}(t, f_I)$ by solving the equations (4.1)–(4.7).

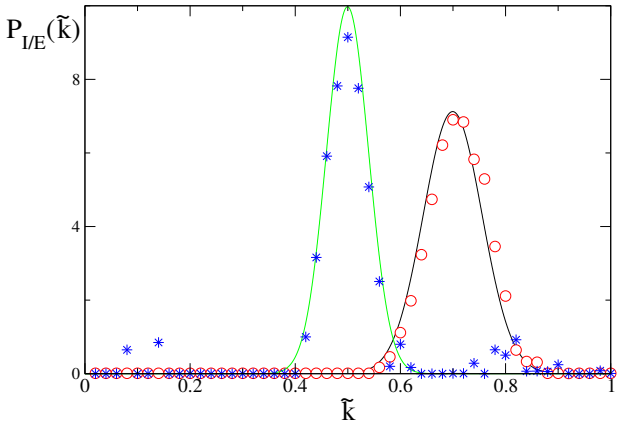

Figure 4.5: Reconstruction of $P_E(\tilde{k})$ and $P_I(\tilde{k})$ for the network of Fig. 4.1. Continuous curves are the expected distributions while red circles (excitatory neuronss) and blue stars (inhibitory neurons) are the reconstruction obtained with the self–consistent equation.

One can then reconstruct the global filed

$$\tilde{Y}_*(t) = \int_0^1 P_*(\tilde{k}) \mathrm{y}_{\tilde{k}}^{(\cdot,*)}(t, f_I) d\tilde{k}, \tag{4.12}$$

then $\tilde{Y}_*(t) = -f_I \tilde{Y}_{*I} + f_E \tilde{Y}_{*E}$ and $\tilde{Y}(t) = f_E \tilde{Y}_E(t) + f_I \tilde{Y}_I(t)$. Clearly the field $\tilde{Y}(t)$ depends on the choice of the parameters to be inverted, i.e. the distributions $P_E(\tilde{k})$, $P_I(\tilde{k})$ and f_I. Therefore one can obtain the best estimate for $P_E(\tilde{k})$, $P_I(\tilde{k})$ and f_I by minimizing the quantity

$$\frac{1}{t_1 - t_0} \int_{t_0}^{t_1} (\tilde{Y}(t) - Y(t))^2 dt \tag{4.13}$$

where $[t_0, t_1]$ is the time interval where $Y(t)$ is known and the minimization procedure can be achieved by means of a zero temperature Montecarlo algorithm (as in the purely excitatory case, see Appendix A). In Fig. 4.5 we show the reconstruction of the two distributions in the case of Fig. 4.1. The procedure reconstructs pretty well the distributions and the fraction of inhibitory neurons $f_I = 0.1$.

This analysis shows how one can invert global signals in the case of network with inhibitory neurons. Nevertheless, this method can be applied to more realistic situations where inhibitory neurons are the hubs of a scale free distribution of connectivities, as observed in experiments [73].

4.4 Bursting regime dynamics

In this last section we discuss the possibility to apply the heterogeneous mean field approach to the model presented in Sec. 2.2 where disorder is present on the leakage currents a. In this regime neurons are not periodic and the dynamics is characterized by quite long silent periods separated by bursts where all neurons fire more then once in short time intervals. The time interval between two consecutive bursts do not show any regularity and is distributed according to a long tail distribution. Let us consider a globally excitatory coupled network where the excitability a of neurons is distributed according to a distribution $P(a)$. As done for the HMF for random networks, where disorder was set on the specific connectivity $\tilde{k}$ of neurons, also in this case we can write a dynamical equation for every class of neurons sharing the same excitability a. Accordingly, the

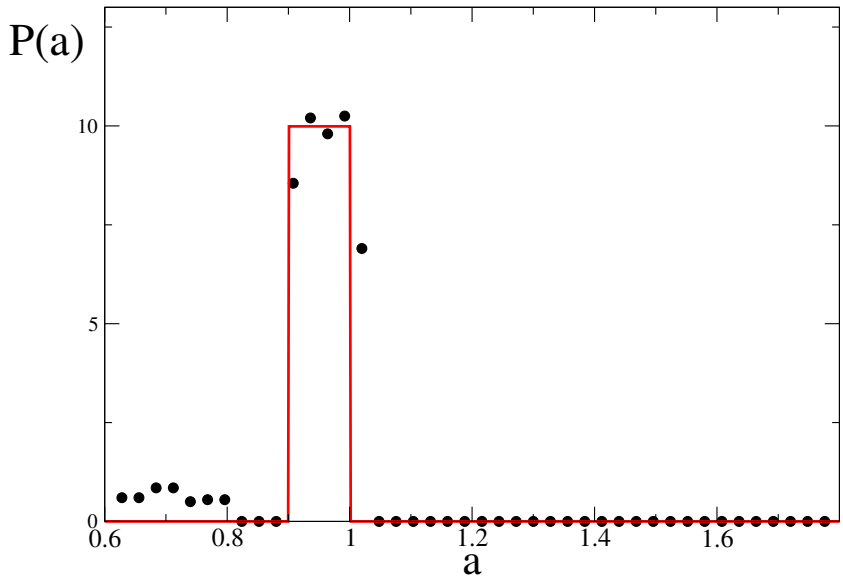

Figure 4.6: Reconstruction of $P(a)$ from a network of $N = 500$ neurons. Red curve is the original uniform distribution of $P(a)$ with $a \in [0.9005, 1, 0006]$ and black dots are the reconstruction. The network is globally coupled and the parameters are the same of Fig. 2.11.

HMF model in this case reads

$$\dot{v}_a = a - v_a + gY \tag{4.14}$$

$$\dot{y}_a = -\frac{y_a}{\tau_{\text{in}}} + ux_a S_a \tag{4.15}$$

$$\dot{z}_a = \frac{y_a}{\tau_{\text{in}}} - \frac{z_a}{\tau_{\text{r}}} \tag{4.16}$$

$$Y = \int P(a) y_a da, \tag{4.17}$$

where a is a continuous variable defined in the set of real numbers (then the distribution $P(a)$ selects the values of a to take into account).

In order to observe the PB dynamical phase we are interested in, let us choose a uniform distribution in the interval $[0.9005, 1.006]$, where the network dynamics is described in Fig. 2.11. Even if the HMF model is able to reproduce qualitatively the finite size dynamics (i.e. the presence of PB alternating seconds of silence), finite size fluctuations are fundamental for the exponent characterizing the distribution of the IPBI (i.e. the time in between two consecutive peaks of global activity Y, see Fig. 2.11). This point is still under investigation and needs further improvements that will be reported in future works. Nevertheless, the HMF formulation permits us to formulate the inverse problem, i.e. the reconstruction of $P(a)$ given the global field $Y(t)$ deriving from finite size network dynamics. The procedure works in the same way described for the reconstruction of $P(\tilde{k})$ in the fully excitatory case (see Sec.3.4 and Appendix A). In Fig. 4.6 we show the reconstruction from a series of around 100 seconds, where three peaks of activity appear. We see that the inversion procedure, based on the HMF equations is able to reconstruct confidently the distribution. From this result it seems that the information relying in few peaks of the global signal is sufficient for the self consistency equation 4.17 to produce the exact result. This point needs to be further investigated but these results confirm the power of the HMF to reconstruct the distribution of network disorder.

General Conclusions

In this thesis we have investigated a model for neural dynamics that turned out to be able to generate a rich variety of dynamical phases. The minimal model taken under consideration, made up of purely excitatory neurons, yields non trivial synchronization patterns typically observed in experimental setups. In fact, the only introduction of disorder in neurons connections is sufficient to generate a dynamical phase where collective oscillations arise as a result of specific microscopic organization. Neurons divide in two families, mainly on the basis of their in–degree, showing different dynamical behavior. Locked neurons are periodic and emit spikes almost synchronously while unlocked neurons are aperiodic and not synchronized with the rest of the network. Furthermore, the introduction of disorder on excitability of neurons is able to yield a completely different dynamical regime observed in in–vitro setups where bursts of spiking neurons alternate with very long periods of silence. The collective field does not show any regularity anymore and the time lapse in between two consecutive bursts is distributed according to a long tail distribution. Taking first under consideration the model with disorder on network topology made up of excitatory neurons, it has been proposed a mean field model able to capture the finite size dynamics that represents the time evolution of a real sample. Such a mean field model, called heterogeneous mean field as it keeps track of the disorder present in the neural ensemble, permits a clearer understanding of the overall dynamics. In particular, a stability analysis, impossible on the finite size model, provides a quite clear picture on the microscopic level. The neurons in–degree plays the role of a bifurcation parameter determining the dynamics of single units that organize in such a way to give rise to global os-

cillations. Furthermore, the probability distribution of in–degrees determines the synchronization pattern of the network and, accordingly, the dynamics of the global activity field. In particular, when the distribution is too broad, the network falls in an asynchronous regime where the average electric field does not show oscillations anymore. The heterogeneous mean field applied to the model we have taken under consideration is quite complex to be solved analytically and it has not permitted us a analytical picture of the dependence of the global field on the distribution of in–degrees. This point is going to be addressed in future works, applying this approach to different models where the dynamical equations can be solved analytically [61].

The generality of the method makes this mean field procedure able to be applied to different models. Accordingly, in the last chapter, we have shown how this procedure applies to network of excitatory and inhibitory neurons and to ensembles where disorder is applied on excitability of neurons.

A great advantage of the heterogeneous mean field has been the possibility to recover the disorder probability distributions from the knowledge of the global activity field, that is the observable more easily measured in experiments. Its robustness with respect to different neural model is a natural continuation of this work and is functional in order to compare our results with experimental data. Nevertheless, as the inversion is based on the knowledge of global signals, one can expect that the result does not depend crucially on the detail of the single unit dynamics, at variance with local approaches to inverse problem where the exact network structure of the network is reconstructed from single neurons records.

Appendices

APPENDIX A

Inversion procedure for excitatory neurons

In this appendix we provide details of the algorithmic procedure adopted for solving the inverse problem, i.e. reconstructing the distribution $P(\tilde{k})$ from Eq. (3.22). In the HMF formulation, the field $Y(t)$ is generated by an infinite number of neurons and $\tilde{k}$ is a continuous variable in the interval $(0, 1]$. In practice, we can sample uniformly this unit interval by L disjoint subintervals of length $1/L$, labelled by the integer i. This corresponds to an *effective neural index* i, that identifies the class of neurons with in-degree $\tilde{k}_i = i/L$. In this way we obtain a discretized definition converging to Eq.(3.22) for $L \to \infty$:

$$Y(t) = \int_0^1 P(\tilde{k}) \mathsf{y}_{\tilde{k}}(t) d\tilde{k} \simeq \frac{1}{L} \sum_{i=0}^{L-1} P(\tilde{k}_i) \mathsf{y}_{\tilde{k}_i}(t) \ . \tag{A.1}$$

In order to improve the stability and the convergence of the algorithm by smoothing the fluctuations of the fields $\mathsf{y}_{\tilde{k}_i}(t)$, it is convenient to consider a coarse–graining of the sampling by approximating $Y(t)$ as follows

$$Y(t) = \frac{1}{L'} \sum_{i=0}^{L'-1} P(\tilde{k}_i) \langle \mathsf{y}_{\tilde{k}_i}(t) \rangle. \tag{A.2}$$

where $\langle \mathsf{y}_{\tilde{k}_i}(t) \rangle$ is the average of L/L' synaptic fields of connectivity $\tilde{k} \in [\tilde{k}_i, \tilde{k}_{i+1}]$. This is the discretized Fredholm equation that one can solve to obtain $P(\tilde{k}_i)$ from the knowledge of $\langle \mathsf{y}_{\tilde{k}_i}(t) \rangle$ and $Y(t)$. For this aim we use a Monte Carlo (MC) minimization procedure, by introducing at each MC step, n, a trial solution, $P_n(\tilde{k}_i)$, in the form of a normalized non-negative in-degree distribution. Then, we evaluate the field $Y_n(t)$ and the distance

γ_n defined as:

$$Y_n(t, P_n(\tilde{k}_i)) = \frac{1}{L'} \sum_{i=0}^{L'-1} P_n(\tilde{k}_i) \langle \mathsf{y}_{\tilde{k}_i}(t) \rangle \tag{A.3}$$

$$\gamma_n(P_n(\tilde{k}_i))^2 = \frac{1}{t_2 - t_1} \int_{t_1}^{t_2} \frac{\Big[Y_n(t, P_n(\tilde{k}_i)) - Y(t) \Big]^2}{Y^2(t)} dt \ . \tag{A.4}$$

The time interval $[t_1, t_2]$ has to be taken large enough to obtain a reliable estimate of γ_n. For instance, in the case shown in Fig.3.2, where $Y(t)$ exhibits an almost periodic evolution of period $T \approx 1$ in the adimensional units of the model, we have used $t_2 - t_1 = 10$. The overall configuration of the synaptic fields, at iteration step $n+1$, is obtained by choosing randomly two values $\tilde{k}_j$ and $\tilde{k}_l$, and by defining a new trial solution $\bar{P}_{n+1}(\tilde{k}) = P_n(\tilde{k}) + \epsilon \delta_{\tilde{k},\tilde{k}_j} - \epsilon \delta_{\tilde{k},\tilde{k}_l}$, so that, provided both $\bar{P}_{n+1}(\tilde{k}_j)$ and $\bar{P}_{n+1}(\tilde{k}_l)$ are non-negative, we increase and decrease $P_n(\tilde{k}_j)$ of the same amount, ϵ, in $\tilde{k}_j$ and $\tilde{k}_l$ respectively. A suitable choice is $\epsilon \sim \mathcal{O}(10^{-4})$. Then, we evaluate $\gamma_{n+1}(\bar{P}_{n+1}(\tilde{k}_i))$: If $\gamma_{n+1}(\bar{P}_{n+1}(\tilde{k}_i)) < \gamma_n(P_n(\tilde{k}_i))$ the step is accepted i.e. $P_{n+1} = \bar{P}_{n+1}$, otherwise $P_{n+1} = P_n$. This MC procedure amounts to the implementation of a *zero temperature dynamics*, where the cost function $\gamma_n(P_n(\tilde{k}_i))$ can only decrease. In principle, the inverse problem in the form of Eq.(A.2) is solved, i.e. $Y_n(t, P_n(\tilde{k}_i)) = Y(t)$, if $\gamma_n(P_n(\tilde{k}_i)) = 0$. In practice, the approximations introduced by the coarse-graining procedure do not allow for a fast convergence to the exact solution, but $P_n(\tilde{k}_i)$ can be considered a reliable reconstruction of the actual $P(\tilde{k})$ already for $\gamma_n < 10^{-2}$. We have checked that the results of the MC procedure are quite stable with respect to different choices of the initial conditions $P_0(\tilde{k}_i)$, thus confirming the robustness of the method. We give in conclusion some comments on the very definition of the coarse-grained synaptic field $\langle \mathsf{y}_{\tilde{k}_i}(t) \rangle$. Since small differences in the values of $\tilde{k}_i$ reflect in small differences in the dynamics, for not too large intervals $[\tilde{k}_i, \tilde{k}_{i+1}]$ the quantity $\langle \mathsf{y}_{\tilde{k}_i}(t) \rangle$ can be considered as an average over different initial conditions. For locked neurons the convergence of the average procedure defining $\langle \mathsf{y}_{\tilde{k}_i}(t) \rangle$ is quite fast, since all the initial conditions tend to the stable fixed point, identified by the return map described in the previous subsection. On the other hand, the convergence of the same quantity for unlocked neurons should require an average over a huge number of initial conditions. For this reason, the broader is the distribution, i.e. the bigger is the unlocked component (see Fig.3.7), the more computationally expensive is the solution of the inverse problem. This numerical drawback for

broad distributions emerges in our tests of the inversion procedure described in Fig. 3.11. Moreover, such tests show that the procedure works insofar the QSE are not negligible, but it fails in the absence of the locking mechanism. In this case, indeed, the global field $Y(t)$ is constant and also $\langle \mathsf{y}_{\tilde{k}_i}(t) \rangle$ become constant, when averaging over a sufficiently large number of samples. This situation makes Eq.(A.2) trivial and useless to evaluate $P(\tilde{k}_i)$. We want to observe that, while in general $\mathsf{y}_{\tilde{k}_i}(t) \neq y_{\tilde{k}_i}(t)$, one can reasonably expect that $\langle \mathsf{y}_{\tilde{k}_i}(t) \rangle$ is a very good approximation of $\langle y_{\tilde{k}_i}(t) \rangle$. This remark points out the conceptual importance of the HMF formulation for the possibility of solving the inverse problem.

Bibliography

[1] D. de Santos–Sierra, I. Sendina–Nadal, I. Leyva, J. A. Almendral, S. Anava, A. Ayali, D. Papo, and S. Boccaletti, PLoS ONE 9(1): e85828 (2014).

[2] V. Volman, I. Baruchi, E. Persi e E. Ben-Jacob, Physica A **335**, 249 (2004).

[3] Hidalgo J, Seoane LF, Cortés JM, Muñoz MA, PLoS ONE **7(8)**, e40710 (2012).

[4] J. F. Mejias, H. J. Kappen and J. J. Torres, PLoS ONE 5(11), e13651 (2010).

[5] M. Tsodyks, A. Uziel and H. Markram, The Journal of Neuroscience 20, RC1 (1-5) (2000).

[6] A. Barrat, M. Bartelemy, and A. Vespignani, *Dynamical Processes on Complex Networks* Cambridge University Press, Cambridge, (2008).

[7] Pastor-Satorras, R. & Vespignani, Phys. Rev. Lett. **86**, 3200 (2001).

[8] A. Vespignani, Nature Physics **8**, 39 (2012).

[9] Shneidman, E., Berry, M.J., Segev, R. & Bialek, Nature **440**, 1007 (2006)

[10] Cocco, S., Leibler, S. & Monasson, R., R. Proc. Natl. Acad. Sci. U.S.A. **106**, 14058 (2009).

[11] Shandilya, S.G. & Timme, M., New J. Phys. **13**, 013004 (2011).

[12] Zheng, H.L., Alava, M., Aurell, E., Hertz, J. & Roudi, Y., Phys. Rev. Lett. **110**, 210601 (2013).

[13] Huettel S. A., Song A. W. and McCarthy G. *Functional Magnetic Resonance Imaging* (2 ed.), Massachusetts: Sinauer, (2009).

[14] Niedermeyer E. and da Silva F.L. *Electroencephalography: Basic Principles, Clinical Applications, and Related Fields.* Lippincot Williams & Wilkins (2004).

[15] Tanzer Oguz I. *Numerical Modeling in Electro- and Magnetoencephalography*. Ph.D. Thesis. Helsinki University of Technology (2006).

[16] Hamill OP, Marty A, Neher E, Sakmann B, Sigworth FJ., Pflugers Archiv European Journal of Physiology 391 (2): 85–100 (1981).

[17] Pelvig DP, Pakkenberg H, Stark AK, Pakkenberg B, *Neocortical glial cell numbers in human brains*. Neurobiology of Aging 29 (11): 1754–1762 (2008).

[18] Kandel E.R., Schwartz J.H., Jessell T.M., *Principles of Neural Science* (4th ed.), McGraw-Hill, New York (2000).

[19] Harvey Lodish, Arnold Berk, S Lawrence Zipursky, Paul Matsudaira, David Baltimore, and James Darnell, *Molecular Cell Biology* (4–th ed.), New York: W. H. Freeman (2000).

[20] Haas L F, Journal of Neurology, Neurosurgery & Psychiatry 74 (1) (2003).

[21] Srinivasan Ramesh, International Journal 1 (1): 102–11 (1999).

[22] Nunez PL, Srinivasan R., *Electric fields of the brain: The neurophysics of EEG*, Oxford University Pres (1981).

[23] Jaakko Malmivuo and Robert Plonsey, *Bioelectromagnetism*, Oxford University Press, New York, (1995).

[24] Boven K–H, Fejtl M, Moller A, Nisch W, Stett A., *On Micro-Electrode Array Revival*, Baudry M, Taketani M, eds. Advances in Network Electrophysiology Using Multi-Electrode Arrays. New York: Springer Press (2006).

[25] Raichman, N., and Ben–Jacob, E., J. Neurosci. Methods 170, 96–110 (2008).

[26] Pikovsky, Arkady, Michael Rosenblum, and Jurgen Kurths, *Synchronization, a universal concept in nonlinear sciences* Self 2 (2001): 3.

[27] Diestel Reinhard, *Graph Theory* (3rd ed.). Berlin, New York: Springer-Verlag (2005).

[28] Bollobás B. *Random Graphs* Academic Press; London (1985).

[29] M. E. J. Newman, S. H. Strogatz, and D. J. Watts, Phys. Rev. E 64, 026118 (2001).

[30] Erdős–Rényi, *The evolution of random graphs*, Magyar Tud. Akad. Mat. Kutató Int. Kozl. 5: 17–61 (1960).

[31] Albert, R'eka, and Albert-László Barabási, Reviews of modern physics 74.1: 47 (2002).

[32] Chung, F., Lu, L. *Complex Graphs and Networks*, CBMS Series in Mathematics, AMS (2004).
[33] Baker P. F., A. L. Hodgkin, and T. I. Shaw, The Journal of physiology 164.2 : 355 (1962).
[34] Hodgkin A. and Huxley A., J. Physiol. (1952).
[35] Eugene M. Izhikevich, *Dynamical Systems in Neuroscience*, Massachusetts Institute of Technology, (2007).
[36] Morris C. and Lecar H., Biophys. J. 35. (1981).
[37] L. Lapicque, J. Physiol. Pathol. Gen. 9, 620 (1907).
[38] S. Luccioli, T. Kreuz and A. Torcini, Phys. Rev. E 73, 041902 (2006).
[39] Hormuzdi SG, Filippov MA, Mitropoulou G, Monyer H, Bruzzone R, Biochim. Biophys. Acta 1662 (1–2): 113–37 (2004).
[40] Bullock, TH, Orkand, R; Grinnell, A, *Introduction to Nervous Systems. A series of books in biology*, San Francisco: W. H. Freeman (1977).
[41] Llinás R, Steinberg IZ, Walton K,. Biophysical Journal 33 (3): 323–351 (1981).
[42] Bear, Mark F., Barry W. Connors, and Michael A. Paradiso, eds. Neuroscience. Vol. 2. Lippincott Williams & Wilkins, (2007).
[43] Elias, L. J, & Saucier, D. M., *Neuropsychology: Clinical and Experimental Foundations*, Boston: Pearson (2005).
[44] Abeles M., *Corticonics*, New York: Cambridge UP (1991).
[45] Gaiarsa, J.L.; Caillard O., and Ben-Ari Y., Trends in Neurosciences 25 (11): 564–570 (2002).
[46] Hebb, D.O., *The Organization of Behavior*, New York: Wiley & Sons (1949).
[47] C. Koch, *Biophysics of computation*, Oxford University Press, New York (2004).
[48] Tsodyks M, Markram H,Proc Natl Acad Sci USA 94:719 –723 (1997).
[49] Markram H, Wang Y, Tsodyks M, Proc Natl Acad Sci USA 95:5323–5328 (1999).
[50] S. Olmi, R. Livi, A. Politi, A. Torcini, Phys. Rev. E 81 046119 (2010).
[51] C-C. Chen and D. Jasnow, Phys. Rev. E 84, 031908 (2011).
[52] M. di Volo, R. Livi, S. Luccioli, A. Politi and A. Torcini, Phys. Rev. E 87, 032801 (2013).
[53] C. van Vreeswijk, L.F. Abbott, and G. Bard Ermentrout, J. Comp. Neuroscience 1 313-321 (1994).
[54] D. Hansel and G. Mato and C. Meunier, Neural Computation 7, 307 (1995).

[55] A. Pikovsky, O. Popovych and Yu. Maistrenko, Phys. Rev. Lett. 87, 044102 (2001).

[56] M. Tsodyks, I. Mitkov, and H. Sompolinsky, Phys. Rev. Lett. 71, 1280-1283 (1993).

[57] R. Zillmer, R. Livi, A. Politi, and A. Torcini, Phys. Rev. E 76, 046102 (2007).

[58] C. van Vreeswijk, Phys. Rev. E 54 5522-5537 (1996).

[59] S. Olmi, A.Politi, and A. Torcini, Frontiers in Computational neuroscience (2014).

[60] Raffaella Burioni, Serena di Santo, Matteo di Volo, and Alessandro Vezzani, Phys. Rev. E 90, 042918 (2014).

[61] Y. Kuramoto, *Chemical oscillations, waves, and turbulence*, Dover Publications (2003).

[62] S. Luccioli, S. Olmi, A. Politi and A. Torcini, Phys. Rev. Lett. 109, 138103 (2012).

[63] G. Benettin, L. Galgani, A. Giorgilli and J.M. Strelcyn, Meccanica 15, 21 (1980).

[64] J. L. Kaplan and J. A. Yorke, *Chaotic behavior of multidimensional difference equations in Functional Differential Equations and Approxi-mation of Fixed Points*, Lect. Not. Math. 13, 730 (1979).

[65] Segev R, Shapira Y, Benveniste M, Ben-Jacob E, Phy Rev E 64:011920-1–9 (2001).

[66] Beggs JM, Plenz D., J. Neurosci. 23(35):11167–77 (2003).

[67] L. de Arcangelis, C. Perrone–Capano and Hans J. Herrmann, Phys. Rev. Lett. **96**, 028107 (2006).

[68] E. Tagliazucchi & D.R. Chialvo, *The collective brain is critical.* (2011) .

[69] M. di Volo and R. Livi, J. of Chaos Solitons and Fractals 57, 54–61 (2013).

[70] R. Burioni, M. di Volo, M. Casartelli, R. Livi and A. Vezzani, Scientific Reports 4, 4336 (2014).

[71] M. di Volo, R. Burioni, M. Casartelli, R. Livi and A. Vezzani, Phys. Rev. E 90, 022811 (2014).

[72] Kress, R. Linear Integral equations, Applied numerical sciences, **82**, Springer-Verlag, New York, (1999).

[73] P. Bonifazi, M. Goldin, M. A. Picardo, I. Jorquera, A. Cattani, G. Bianconi, A. Represa, Y. Ben–Ari, and R. Cossart, Science, 326(5958), (2009).

[74] S. Royer and D. Paré, Nature 422, 518 (2003)

[75] V. Capano, H.J. Hermann and L. De Arcangelis,*Optimal percentage*

of inhibitory synapses in multi-task learning, preprint 2014.

Acknowledgments

Vorrei ringraziare la Prof.ssa Burioni per aver creduto fin da principio in questo progetto di ricerca, per i preziosi consigli e per avermi spronato con entusiasmo e sensibilità. Mi sono sentito fin da subito accolto e reso partecipe delle attività di ricerca del gruppo di lavoro e tutto ciò ha rappresentato una forza motrice fondamentale per la realizzazione di questo lavoro di tesi.

Vorrei inoltre ringraziare il Prof. Livi, il Dott. Vezzani e il Prof. Casartelli per la collaborazione e i proficui suggerimenti. Ma ciò che è più importante per avermi fatto sentire parte di un gruppo di ricerca sano e appassionato.

Un ringraziamento speciale è per la mia famiglia. Voi siete il mio punto di riferimento e il perno sul quale ho fatto e farò sempre forza. Cerco ogni giorno di ricambiare tutto quello che fate e avete fatto per me.

Inoltre, in questi anni tanti amici mi hanno sostenuto nei momenti più difficili, fatto scatenare al vipera e in giro per il mondo, sbazzare davanti a Kikko, sudare nella ping caverna o nel nuovo stabilimento outdoor. Non sento la necessità di fare nomi, ma di ringraziare tutte queste persone.